Active Sonar Tracking Under Realistic Conditions

ACTIVE SONAR TRACKING UNDER REALISTIC CONDITIONS

BY

BEN LIU, M.Sc.

A THESIS

SUBMITTED TO THE DEPARTMENT OF ELECTRICAL & COMPUTER ENGINEERING

AND THE SCHOOL OF GRADUATE STUDIES

OF MCMASTER UNIVERSITY

IN PARTIAL FULFILMENT OF THE REQUIREMENTS

FOR THE DEGREE OF

DOCTOR OF PHILOSOPHY

Doctor of Philosophy (2019) McMaster University

(Electrical & Computer Engineering) Hamilton, Ontario, Canada

TITLE:	Active Sonar Tracking Under Realistic Conditions
AUTHOR:	Ben Liu M.Sc., (Pattern Recognition & Intelligence Systems) University of Chinese Academy of Sciences, Beijing, China
SUPERVISOR:	Prof. T. Kirubarajan
NUMBER OF PAGES:	xiii, 145

To my family

Abstract

This thesis focuses on the problem of underwater target tracking with consideration for realistic conditions using active sonar. This thesis addresses the following specific problems: 1) underwater detection in three dimensional (3D) space using multipath detections and an uncertain sound speed profile in heavy clutter, 2) tracking a group of divers whose motion is dependent on each other using sonar detections corrupted by unknown structured background clutter, 3) extended target tracking (ETT) with a high-resolution sonar in the presence of multipath detection and measurement origin uncertainty.

Unrealistic assumptions about the environmental conditions may degrade the performance of underwater tracking algorithms. Hence, underwater target tracking with realistic conditions is addressed by integrating the environment-induced uncertainties or constraints into the trackers. First, an iterated Bayesian framework is formulated using the ray-tracing model and an extension of the Maximum Likelihood Probabilistic Data Association (ML-PDA) algorithm to make use of multipath information. With the ray-tracing model, the algorithm is able to handle more realistic sound speed profile (SSP) instead of using the commonly-assumed constant velocity model or isogradient SSP. In addition, by using the iterated framework, we can

simultaneously estimate the SSP and target state in uncertain multipath environments. Second, a new diver dynamic motion (DDM) model is integrated into the Probability Hypothesis Density (PHD) to track the dependent motion diver targets. The algorithm is implemented with Gaussian Mixtures (GM) to ensure low computational complexity. The DDM model not only includes inter-target interactions, but also the environmental influences (e.g., water flow). Furthermore, a log-Gaussian Cox process (LGCP) model is seamlessly integrated into the proposed filter to distinguish the target-originated measurement and false alarms. The final topic of interest is to address the ETT problem with multipath detections and clutter, which is practically relevant but barely addressed in literature. An improved filter, namely MP-ET-PDA, with the classical probabilistic data association (PDA) filter and random matrices (RM) is proposed. The optimal estimates can be provided by MP-ET-PDA filter by considering all possible association events. To deal with the high computational load resulting from the data association, a Variational Bayesian (VB) clustering-aided MP-ET-PDA is proposed to provide near real-time processing capability.

The traditional Cramér-Rao Lower Bound (CRLB), which is the inverse of the Fisher information matrix (FIM), quantifies the best achievable accuracy of the estimates. For the estimation problems, the corresponding theoretical bounds are derived for performance evaluation under realistic underwater conditions.

Acknowledgements

I would like to take this opportunity to acknowledge my deepest gratitude to my supervisor, Prof. T. Kirubarajan, for accepting me as a Ph.D student, for supporting me financially and spiritually, for the generous expert advise and guidance motivated me to complete my thesis work, and for the trusting in my abilities and encouragement throughout the course of my Ph.D career.

I would like to thank to Dr. R. Tharmarasa for his much needed help and advise during last three years. His creative and comprehensive advice and comments greatly improve the quality of my research work. I also want to express my gratitude to my committee members, Prof. I. Bruce and Prof. J. Chen for suggesting their valuable feedback on my research work and the time they took spent on my supervisory meetings and reading this thesis.

I want to thank Prof. Y. Zuo, Prof. W. Wang, Prof. Y. Guo , Prof G. Zhou and Prof. X. Tang for their supports on my research papers. Thanks to all my friends, in particular, Yuanhao, Qingsong, Yinghui, Krishanth, Dan, Keqi, Jianfeng, Mehrnoosh, Tongyu, Bin, Song, Markimba, Jingqun, Keyi, Zhen, Yi for their help during my Ph.D career.

Last, but by no means least, I would like to express my special gratitude to my parents for their unconditional love and support throughout all these years.

Abbreviations

2D	Two Dimensional
3D	Three Dimensional
cdf	Cumulative Distribution Function
CR	Coordinate Registration
CRLB	Cramér-Rao Lower Bound
CSS	Constant Sound Speed
CV	Constant Velocity
DA	Data Association
DDM	Diver Dynamic Motion
DDS	Diver Detection Sonar
DSS	Directed Subspace Search
EOF	Empirical Orthogonal Function
ET	Extended Target

ETT	Extended Target Tracking
EVT	Extreme Value Theory
FIM	Fisher Information Matrix
FISST	Finite Set Statistics
GM	Gaussian Mixture
GM-PHD	Gaussian Mixture Probability Hypothesis Density
GML	Global Maximum Likelihood
GNN	Global Nearest Neighbor
GS	Genetic Search
IRF	Information Reduction Factor
JLLR	Joint Log Likelihood Ratio
JPDA	Joint Probabilistic Data Association
KF	Kalman Filter
LGCP	Log Gaussian Cox Process
LLR	Log Likelihood Ratio
MHT	Multiple Hypotheses Tracking
ML	Maximum Likelihood
ML-PDA	Maximum Likelihood Probabilistic Data Association

ML-PMHT Maximum Likelihood Probabilistic Multi-Hypothesis Tracker

MLE Maximum Likelihood Estimation

MMC Modified Measurement Covariance

MP-ML-PDA
Multipath Maximum Likelihood Probabilistic Data Association

MPG Multi-Pass Grid

MSE Mean Square Error

MTT Multitarget Tracking

NEES Normalized Estimation Error Squared

PCRLB Posterior Cramér-Rao Lower Bound

pdf Probability Density Function

PHD Probability Hypothesis Density

PPP Poisson Point Process

PSO Particle Swarm Optimization

RFS Random Finite Set

RoI Region of Interest

SFM Social Force Model

SNR Signal-to-Noise Ratio

SSP	Sound Speed Profile
ToD	Target-Originated Detection
ToF	Time of Flight
ToI	Target of Interest
TRV	Target Related Variable
UKF	Unscented Kalman Filter
UT	Unscented Transformation
UWSN	Underwater Wireless Sensor Network
VB	Variational Bayesian
VLO	Very Low Observable

Declaration of Academic Achievement

This research presents analytical and computational work carried out solely by Ben Liu, herein referred to as "the author", with advice and guidance provided by the academic supervisor Prof. T. Kirubarajan. Information that is presented from outside sources which has been used towards analysis or discussion, has been cited when appropriate; all other materials are the sole work of the author.

Contents

List of Figures

Chapter 1

Introduction

1.1 Introduction

1.1.1 Background of Target Tracking

Target tracking has a long history spanning over more than half a century and it refers to jointly estimating target related variables (TRVs) (e.g., number of targets, target appearance or environment parameters) and the targets' state (e.g., position, velocity and acceleration) conditioned on sensor data. By incorporating the evolution models of TRVs into the trackers, we aim to obtain accurate estimates over time.

Tracking algorithms usually handle the tracking problems in two stages: 1) Data association (DA) techniques (e.g., optimal assignment) are used to address the measurement-origin uncertainty caused by missed detections, multipath detection or clutter, 2) State estimation techniques (e.g., recursive Bayesian) are applied to update the states of targets given the associated measurement events. Several DA techniques have been proposed in the literature. The global nearest neighbor (GNN) approach,

joint probabilistic data association (JPDA) filter [1, 2, 3] and the multiple hypotheses tracking (MHT) [4] method are widely used to handle the measurement origin uncertainty problem. The GNN chooses the best observation within the gating region to update a track [5]. The basic idea behind JPDA is to update a track using all observations in a neighborhood (or gate) with different weights. To handle the association uncertainty, the GNN and the JPDA try to inflate the covariance matrix, which may result in more false detections within the gate. Also, the performance of JPDA will degrade when two targets evolve close to each other. Compared with JPDA, MHT is a measurement-oriented tracking method, which assigns feasible observations in the gate to tracks and builds multiple hypotheses [6]. Instead of choosing the most likely hypothesis as in GNN or fusing all possible hypotheses as in JPDA, all possible hypotheses in MHT are propagated to the subsequent time step and updated with future observations. The computational load of MHT is, however, quite high and highly improbable hypotheses are usually pruned to reduce the computational load.

Recently, Probability Hypothesis Density (PHD) filter, which is based on the Random Finite Set (RFS) theory [7], has been applied to track a time-varying number of targets. The PHD filter propagates the first moment of the intensity function of PHD, which is a sub-optimal but practical alternative to propagating the actual multitarget probability density function (pdf) [8]. The data association between measurements and tracks is avoided within the PHD framework. The Sequential Monte Carlo (SMC) method is often used to implement the PHD with a large set of particles, resulting in the SMC-PHD algorithm [9]. Alternatively, the Gaussian Mixture PHD (GM-PHD) filter, which uses a Gaussian mixture (GM) approximation to the pdf, is used as well [10] with reduced computational complexity compared with

the SMC-PHD.

In addition to the methods described above, which assume prior distributions and an evolution model on the kinematics state, parameter estimation techniques within the maximum likelihood estimation (MLE) framework assume a deterministic target motion model (i.e., no process noise) and find the optimal estimates by optimizing the measurement likelihood. The MLE algorithms are batch processing methods to estimate the kinematics state of the target in contrast to the recursive GNN, JPDA, MHT and PHD algorithms. The Maximum Likelihood Probabilistic Data Association (ML-PDA) algorithm [11], and the maximum likelihood probabilistic multi-hypothesis tracker (ML-PMHT) [12, 13] are two commonly used methods for tracking low signal-to-noise ratio (SNR) targets. ML-PDA uses the probabilistic data association (PDA) technique to solve the measurement-origin uncertainty assuming that at most one target exists. An extension of ML-PDA using joint PDA that can be used in multiple targets scenarios is available as well [14]. In contrast to ML-PDA, ML-PMHT does not restrict the number of measurements being assigned to a target.

1.1.2 Active Sonar Tracking: A Brief Review

Underwater target tracking has applications in marine surveillance, search and rescue, and ocean explorations. Due to the high transmission loss of radio waves passing through water, a passive or an active sonar is widely used in wide-area underwater surveillance. Underwater acoustic communication suffers from multipath, low SNR, limited transmission rate and the varying sound speed profile (SSP) depending on oceanographical factors. The performance of the trackers is affected by the complex underwater environment (e.g., rough seabed, water flow movement).

Originally, a passive sonar on a single platform was used to detect and track maritime targets [15][16][11]. Numerous algorithms to handle the high nonlinearity, low observability [17], and the low detection probability [11] of passive underwater tracking systems have been proposed. To ensure observability and to improve the accuracy of the estimates, multiple sonar sensors [18] or sonobuoy-based networks [19][20][21] are increasingly used to localize and track underwater targets.

With the recent advances in acoustic noise quietening techniques [22][23], however, it is becoming more difficult to detect underwater targets with a passive sonar, leading to increased interest in active sonar to detect and track stealthy targets. In the context of active sonar, transmitter and receiver operate by emitting acoustic pulse signals into the water and detecting the signal reflected from the target of interest (ToI), respectively. Horizontal azimuth and time of flight (ToF) captured by the receiver are used to localize targets. Compared with a passive sonar, active sonar enables the detection and tracking of a stealthy target at longer ranges albeit at the expense of the requirement for a signal transmitter.

Classical approaches [24][25] to active sonar tracking problem have been concerned with target localization in a two-dimensional (2D) azimuth plane. Most works on clutter modeling assume that the clutters are uniformly distributed in the surveillance region [11], but such assumptions may not be valued in the real underwater environments. For example, the wake phenomenon, which generates a stronger clutter behind the targets, often confuses the trackers since wake measurements violate the uniform distribution assumption. In [26, 27], multi-target tracking algorithms are proposed to track divers in the proposed of state-dependent clutter by correctly modeling the wake-generated false alarms behind the divers. Instead of assuming that

the signal amplitude information (AI) is Gaussian or Rayleigh distributed, a modified version of the PDA filter is proposed by using the heavy-tailed clutter model [28], which can yield more robust performance than conventional trackers. Increased interest in depth estimation has lead to the development of three-dimensional (3D) active tracking methodologies with application to stealthy target tracking. In [29], a 3D multitarget tracking (MTT) tracking method was proposed by taking advantage of instantaneous 3D detections from signal pings. In [30], the target range and depth were estimated using the elevation and time of flight (ToF) measurements assuming that the relative azimuth between the sensor and target are known a priori. Also, the combined acoustic rays, a special multipath property, were used in [30] to increase the accuracy of estimates. Underwater wireless sensor networks (UWSNs) are also widely used for 3D target localization with multiple detections from one target [31][32]. To obtain 3D localization information, some methods have been extended to multipath-based trackers [33][34][35][36][37]. These multipath-enabled trackers can provide better performance by exploiting multipath detections, but suffer from high computational complexity in low SNR (high clutter) environments. In [38], the Maximum Likelihood Probabilistic Data Association (ML-PDA) algorithm was extended to handle heavy clutter and multipath detections to yield the multipath ML-PDA (MP-ML-PDA) tracker for low observable target states initialization. With the advances in sensor revolution, extended target tracking based on high-resolution sonar (e.g., diver detection sonar (DDS)) has become possible. A brief introduction on extended target tracking can be found in Chapter 4.

Because of the significant impact of the surrounding environment on underwater tracking performance, the modeling and the estimation of the environmental factors

are essential steps in underwater target trackers. The complex marine environment provides the motivation for this thesis including. The specific problems addressed in this thesis are:

- Curvilinear acoustic propagation channel caused by an uncertain SSP, which may degrade the accuracy of coordinate registration techniques using a simple/idealized SSP model (i.e., constant velocity model [38], isogradient SSP [39]).
- Multiple signals from one target via different propagation paths and high false alarm rates in the region of interest (RoI), leading to difficulties in measurement-to-track association and track initialization [38].
- Unknown structured clutter distribution caused by the nonuniform environment (e.g., bathymetry, movement of water flow), which conflicts with the assumption that clutter is uniformly distributed over the RoI with a known density in traditional trackers [9, 10, 40].
- Unknown number of the targets and the special dynamic motion model influenced by the interactions among targets and by the surrounding environment (e.g., water flow, terrain shape).
- More complex data association problem due to the multipath phenomena and extended target (ET) detections in clutter using a high-resolution active sonar system.

The main objective of this thesis is to propose better models to represent the SSP-influenced acoustic propagation model, the structured clutter distribution, the

dynamic motion including environmental interactions and the coexistence of multipath phenomena and ET detections in clutter environment to improve the performance and efficiency of underwater target tracking algorithms.

In most traditional underwater target trackers, the realistic environmental factors are usually ignored or approximated with a simple/idealized model, which may result in model mismatches. For example, a straight propagation model is used in previously proposed trackers [21][38][41][42], interactions among underwater group targets and with the environment are ignored in existing diver tracking algorithms [26, 27, 28] and the problem of extended target tracking (ETT) in multipath clutter environment is rarely addressed [43] until now.

To improve the performance and accuracy of the trackers using an active sonar, realistic conditions/models representing the underwater environment state must be properly integrated into the algorithms. The second chapter of this dissertation is dedicated to deal with target detection taking into consideration the uncertain multipath environment in heavy clutter. The ray-tracing method is utilized to account for the phenomena of bending and multipath with a given SSP [39][44]. To represent the sound speed variation efficiently in general cases, a combination of Muck profile [45] and multiple Empirical Orthogonal Functions (EOFs) [46] is used in the SSP modeling. By uniting the ray-tracing method and the Munk-based SSP model, a characteristic ToF measurement model for active sonar that handles the bending acoustic channel and uncertain ocean factors can be obtained. Further, to deal with measurement origin uncertainty arising from the heavy clutter and multipath detections, a new expanded version of ML-PDA, called MP-ML-PDA, is presented. An iterated MP-ML-PDA (IMP-ML-PDA) framework that can estimate the state of the

underwater target in an uncertain multipath environment with heavy clutter, is finally proposed.

High-resolution active sonar systems are now commonly used in underwater surveillance (e.g., DDS) to provide more information on the targets of interest. In chapter 3, a new diver dynamic motion (DDM) model for divers moving in a group is presented based on the social force model (SFM) [47]. The novel DDM model derived from the SFM not only includes the inter-target interactions, but also the influences arising from the water flow surrounding the divers. Another challenge in underwater target tracking is the existence of unknown structured background clutter arising from the noisy and non-stationary surrounding environment, violating the assumptions in traditional trackers [9, 10, 40]. Here, the log-Gaussian Cox process (LGCP) [48] is utilized to estimate the environment-induced structured clutter spatial intensity over the whole measurement space. By integrating the novel DDM and the LGCP-based clutter estimator into the widely used GM-PHD filter, a unified recursive framework is formed to track a group divers consisting of an unknown number of targets with environmental-influenced dynamics and unknown clutter distribution density.

Another challenging problem that emerges with a high-resolution active sonar system is tracking an extended target in a multipath clutter environment. Extended target tracking, where a target occupies more than one resolution cells, has received attention in the literature [49]. However, in scenarios where an extended target appears, one may receive target-originated detections (ToDs) via multiple propagation modes (e.g., non-line-of-sight, line-of-sight) when ET travels in a confined underwater environment due to reflections at the surface and bottom. This ET tracking problem accompanied by the multipath phenomenon, called the MP-ET problem, is realistic

and needs efficient solutions. The multipath detections may confuse the traditional trackers [50, 51, 51, 52, 53, 54, 55, 56, 57, 58] that assume only a single propagation path. To the best our knowledge, the ETT problem with multipath detections has been only discussed in [43]. The method in [43] does not provide the target shape information, which is deemed vital in ETT problems with measurement origin uncertainty [59]. In chapter 4, a newly expanded version of the PDA filter that integrates the random matrix model is derived to jointly estimate the kinematic state and target extent. Further, a Variational Bayesian (VB) clustering-aided algorithm with a lower computational load is presented to provide real-time capable solution for the ETT problem in an uncertain multipath environment. In addition to using a constant velocity motion model, a new terrain constrained motion model is presented for scenarios with terrain-following autonomous vehicles.

1.2 Objectives of the Thesis

In compliance with the terms and regulations of McMaster University, this dissertation has been written in *sandwich thesis* format by assembling three articles. These articles represent the independent research performed by the author of this dissertation, Ben Liu.

These articles included in the dissertation are focused on underwater target localization and tracking using an active sonar under realistic conditions. The objectives of the thesis are the following:

- To provide an overview of the challenging problems arising from realistic conditions in active sonar tracking (Papers I, II and III).

- To formulate an algorithmic framework of detecting an unknown underwater target considering realistic ocean environment uncertainty (Paper I).
- To mathematically formulate the new motion model for divers including the inter-target interactions and influences from water flow (Paper II).
- To seamlessly integrate the multi-diver tracking algorithm with the structured clutter density estimator to distinguish the target-originated measurement with false alarms efficiently (Paper II).
- To develop an algorithm for extended target state estimation with the multipath phenomenon (Paper III).

1.3 Related Publications

1.3.1 Journal Articles

- **B. Liu**, X. Tang, R. Tharmarasa, T. Kirubarajan, R. Jassemi, S. Hallé, "Underwater Target Tracking in Uncertain Multipath Ocean Environments", Submitted to *IEEE Transactions on Aerospace and Electronic Systems*, 2018.
- **B. Liu**, R. Tharmarasa, M. Florea, R. Jassemi, T. Kirubarajan, "Diver Tracking in Unknown Structured Clutter Background using a Force-based GM-PHD Filter", Submitted to *IEEE Transactions on Aerospace and Electronic Systems*, 2019.
- **B. Liu**, R. Tharmarasa, R. Jassemi, D. Brown, T. Kirubarajan, "Extended Target Tracking with Multipath Detections, Terrain-Constrained Motion Model

and Clutter", Submitted to *IEEE Transactions on Intelligent Transportation Systems*, 2019.

1.3.2 Conference Publications

- **B. Liu**, R. Tharmarasa, S. Hallé, R. Jassemi, M. Florea, T. Kirubarajan, "Divers Tracking with Improved Gaussian Mixture Probability Hypothesis Density Filter", In *22nd International Conference on Information Fusion*, Ottawa, Canada, July 2019.

Chapter 2

Underwater Target Tracking in Uncertain Multipath Ocean Environments

2.1 Abstract

In order to address the problem of three dimensional (3D) localization of an underwater target using a two dimensional (2D) active sonar with unknown oceanographic factors in a multipath environment with heavy clutter, a novel iterative framework based on ML-PDA, which considers ocean SSP uncertainty and utilizes multiple detections to realize 3D position estimation with only bearing and ToF measurements, is proposed. ML-PDA is highly effective in low SNR target detection. However, it is limited by its assumption of at most one target-originated detection within a scan. We first extend the ML-PDA into a multipath ML-PDA by enumerating the combined association events formed from multiple detection patterns. In addition, an

SSP-dependent ToF measurement model is derived for both the direct path and the surface-reflected path between two remote nodes, so that the SSP uncertainty can be addressed systematically. By adopting an iterative Bayesian framework, both the target states and the SSP coefficients can be estimated simultaneously.

In addition, the Cramér-Rao Lower Bound (CRLB), which quantifies the best possible accuracy in the presence of SSP uncertainties, is derived and analyzed. Numerical simulations confirm the underwater target localization performance of the proposed method in the presence of heavy clutter in an unknown ocean environment with a realistic sound propagation model.

2.2 Introduction

Detection and tracking of underwater targets is a fundamental component in underwater surveillance, search and rescue, and in ocean exploration. Due to the high transmission loss of radio waves passing through water, passive or active sonar is widely used in wide-area underwater surveillance. Underwater acoustic communication suffers from multipath, low SNR, limited transmission rate and varying SSP dependent on oceanographical factors. Originally, passive sonar on a single platform was used to detect and track maritime targets [15][16][11]. Numerous algorithms to handle the high nonlinearity, low observability [17], and low detection probability [11] of passive underwater tracking systems have been proposed. To ensure observability and to improve the accuracy of the estimates, multiple sonar sensors [18] or sonobuoy-based networks [19][20][21] are increasingly used to localize and track underwater targets. With the advances in acoustic noise quietening techniques [22][23], however, it is becoming more and more difficult to detect underwater targets with a

passive sonar, leading to increased interest in active sonar to detect and track stealthy targets.

Classical approaches [24][25] to active sonar based tracking have been concerned with target localization in a 2D azimuth plane. Increased interest in depth estimation has lead to the development of 3D active tracking methodologies with application to stealthy target tracking. In [29], a 3D multitarget tracking (MTT) tracking method was proposed by taking advantage of instantaneous 3D detections from signal pings. In [30], the target range and depth were estimated using the elevation and ToF measurements assuming that the relative azimuth between the sensor and target are known a priori. Also, the combined acoustic rays, a special multipath property, were used in [30] to increase the accuracy of estimates. UWSNs are also widely used for 3D target localization with multiple detections from one target [31][32].

In order to obtain 3D localization information, the above methods attempt to diversify the measurements space, which increases the complexity and cost of the tracking system. As stated before, the existence of multiple propagation paths between two nodes poses an added challenge to sonar trackers, however, it also affords an opportunity to improve the tracking results. The information contained within the multipath returns in the receiver can help improve the observability in 3D sonar tracking systems. Some methods have been extended to multipath-based trackers [33][34][35][36][37]. These multipath-enabled trackers can provide better performance by exploiting multipath detections, but suffer from high computational complexity in low SNR detection clutter environments. In [38], the ML-PDA algorithm was extended to handle heavy clutter and multipath detections to yield the multipath Maximum Likelihood Probabilistic Data Association (MP-ML-PDA) tracker for low

observable target states initialization. But, these multipath-enabled methods, including the MP-ML-PDA algorithm, assume that coordinate registration (CR), whereby a sensor measurement is converted into the ground coordinate, can be carried out accurately for different paths. However, due to the idiosyncrasies of the environment, accurate CR is not practical in underwater environments.

To accurately estimate the location of the target, an accurate CR process is required. In contrast to terrestrial radio propagation, underwater sound propagation speed is not constant but varies with salinity, pressure and temperature. Due to this environmental dependency, acoustic propagation model is not necessarily linear but often curvilinear, which makes the traditional trackers [21][38][41][42] that assume propagation along straight lines between the sensor and the target inaccurate. In [30], by taking advantage of an assumed and known SSP, the target depth information was obtained from multipath detections. In [39], 3D target position was estimated from acoustic ToF measurements with an assumed isogradient SSP. In practice, the ocean environment is not known exactly. Even though the ocean parameters can be identified by various sensors (e.g., conductivity, temperature and density or CTD sensor), there is still uncertainty due to sensor noise. Also, the ocean state does not remain constant, but varies due to changing ocean current and sun light. Thus, the SSP calculated from ocean variables has to account for the uncertainty when the SSP is applied to generate the sound propagation path. The inaccurate and varying SSP, combined with high nonlinearity and measurement uncertainty due to heavy clutter and missing detection, makes underwater target detection a non-trivial problem.

To the best of our knowledge, there are no existing solutions to handle underwater target tracking with both environment and measurement origin uncertainties. In

[60], the idea of argumented state is utilized to estimate sensor registration errors, but with the requirement of Doppler measurement information, which is satisfied only by narrowband sonar. A variational Bayesian filter is presented in [61] to deal with uncertain process and measurement noise covariance matrices. To handle sensor location uncertainty in heavy clutter, an iterated ML-PDA is proposed in [18] to simultaneously estimate both the states of the target and the sensor. However, the framework presented in [18] is only for a passive surveillance system with multiple sensors and cannot handle the case of multipath detections. In addition, the oceanographic parameter uncertainty cannot be introduced into the framework in [18] without using a specific ocean environment dependent measurement model.

The objective of this paper is to propose an algorithm that estimates the ocean environment parameters and the target state simultaneously by incorporating a realistic SSP-dependent propagation model. In addition, the 3D motion information is obtained by the proposed algorithm without using a 3D sonar or a multi-sensor system, but only by using a single monostatic 2D active sonar platform. The problem addressed in this paper is both challenging and realistic. To incorporate the ocean environment uncertainty, realistic and highly nonlinear acoustic propagation paths dependent on varying SSP are required. Measurement origin uncertainty via multiple propagation paths in heavy clutter has to be considered as well. To address these real-world issues, in this paper, an iterated MP-ML-PDA (IMP-ML-PDA) algorithm is proposed to tackle the underwater target localization problem with heavy clutter in a multipath ocean environment using a practical sound signal propagation model.

In the proposed algorithm, the SSP model that is dependent on ocean parameters

is described using a stratification technique. Then, a set of highly nonlinear ToF measurement formulas for monostatic active sonar is derived using Snell's law based on the stratified ocean environment model. With this SSP-dependent model, a deterministic sampling-based method [62] is used to handle the highly nonlinear problem and to account for the uncertainty in predicted ocean state as part of the measurement covariance, resulting in a set of new and modified covariances for all possible target measurement models. With the extension of the ML-PDA to the MP-ML-PDA, the new modified covariances are used to build a new joint log likelihood ratio (JLLR). Finding the JLLR global optimal point is a non-trivial non-convex problem with a large number of local maxima distributed throughout the six-dimensional parameter space. A hybrid optimization solution consisting of grid search and particle swarm optimization (PSO) is presented to handle the complex objective function. Grid search can help find an initial RoI, and then the final estimate can be obtained by PSO. Finally, a sequential update technique is adopted to fuse the information from multiple measurements.

In this paper, we focus on the 3D underwater target localization with uncertainties in both oceanographic parameters and measurement origin using multipath detections with a realistic acoustic propagation model. The paper is organized as follows: Section II describes the problem and the system models including target motion model, ocean SSP model, sensor measurement model with multipath and the ray-tracing model derived from an arbitrary SSP. In Section III, the basic framework of ML-PDA and its extension MP-ML-PDA based on [38] are presented, followed by the new IMP-ML-PDA algorithm to address the SSP uncertainty problem. The CRLB that qualifies the achievable accuracy in the presence of false alarms, missed detections, multipath

and SSP uncertainty is derived in Section IV. In Section V, simulation results are presented while conclusions are discussed in Section VI.

2.3 Problem Formulation

2.3.1 Target Dynamical Model

This paper is limited to tracking the non-maneuvering and noise-free motion of a deep sea target using a single active sonar. A constant velocity motion model is utilized in this paper, but the algorithm can also be applied to other models such as the constant acceleration motion model. For simplicity, we assume submarine target tracking under an ocean environment with single-hop propagation reflected by a flat surface and the direct propagation without any contact with a boundary. Bottom-reflected paths and other multiple-hop reflected paths can also be utilized and improve the accuracy of the proposed tracker without any changes to the theoretical framework.

Figure 2.1 illustrates the geometric locations of the target and the sonar platform. The state variables at the k-th scan for a constant velocity (CV) target are the position vector $(x_t^k, y_t^k, \zeta_t^k)$ and the velocity vector $(\dot{x}_t^k, \dot{y}_t^k, \dot{\zeta}_t^k)$ in 3D Cartesian coordinates. We denote the state of target at time k as

$$X_t^k = [x_t^k, \dot{x}_t^k, y_t^k, \dot{y}_t^k, \zeta_t^k, \dot{\zeta}_t^k]', \tag{2.1}$$

where $'$ denotes transposition.

A linear, discrete-time state evolution equation with no process noise can be written as

$$X_t^{k+1} = F_t^k X_t^k, \tag{2.2}$$

where the state transition matrix F is given by

$$F = \begin{bmatrix} 1 & T & 0 & 0 & 0 & 0 \\ 0 & 1 & 0 & 0 & 0 & 0 \\ 0 & 0 & 1 & T & 0 & 0 \\ 0 & 0 & 0 & 1 & 0 & 0 \\ 0 & 0 & 0 & 0 & 1 & T \\ 0 & 0 & 0 & 0 & 0 & 1 \end{bmatrix} \tag{2.3}$$

with T being the sampling time.

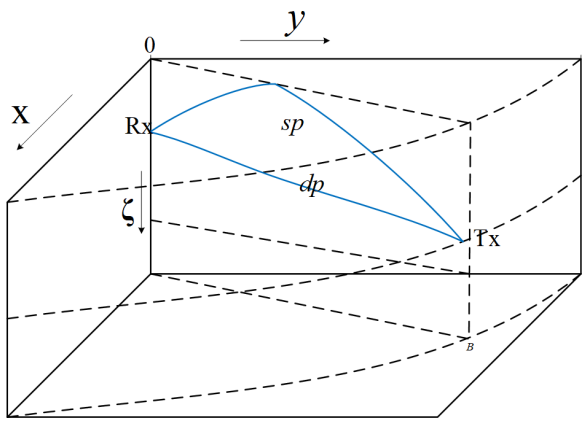

Figure 2.1: Geometry of the vertical planar sonar measurement model.

2.3.2 Stratified Ocean Environment Model

As stated before, by assuming a known SSP, a sensor measurement can be accurately mapped to the target state. However, in practical scenarios, there is uncertainty about the oceanographic parameters and the SSP information is not perfect, which degrades the performance of sonar trackers. Thus, to quantify the uncertainty in SSP and to account for the uncertainty in target tracking, a general, albeit approximate, SSP model needs to be incorporated into the tracker.

The SSP can generally be expressed using empirical variables and functions obtained from historical data or field experiments. In reality, it is impossible to measure the SSP continuously from sea surface to ocean bottom, but possible only at discrete depths layers. As a reasonable and simple model for underwater sound speed, the Munk profile [45] is adopted to capture the feature of varying underwater SSP. Also, the EOFs [46] can efficiently represent the sound speed variation in many cases with low computational load. Thus, EOF vectors are used to make the model more practical. More complex models [63] are also available, but only with additional a priori information. Assuming that N EOFs are used, the SSP model is given by

$$c = c_{\text{munk}} + \sum_{n=1}^{N} a_n E_n, \tag{2.4}$$

where $c = [c(\zeta_1), c(\zeta_2), ..., c(\zeta_J)]'$ is a vector of sound speed samples at various vertical depth layers, J denotes the total number of ocean layers, and

$$c_{\text{munk}} = [c_{\text{munk}}(\zeta_1), c_{\text{munk}}(\zeta_2), ..., c_{\text{munk}}(\zeta_J)]' \tag{2.5}$$

is a Munk profile generated from

$$c_{\text{munk}}(\zeta_j) = 1500\left[1.0 + \rho(\bar{\zeta}_j - 1 + e^{-\bar{\zeta}_j})\right]. \tag{2.6}$$

In the above, $\bar{\zeta}_j = 2(\zeta_j - \zeta_C)/\zeta_C$ and ζ_C is the depth of the minimum sound velocity, and ρ is the perturbation coefficient. Also, a_n is the coefficient of SSP reconstruction and $E_n = [e_n(\zeta_1), e_n(\zeta_2), \cdots, e_n(\zeta_J)]$ is $J \times 1$ orthogonal vector calculated from EoF e_i. To predict the SSP, a state-evolution model based on the coefficients of SSP is defined as

$$X_e^{k+1} = F_e X_e^k, \tag{2.7}$$

where $X_e^k = [a_1^k, a_2^k, \cdots, a_N^k]'$. Within a short time span and surveillance range, a reasonable assumption is that the SSP is independent of time and range [64]. Thus, F_e is an identity matrix. The initial SSP parameters are assumed to be $X_e^0 \sim \mathcal{N}(\bar{X}_e^0, P_e^0)$, where $\bar{X}_e^0$ is the mean vector of environmental variables and P_e^0 is the corresponding covariance. For simplicity, we define $c^k = \mathcal{C}(\zeta, X_e^k)$, where $\zeta = [\zeta_1, \zeta_2, ..., \zeta_J]$ is the ocean depth vector. For a uniformly divided ocean depth in this paper, the size of a single depth layer $\Delta\zeta = \zeta_2 - \zeta_1 = \ldots = \zeta_J - \zeta_{J-1} = (\zeta_J - \zeta_1)/(J-1)$.

The reflection of the acoustic signal occurs because of the existence of the ocean boundary. In this paper, we assume that the ocean bottom and the surface are both flat and their depth information are known as a priori based on bathymetry data.

2.3.3 Sensor Measurement Model in a Multipath Environment

The geometry with a deep-sea target and an active sonar platform illustrated in Figure 2.1 assumes that the target (Tx) moves close to the ocean bottom and that the sonar platform (Rx) is located near the surface. In a monostatic active sonar, the transmitter and the receiver are collocated. For simplicity, two one-way paths between the target and the sonar are assumed in this paper. Other models can also be utilized within the proposed framework to improve performance, albeit at the cost of increased computational complexity. The first is the direct path (*dp*), which defines the acoustic wave travel between two nodes without any reflection, while the second is a single-hop surface-reflected path (*sp*). As discussed previously, the SSP is independent of time and range, so we can specify various active sonar two-way propagation modes by combining *dp* and *sp*. Then, all active propagation models are shown in Table 2.1. Mode 1 and Mode 2 specify that signals from the transmitter go to target via *dp* and then come back to the receive via *dp* and *sp*, respectively. Mode 3 and Mode 4 denote that signals leave the transmitter via *sp* and return to the receiver via *dp* and *sp*, respectively.

Table 2.1: Acoustic Propagation Paths and Modes

Mode	Path	Mode	Path
1	dp-dp	3	sp-dp
2	dp-sp	4	sp-sp

With a 2D active sonar, a received measurement signal consists of the ToF τ and the azimuth θ. Assume that m_k measurements are received by the sensor at time k

and denote the measurement vector by

$$Z_{m_k}^k = [z_1^k, z_2^k, ..., z_{m_k}^k] \tag{2.8}$$

where $z_i^k = [\tau_i^k, \theta_i^k]'$, $i = 1, \cdots, m_k$. For simplicity, we assume that all propagation models have equal probability of detection p_d and that the detection events are independent of one another over time. However, range-dependent p_d can be used as well. Detection z_i^k can be target-originated or from clutter (false alarm). The corresponding measurement equation is given by

$$z_i^k = \begin{cases} \mathcal{M}_l(X_t^k, X_s^k, \hat{c}^k) + w_{l,i}^k & \text{Mode } l \\ \text{clutter} & \text{otherwise} \end{cases} \tag{2.9}$$

where w_l^k is zero-mean white Gaussian noise with covariance R_l^k, $X_s^k = [x_s^k, \dot{x}_s^k, y_s^k, \dot{y}_s^k, \zeta_s^k, \dot{\zeta}_s^k]$ is the sensor state, which is assumed to be stationary without loss of generality, and $\hat{c}^k$ is the predicted SSP from (2.4). The vector nonlinear function $\mathcal{M}_l$ is given by

$$\mathcal{M}_l^k(\bullet) = \begin{bmatrix} \tau \\ \theta \end{bmatrix} = \begin{bmatrix} h_l(X_t^k, X_s^k, \hat{c}^k) \\ \text{actan}(\dfrac{y_t^k - y_s^k}{x_t^k - x_s^k}) \end{bmatrix} \tag{2.10}$$

where l represents the index of propagation model. The measurement covariance is given by

$$R_l^k \triangleq \text{cov}\{w_l^k\} = \begin{pmatrix} \sigma_{\tau_l^k}^2 & 0 \\ 0 & \sigma_{\theta_l^k}^2 \end{pmatrix} \tag{2.11}$$

where $l = 1, 2, \cdots, L$. From the measurement equation, we can see that the ToF

of sensor measurement is dependent on the SSP. With an ideal a priori SSP, one can assume that the measurement model is only disturbed by the thermal noise $w_l^k \sim \mathcal{N}(0, R_l^k)$. In practical situations, however, the SSP is not necessarily measured accurately. That is, the measurement model inevitably suffers from both thermal noise and SSP uncertainty, which is the focus of this paper.

Due to the low SNR of target-originated detections, false alarms or clutter measurements are inevitable, resulting in the measurement origin uncertainty problem. Assume that a clutter measurement $o_i^k = [o_{\tau,i}^k, o_{\theta,i}^k]$ is uniformly distributed over the surveillance space V, $o_{\theta,i}^k \sim \mathcal{U}(\Theta_1, \Theta_2)$, $o_{\tau,i}^k \sim \mathcal{U}(\mathcal{T}_1, \mathcal{T}_2)$ and that the number of false alarms m_k in a frame is Poisson distributed with a known expected value $\lambda\mathcal{V}$ [65]. The probability mass function (pmf) of m_k is given by

$$u_f(m_k) = \frac{(\lambda\mathcal{V})^{m_k} \exp(-\lambda\mathcal{V})}{m_k!} \tag{2.12}$$

where $\mathcal{V} = (\Theta_2 - \Theta_1)(\mathcal{T}_2 - \mathcal{T}_1)$, and λ is the spatial clutter density.

2.3.4 Ray-Tracing Method with Ocean Stratification

As mentioned previously, acoustic propagation is influenced by the uncertain SSP. To calculate the accurate ToF of a received signal, ray-tracing method is adopted here. Ray-tracing accounts for the phenomena of bending and multipath with a given SSP [39][44].

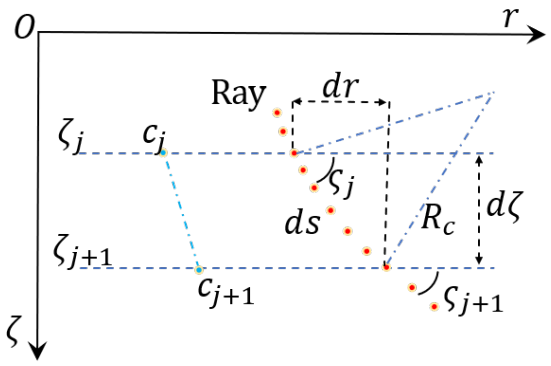

Figure 2.2: Illustration of Snell's law.

In a depth-dependent medium, acoustic rays travel based on Snell's law [66], which is given by

$$\frac{\cos(\varsigma_j)}{c(\zeta_j)} = \frac{\cos(\varsigma_{j+1})}{c(\zeta_{j+1})} = \eta \tag{2.13}$$

where ς is the grazing angle of a single ray, ζ is the depth information and η is the ray parameter, which is constant for a given direct ray. From the differentials, one has

$$d\mathfrak{t} = \frac{ds}{c(\zeta)}, \quad \tan(\varsigma_j) = \frac{d\zeta}{dr}, \quad \sin(\varsigma_j) = \frac{d\zeta}{ds}. \tag{2.14}$$

The travel time $\mathfrak{t}_j$ within the j-th depth layer is expressed as

$$\mathfrak{t}_j = \int_{\zeta_j}^{\zeta_{j+1}} \frac{d\zeta}{c(\zeta)\sqrt{1-\eta^2 c(\zeta)^2}}. \tag{2.15}$$

The ToF of the one-way direct path between two nodes can be expressed as

$$\tau_{dp} = \int_{\zeta_s}^{\zeta_t} \frac{d\zeta}{c(\zeta)\sqrt{1-\eta_{dp}^2 c(\zeta)^2}}. \tag{2.16}$$

Also, the corresponding travel distance is

$$s_{dp} = \int_{\zeta_s}^{\zeta_t} \frac{d\zeta}{\sqrt{1 - \eta_{dp}^2 c(\zeta)^2}} \tag{2.17}$$

As assumed previously, the ocean boundary is flat and can be treated as a mirror surface. The ray parameter remains constant after specular reflection. Therefore, the ToF and travel distance of single-hop *sp* can be respectively expressed as

$$\tau_{sp} = \int_{\zeta_s}^{\zeta_t} \frac{d\zeta}{c(\zeta)\sqrt{1 - \eta_{sp}^2 c^2(\zeta)}}, \tag{2.18}$$

$$s_{sp} = \int_{\zeta_s}^{\zeta_t} \frac{d\zeta}{\sqrt{1 - \eta_{sp}^2 c^2(\zeta)}}. \tag{2.19}$$

From (2.16) and (2.18), one can see that the acoustic travel times via *dp* and *sp* between two nodes are different due to differing ray parameters. The horizontal distance between the target and the sensor is written as

$$r = \int_{\zeta_s}^{\zeta_t} \frac{\eta c(\zeta) d\zeta}{\sqrt{1 - \eta^2 c(\zeta)^2}} = \sqrt{(x_t - x_s)^2 + (y_t - y_s)^2} \tag{2.20}$$

Note that the distance between a pair of nodes is independent of propagation modes. Thus, let $\eta = \eta_{dp}$.

2.3.5 Finding Eigenrays

Eigenrays are the acoustic propagation paths that connect the sensor and the target and are pivotal in determining the ToF and which signals are received [64]. Calculating the acoustic paths in sea water is a complex task. The sound speed varies due to

the differences in temperature, salinity and pressure at different ocean depth, resulting in refraction effects. The reflection of rays at surface and ocean bottom makes the problem more complicated. By assuming a constant sound speed or isogradient sound speed, analytical solutions can be obtained [21][38][39]. However, in practical scenarios with varying sound speed, which are of interest here, an analytical solution is nearly impossible and numerical approximations have to be used [64].

With the discretized SSP, one can numerically calculate the sound signal travel path at an emitting angle $\varsigma \in [-90°, 90°]$ compared to the horizontal level, and estimate the travel time at the same time. By defining a tolerance gap space around the target position, the eigenrays that connect the target and the sensor can be identified when the rays reach the predefined space.

2.4 Multipath Tracking with Uncertain SSP

In this section, the standard ML-PDA is first briefly reviewed and then expanded to the multipath ML-PDA to handle the case of multiple target-originated detections in the same frame. Finally, an iterated ML-PDA based algorithm is presented to track the underwater target in heavy clutter and uncertain ocean environment with a curvilinear sound propagation model.

2.4.1 Outline of ML-PDA

The ML-PDA algorithm for target parameter estimation was first presented in [67], and it has been demonstrated to be an effective tracker of Very Low Observable (VLO) targets in high clutter environments [14]. The assumptions made by the ML-PDA

algorithm are given below [65]:

- Only one target exists per scan with a known detection probability p_d.
- No more than one target-originated measurement can be received by the sensor in each scan.
- Target evolves according to a deterministic target dynamic model, e.g., the perfectly constant velocity model.
- Target-originated measurements are corrupted by zero-mean white Gaussian noise.
- False alarms are uniformly distributed and their cardinality per scan is Poisson distributed with known parameters.

The development of the ML-PDA is described in detail in [68], and the ML-PDA log-likelihood ratio over N_w frames of data is summarized as

$$\mathcal{L}(\mathbf{x}, Z) = \sum_{k=1}^{N_w} \ln \left\{ 1 - p_d + \frac{p_d}{\lambda} \sum_{i=1}^{m_k} p(z_i^k \,|\, \mathbf{x}) \right\} \tag{2.21}$$

where p_d is the target detection probability per frame, N_w is the number of frames of measurements used for estimation and m_k is the number of measurements in the k-th frame.

2.4.2 Derivation of Multipath ML-PDA

Target-originated multipath returns at the receiver is a special case of underwater signal propagation due to the reflection and refraction of acoustic rays. Additional

information about the target state is contained within these multiple returns and it is beneficial to include those multipath measurements into the tracker. However, the ML-PDA is limited to processing at most one detection from a single target [65], which is not suitable for our problems here.

In this section, to deal with the problem of the 3D position estimation using a 2D sonar, multipath ML-PDA algorithm is presented. The MP-ML-PDA can make use of the multipath environment by considering all possible associations events from multiple detections.

To use the MP-ML-PDA, the following assumptions about the statistics of the measurements are made [38]:

- The maximum number of propagation modes is L and the corresponding measurement equations are given by (2.10).
- The target-originated measurements in a scan are statistically independent of each other [69][70], and the measurements from different frames are also mutually independent.
- Each detection from the measurement set can be associated to any single propagation model, but the identity of propagation modes is not known.
- The target's detection probability through various propagation modes is identical.

With above assumptions, for a set of measurements $Z^k_{m_k} = \{z^k_1, \cdots, z^k_{m_k}\}$ including multiple target-originated returns and false alarms, various combinations of detections from $Z^k_{m_k}$ are defined as association events $\Phi^k_{\varphi,n_\varphi}$, where φ means the hypothesized number of target-originated detections at time k and $\varphi \in [0, \varphi_{\max} = \min\{m_k, L\}]$,

and $n_\varphi = C_{m_k}^{\varphi}$ is the number of measurement combinations ε_φ^k, and A_L^φ is the number of corresponding propagation mode combinations ϵ_k^φ; $A_a^b = a!/(a-b)!$, $C_a^b = A_a^b/b!$. Then, one can calculate the total number of all association events $N_{\Phi^k} = \sum_0^{\varphi_{max}} C_{m_k}^{\varphi} A_L^{\varphi}$.

To make the problem clear, an example is presented here. Define a measurement set $Z_3^k = \{z_1^k, z_2^k, z_3^k\}$ with $m_k = 3$ in the k-th sonar scan with $L = 2$ possible propagation modes $h = \{h_1, h_2\}$. Then, one can obtain $\varphi_{max} = 2$, and for $\varphi = 2$, measurement combination set $\varepsilon_2^k = \{(z_1^k, z_2^k), (z_1^k, z_3^k), (z_2^k, z_3^k)\}$ and propagation mode combination set $\epsilon_2^k = \{(h_1, h_2), (h_2, h_1)\}$. The association event for 2 hypothesized target-originated detections within k-th frame is given by $\Phi_{2,3}^k = \{(\phi_{h_1,h_2}^{z_1,z_2}), (\phi_{h_2,h_1}^{z_1,z_2}), (\phi_{h_1,h_2}^{z_1,z_3}), (\phi_{h_2,h_1}^{z_1,z_3}), (\phi_{h_1,h_2}^{z_2,z_3}), (\phi_{h_2,h_1}^{z_2,z_3})\}$ with cardinality $N_{\phi_{2,3}^k} = C_3^2 A_2^2 = 6$.

The feasible association events are

$$\Phi_{\varphi,n_\varphi}^k = \begin{cases} \varphi \text{ out of } m_k \text{ detections are target-originated} \\ \qquad\qquad\qquad\qquad \varphi = 1, ..., \varphi_{\max} \\ \text{all measuremnts are from clutter or false alarms} \\ \qquad\qquad\qquad\qquad \varphi = 0 \end{cases} \tag{2.22}$$

Accordingly, the target-originated measurement model for association event $\phi_{\varphi,n_\varphi}^k$ is given by

$$z_{\varphi,n_\varphi}^k = \begin{bmatrix} \mathcal{M}_{D_1}^k(\bullet) \\ \mathcal{M}_{D_2}^k(\bullet) \\ \vdots \\ \mathcal{M}_{D_L}^k(\bullet) \end{bmatrix} + \begin{bmatrix} w_{D_1}^k \\ w_{D_2}^k \\ \vdots \\ w_{D_L}^k \end{bmatrix} \tag{2.23}$$

where D_l equals to one or zero depending on whether the l-th propagation model is used in association event $\phi^k_{\varphi,n_\varphi}$.

For a target-originated measurement, the likelihood function is given by

$$p(z^k_{\varphi,n_\varphi}|X^k_t) = \mathcal{N}[z^k_{\varphi,n_\varphi}; \mathcal{M}^k_{\varphi,n_\varphi}; R^k_{\varphi,n_\varphi}] \tag{2.24}$$

where

$$\begin{aligned} \mathcal{M}^k_{\varphi,n_\varphi} &= [\mathcal{M}^k_{D_1}, \mathcal{M}^k_{D_2}, \ldots, \mathcal{M}^k_{D_L}]' \\ R^k_{\varphi,n_\varphi} &= \text{blkdiag}\left(R^k_{D_1}, R^k_{D_2}, \ldots, R^k_{D_L}\right) \end{aligned} \tag{2.25}$$

As defined above, only when the sign of D_l is equal to one, can its corresponding parameter be retained in the association event set and used in subsequent calculations.

Applying the total probability theorem, the joint likelihood function of one single frame measurement set is given by

$$\begin{aligned} p(Z^k_{m_k}|X^k_t) &= \sum_{\Phi^k} p(Z^k_{m_k}|\Phi^k_{\varphi,n_\varphi}, X^k_t) \cdot p(\Phi^k_{\varphi,n_\varphi}|X^k_t) \\ &= \sum_{\Phi^k} \frac{(m_k-\varphi)! \times \mu_f(m_k-\varphi)}{p(m_k)m!} \\ &\times \prod_{l=1}^{L} (p^l_d)^{D_l}(1-p^l_d)^{1-D_l} \cdot p(z^k_{\varphi,n_\varphi}|X^k_t) \end{aligned} \tag{2.26}$$

with p^l_d denoting the target detection probability via path l.

Dividing (2.26) by the joint likelihood that all m_k observations are clutter-originated, one can get the joint likelihood ratio of one single frame measurement

$$\mathcal{J}(Z^k_{m_k}, X^k_t) = \sum_{\Phi^k} \alpha_{\varphi,n_\varphi} \cdot p(Z^k_{m_k}, X^k_t) \tag{2.27}$$

where

$$\alpha_{\varphi,n_\varphi} = \frac{1}{\lambda^\varphi} \prod_{l=1}^{L} (p_d^l)^{D_l} (1 - p_d^l)^{(1-D_l)} \tag{2.28}$$

Assuming that the measurement data set are frame independent, the joint likelihood function for all N_w frames of data Z^{N_w} can be expressed as the product of the single frame joint likelihood functions. Taking the logarithm of the result, the JLLR can be therefore given by

$$\mathcal{L}(Z^{N_w}, X_t^k) = \sum_{k=1}^{N_w} \ln \mathcal{J}(Z_{m_k}^k, X_t^k) \tag{2.29}$$

2.4.3 Iterated MP-ML-PDA Method with Uncertain SSP

To deal with uncertain SSP in heavy clutter and multipath environment, an iterated multipath ML-PDA framework is proposed here. By modifying the measurement covariance, the SSP uncertainty is reasonably incorporated into the whole framework. The idea is to estimate the parameters of the SSP and the target state simultaneously in every recursion, and this mainly consists of two stages: prediction stage and update stage.

1) **Prediction Stage**

By using a Kalman filter (KF)-based framework, the modified measurement covariance (MMC) can be approximated. For the nonlinear system in the present paper, the unscented Kalman filter (UKF), a deterministic sampling method, is adopted. By using the unscented transformation (UT) technique, the UKF calculates the statistics of a random variable undergoing a nonlinear transformation. Compared with the extended Kalman filter (linearization method) and the particle filter (random sampling method), the UKF (deterministic sampling method) can provide more accurate

estimates with lower complexity. As previously assumed, the initial $\hat{X}_e^0$ is subject to Gaussian distribution $\hat{X}_e^0 \sim \mathcal{N}(\bar{X}_e^0, P_e^0)$. Then, in the q-th recursion, one can predict

$$\begin{aligned} \hat{X}_e^{k|k-1} &= F_e * \hat{X}_e^{k-1} \\ \hat{P}_e^{k|k-1} &= F_e * \hat{P}_e^{k-1} * F_e \end{aligned} \tag{2.30}$$

where $q = 1, ..., q_{max}$. Then, a matrix $\mathcal{X}$ containing $2U + 1$ sigma vectors is formed based on the following:

$$\begin{aligned} \mathcal{X}_{e,0}^{k|k-1} &= \hat{X}_e^{k-1} \\ \mathcal{X}_{e,u}^{k|k-1} &= \hat{X}_e^{k-1} + (\sqrt{(U+\gamma)\hat{P}_e^{k-1}})_u, \ u = 1, ..., U \\ \mathcal{X}_{e,u}^{k|k-1} &= \hat{X}_e^{k-1} - (\sqrt{(U+\gamma)\hat{P}_e^{k-1}})_{u-U}, \ u = U+1, ..., 2U \end{aligned} \tag{2.31}$$

where γ is a scaling variable.

Given a target state, propagating those sigma vectors through the SSP prediction model (2.4), one can get the predicted SSP

$$\hat{c}_u^{k|k-1} = \mathcal{C}(\zeta, \mathcal{X}_{e,u}^{k|k-1}) \tag{2.32}$$

By transforming $\hat{c}_u^{k|k-1}$ and using a hypothesized target state via the l-th nonlinear measurement model, the predicted sigma points of the target-originated measurement is given by

$$z_{u,l}^{k|k-1} = \mathcal{M}_l(\hat{X}_t^k, X_s^k, \hat{c}_u^{k|k-1}) \tag{2.33}$$

Using a weighted sample mean and covariance of the posterior sigma points, the

predicted measurement $\hat{z}_l^k$ and the corresponding MMC $\hat{R}_l^k$ can be approximated by

$$\begin{aligned}\hat{z}_l^{k|k-1} &= \sum_{u=0}^{2U} w_u z_{u,l}^{k|k-1} \\ \hat{R}_l^k &= \sum_{u=0}^{2U} w_u (z_{u,l}^{k|k-1} - \hat{z}_l^{k|k-1})'(z_{u,l}^{k|k-1} - \hat{z}_l^{k|k-1}) + R_l^k\end{aligned} \tag{2.34}$$

The derivation of the MMC accounts for both the SSP uncertainty and the sensor thermal noise. One can see that the MMC here is not constant but varies with the accuracy of SSP estimation. Before data association and the calculation of the new JLLR function, all measurements are validated first to eliminate outliers and to reduce the number of combinatorial candidate events. The validation gate for propagation mode l is given by

$$G_l^k \triangleq \left\{ z_k^i : (z_k^i - \hat{z}_l^{k|k-1})'(\hat{R}_l^k)^{-1}(z_k^i - \hat{z}_l^{k|k-1}) \leq g_l \right\} \tag{2.35}$$

where $g_l \sim \chi^2_{n_z}$ is the gate threshold for the l-th propagation mode. For simplicity, g_l for various propagation mode is assumed identical. The validated measurement set in the k-th frame is redefined as $\check{Z}^k$ and $\check{Z}^{N_w}$ is the corresponding measurement set over N_w frames.

With the above MMC and (2.26), one can calculate a new JLLR function as follows:

$$\begin{aligned}\mathcal{L}(\check{Z}^{N_w}, \hat{X}_t^k) &= \sum_{k=1}^{N_w} \ln \mathcal{J}(\check{Z}^k, \hat{X}_t^k) \\ &= \sum_{k=1}^{N_w} \sum_{\Phi^k} \ln \left(\prod_{l=1}^{L} (1 - p_d^l) + \alpha_{\varphi,n_\varphi} \times p(\check{z}_{\varphi,n_\varphi}^k | \hat{X}_t^k) \right)\end{aligned} \tag{2.36}$$

Algorithm 1: PSO Algorithm for MP-ML-PDA

Input:

Recursion index q

Predicted SSP $\hat{c}^{k,q}$

Target state estimates at last recursion $\hat{X}_t^{k,q-1} (q > 1)$

Output:

Global optimal target state estimate $\hat{X}_t$

Initialization:

Define a constrained search space with:

Upper bound on target state $[x^+, \dot{x}^+, y^+, \dot{y}^+, \zeta^+, \dot{\zeta}^+]$

Lower bound on target state $[x^-, \dot{x}^-, y^-, \dot{y}^-, \zeta^-, \dot{\zeta}^-]$

Let iteration index $I = 1$

Generate an initial population with random position and velocity vectors

Start:

Evaluate the objective function JLLR with initial particles

while $I < I_{\max}$ **do**

    Update iteration index $I = I + 1$

    Update the position and velocity of particles

    Evaluate the objective function JLLR with the new population

    if (Convergence) **or** $(I > I_{\max})$ **then**

        Output final estimate of target state $\hat{X}_t^{k,q}$

        Exit

    end

end

2) **Search for Optimal Solution**

The proposed iterated MP-ML-PDA approach is still a maximum likelihood method, and the optimal target state estimate that maximizes the JLLR function can be obtained by searching the constrained target state space. Due to the highly non-convex nature of the above JLLR, the traditional gradient-based optimization methods [71] surfer from the existence of local maxima [69]. Multi-Pass Grid (MPG) Search [11], Genetic Search (GS) [72] and Directed Subspace Search (DSS) [24] have been studied by prior researchers. Compared with MPG Search, GS and DSS are better at finding the global maximum and have lower computational complexity in ML optimization problems [69]. As a stochastic algorithm, PSO has been successfully applied in searching for global maximum mikelihood (GML) solutions [73][74] and shown to be superior with computational efficiency and convergence over the Genetic Algorithm (GA) approach [75, 76].The PSO starts by initializing a population of random solutions in a constrained search space and searches for the best "fitness" value by updating generations.

To mitigate the high computational cost in high dimensional maximum mikelihood (ML) problems, a hybrid approach consisting of grid search and PSO is applied here. The key to this method is to obtain an initial estimate of a smaller search space where a target is likely existent with a coarse grid search, and then use PSO to find a more accurate solution. The main step in the PSO algorithm with application to the current ML problem is illustrated in Algorithm 1. Since PSO is implemented within the iterated MP-ML-PDA framework, the final solution from the last recursion can be utilized to initialize the search space adaptively, which improves the efficiency and accuracy of the optimization method.

In addition, for the specific problem here, the azimuth measurements are independent of the ray-tracing model and ocean environment state. Thus, within the hybrid optimization framework, we first find the azimuth estimate $\hat{\theta}_t^k$ by maximizing the azimuth JLLR given by

$$\begin{aligned} \mathcal{L}(\check{\theta}^{N_w}, \hat{\theta}_t^k) &= \sum_{k=1}^{N_w} \sum_{\Phi^k} \ln \left(\prod_{l=1}^{L} (1 - p_d^l) + \alpha_{\varphi,n_\varphi} \times p(\check{\theta}_{\varphi,n_\varphi} | \hat{\theta}_t^k) \right) \\ p(\check{\theta}_{\varphi,n_\varphi} | \hat{\theta}_t^k) &= \mathcal{N}[\check{\theta}_{\varphi,n_\varphi}^k; \hat{\theta}_{\varphi,n_\varphi}^k; \hat{\sigma}_{\theta,(\varphi,n_\varphi)}^2] \end{aligned} \tag{2.37}$$

Then, we estimate the other 5-dimensional propagation mode-dependent target state $X_t^k = ([x_t^k = r_t^k \cos(\hat{\theta}_t^k),\ \dot{x}_t^k,\ y = r_t^k \sin(\hat{\theta}_t^k),\ \dot{y}_t^k,\ \zeta_t^k,\ \dot{\zeta}_t^k])$ using the azimuth estimate, where $r_t^k = \sqrt{(x_t^k)^2 + y(_t^k)^2}$.

For a grid search method with χ_g uniformly distributed cells over each dimension of the target state space, the computational complexity of (2.36) is $O(\chi_g^{d_z})$, where d_z is the dimension of the target state space, and that of (2.37) is $O(\chi_g^{d_z-1} + \chi_g)$ [18]. The computational complexity of PSO depends on the total number of iterations I, size χ_p of the population and the dimension of the target state space, and it can be written as $I * O(\chi_p^{d_z})$. With the hybrid method consisting of GS and PSO, the overall computational complexity here is $O(\hat{\chi}_g^{d_z-1} + \hat{\chi}_g) + I * O(\chi_p^{d_z})$. One can see that the hybrid optimization solution with a coarse grid strategy is more computationally efficient than the pure grid-based search method because of $\hat{\chi}_g \ll \chi_g$.

3) **Sequential Update**

In a multipath environment, multiple target-originated measurements can be received by the sonar sensor. To extract all the information in those redundant measurements

about the target state and to estimate the SSP parameters accurately, a sequential update strategy is applied here.

Define $\check{Z}_l^k$ as the mutual exclusive validated measurements set corresponding to the l-the measurement model. The basic idea behind sequential update is to treat each $\check{Z}_l^k$ as a new data point at the current prediction time sequentially [77] and update the state, gain and the covariance using all L validated measurements set one after another. In order to simplify the notation, the frame index k is omitted in the following subsection.

The predicted output from the $(q-1)$-th recursion $\hat{X}_e^{q-1}$ and the corresponding covariance $\hat{P}_e^{q-1}$ along with the target state estimate $\hat{X}_t^{q-1}$ are used as the prior information for $l=0$ in the next recursion. For the l-th ($l>0$) propagation model, the measurement innovation $\tilde{z}_l^q$ can be written as [78]

$$\tilde{z}_l^q = \sum_{\check{z}_{l,j} \in \check{Z}_l} \omega_{l,j}^q \tilde{z}_{l,j}^q \tag{2.38}$$

where $\tilde{z}_{l,j}^q = \check{z}_{l,j} - \hat{z}_{l|l-1}^q$ and

$$\omega_{l,j}^q = \frac{\exp\left\{-(\tilde{z}_{l,j}^q)^{\mathrm{T}}(\hat{R}_l^q)^{-1}(\tilde{z}_{l,j}^q)\ /\ 2,\right\}}{\beta + \sum_{\check{z}_{l,j} \in \check{Z}_l} \exp\left\{-(\tilde{z}_{l,j}^q)^{\mathrm{T}}(\hat{R}_l^q)^{-1}(\tilde{z}_{l,j}^q)\ /\ 2\right\}} \tag{2.39}$$

Then, the measurement update equations can be expressed as [78][79]

$$
\begin{aligned}
P^q_{l,X_eZ} &= \sum_{u=0}^{2U} w_u(\mathcal{X}^{l|l-1}_{e,u} - \hat{X}^{l|l-1}_e)(z^{q|q-1}_{u,l} - \hat{z}^q_{l|l-1})' \\
\mathcal{K}^l &= P^q_{l|l-1,X_eZ}(\hat{R}^q_l)^{-1} \\
P^q_{l,\tilde{z}\tilde{z}} &= \mathcal{K}^l \left[\sum_{\check{z}_{l,j}\in\check{Z}_l} \omega^q_{l,j}(\tilde{z}^q_{l,j})(\tilde{z}^q_{l,j})' - \tilde{z}^q_l(\tilde{z}^q_l)' \right] \mathcal{K}^l \\
\hat{X}^q_{e,l} &= \hat{X}^q_{e,l|l-1} + \mathcal{K}^l\tilde{z}^q_l \\
P^q_{e,l} &= P^q_{e,l|l-1} - (1-\omega^q_{l,0})\mathcal{K}^l\hat{R}^q_l\mathcal{K}^l + P^q_{l,\tilde{z}\tilde{z}}
\end{aligned}
\tag{2.40}
$$

where

$$
\omega^q_{l,0} = \frac{\beta}{\beta + \sum_{\check{z}_{l,j}\in\check{Z}_l} \exp\left\{-(\tilde{z}^q_{l,j})^{\mathrm{T}}(\hat{R}^q_l)^{-1}(\tilde{z}^q_{l,j}) \,/\, 2\right\}}
\tag{2.41}
$$

where $\beta = (2\pi)^{d_z/2}\lambda|\hat{R}^q_l|^{1/2}(1-p_dp_g)/p_d$ and p_g is the probability that the target-originated measurement, if detected, lies within the gate [78].

Algorithm 2: Iterated MP-ML-PDA

Input:

Initial environment state X_e^0 and covariance P_e^0

N_w frames of sensor measurement data set Z^{N_w}

3D surveillance area of interest

Output:

Optimal target state estimate $\hat{X}_t$

Initialization:

Initialize X_e^1 and P_e^1 with X_e^0 and P_e^0

Initialize recursion index $q = 1$

Start:

while $q < q_{\max}$ **do**

  Predict $\hat{X}^q_{e,l=0}$ and $P^q_{e,l=0}$ based on $\hat{X}_e^{q-1}$ and P_e^{q-1}

  Predict SSP information for all sigma points using (2.32)

  Given the predicted SSP, find the optimal solution of target state (see Algorithm 1)

  Update $\hat{X}^q_{e,l}$ and $\hat{P}^q_{e,l}$ based on equations(2.38)–(2.40) and produce global $\hat{X}_e^q$ and P_e^q

  Update recursion index $q = q + 1$:

  if (Convergence) **or** $(I > I_{\max})$ **then**

    Output final estimate $\hat{X}_t$ and $\hat{X}_e$

    Exit

  end

end

2.4.4 Track Validation

As stated before, the above optimization may not necessarily converge to the true target state due to the high non-convexity of the JLLR function. That is, the algorithm may end up with an estimate at a local maximum, resulting in a false track. Thus, to determine the existence of a target at the estimate, the output $\hat{X}_t$ must be validated [80].

To validate the output from the proposed iterated MD-ML-PDA approach, a binary hypothesis validation method from [80] is implemented. Define two hypotheses, namely H_1 corresponding to target existence and H_0 corresponding to no target at $\hat{X}_t$. The objective of the validation procedure is to have the most powerful test to choose between H_0 and H_1 by comparing the LLR global maximum at the track estimate to a certain threshold $\mathrm{Th_v}$. Based on the result of extreme value theory (EVT) [81], a Gumbel distribution instead of the Gaussian distribution, is applied to approximate the log-likelihood ratio (LLR) at the track estimate in the absence of a target. The corresponding cumulative distribution function $F_w(w)$ is given by

$$F_w(w) = \exp\{-\exp[-a_n(w - u_n)]\} \tag{2.42}$$

where a_n and u_n are the Gumbel parameters that need to be estimated. The offline method from [80] to estimate the Gumbel parameters is applied here. That is, the unknown parameters a_n and u_n can be calculated from a set of N_c global JLLR maxima $\{w_\iota\}$ with mean value $\bar{w}$ from Monte Carlo simulations and the parameter

estimates are given by

$$\begin{aligned}\hat{a}_n &= \left[\bar{\omega} - \frac{\sum_{\iota=1}^{N_c} \omega_\iota \exp\left(-\hat{a}_n \omega_\iota\right)}{\sum_{\iota=1}^{N_c} \exp\left(-\hat{a}_n \omega_\iota\right)}\right]^{-1} \\ \hat{u}_n &= \frac{1}{\hat{a}_n} \ln\left[\frac{c}{\sum_{\iota=1}^{N_c} \exp\left(-\hat{a}_n \omega_\iota\right)}\right]^{-1}\end{aligned} \tag{2.43}$$

Thus, the threshold $\mathrm{Th_v}$ can be calculated as

$$\mathrm{Th_v} = F_\omega^{-1}(1 - P_{\mathrm{FT}}) \tag{2.44}$$

where P_{FT} is the given false track acceptance probability.

2.5 Cramér–Rao Lower Bound for IMP-ML-PDA

In this section, to validate the performance of the proposed IMP-ML-PDA, the CRLB on the estimation errors in the presence of SSP uncertainty and measurement origin uncertainty is derived using a modified likelihood function. The CRLB is the lower bound on the minimum mean square error (MSE) of any unbiased estimator. Assume $\hat{X}$ is an unbiased estimate of X. Then, the standard CRLB is expressed as

$$\mathcal{E}\{[\hat{X}(Z^{N_w}) - X][\hat{X}(Z^{N_w}) - X]'\} \geq J^{-1} \tag{2.45}$$

where $\mathcal{E}$ represents the expectation operation and

$$\mathbf{J} = \mathcal{E}\{[\nabla_X \ln p(Z^{N_w}|X)][\nabla_X \ln p(Z^{N_w}|X]'\}|_{X=X_{\mathrm{true}}} \tag{2.46}$$

is the Fisher information matrix (FIM) that is calculated at the true value of $X = X_{\text{true}}$ [68].

Substituting (2.26) into (2.46) and after several manipulations, the FIM for the batch-estimation problem in the presence of SSP and measurement origin uncertainties is given by

$$\begin{aligned}\mathbf{J} &= \sum_{k=1}^{N_w} \mathbf{J}_k \\ &= \sum_{k=1}^{N_w} \mathcal{E}\{[\nabla_{X^*} \ln p(Z_{m_k}^k|X^*)][\nabla_{X^*} \ln p(Z_k|X^*]^{\mathrm{T}}\}|_{X^*=X_{\text{true}}^*} \\ &= \sum_{k=1}^{N_w} \sum_{\Phi_k} q_{\varphi,n_\varphi} \cdot [\mathbf{M}_{\varphi,n_\varphi}^k]^{\mathrm{T}} (R_{\varphi,n_\varphi}^k)^{-1} \cdot [\mathbf{M}_{\varphi,n_\varphi}^k]\end{aligned} \tag{2.47}$$

where $X^* = [X_t, X_e]'$ and

$$\mathbf{M}_{\varphi,n_\varphi} = \frac{\partial \mathcal{M}_{\varphi,n_\varphi}(X^*)}{\partial X^*} \tag{2.48}$$

The analytical forms of the partial derivative $\partial \mathcal{M}^l / \partial X^*$ for various propagation models can be found in Appendix A. Also,

$$q_{\varphi,n_\varphi} = E\left[\frac{(\beta_{\varphi,n_\varphi})^2 \cdot p(\hat{z}_{\varphi,n_\varphi}|X^*)}{p(Z^k|X^*)}\right] \tag{2.49}$$

is the less-than-unity scalar information reduction factor (IRF), which quantifies the loss of information due to measurement origin uncertainty.

2.6 Numerical Simulations

In this section, 50 Monte Carlo simulations are used to evaluate the performance of the proposed IMP-ML-PDA approach with a practical acoustic propagation model in estimating the 3D target motion information with a 2D active sonar in an uncertain ocean environment in heavy clutter. The baseline is the estimator assuming the straight line propagation model, which is used in most conventional underwater target localization algorithms [21][38][41][42]. Also, the CRLB provides the benchmark for quantifying the accuracy achievable by any estimator.

To formulate the SSP, we assume the parameters in Munk model as $z_C = 1300$, $\epsilon = 0.00737$. For simplicity, two EoFs are applied here, and the corresponding coefficients are $X_e = [15, -3]$. To simulate the SSP uncertainty, we assume that the initial covariance of X_e is $P_e^0 = \text{diag}(9, 9)$. Moreover, the ocean depth is divided into 13 layers with $\Delta\zeta = 400$m. The Munk profile, EoFs and the modeled SSP can be found in Figure 2.3. As depicted in Figure 2.1, the sonar platform Rx is positioned at $(0, 0, 400)$m, and the unknown underwater target travels near the ocean bottom with a constant velocity. As stated before, a numerical ray-tracing method is applied to approximate the ToF of acoustic signals between the sensor and the target, making the estimation accuracy sensitive to the size of the depth searching range and the intensity of rays. In our simulation, 2,000 rays are traced and a tolerance gap $[\zeta_t^k - 25, \zeta_t^k + 25]$ (in meters) around target depth is selected so that the eigenrays can be found efficiently with an acceptable error.

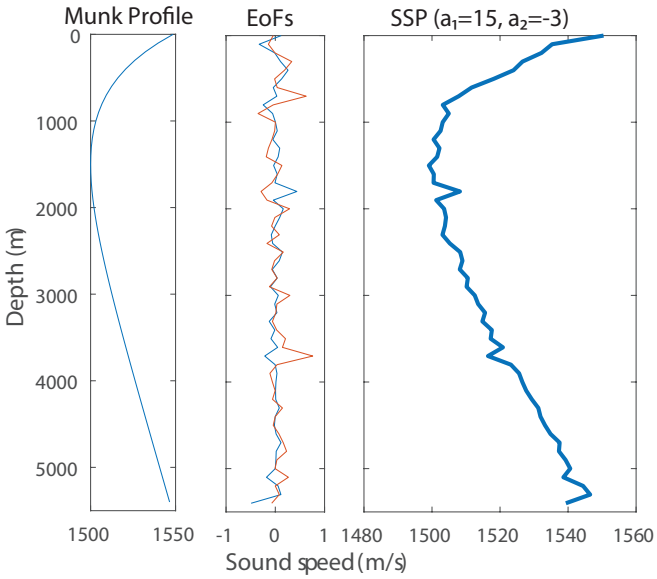

[h]

Figure 2.3: SSP model

To simulate the environment with a VLO target under heavy clutter, we assume Rayleigh fading amplitude to approximate the sonar measurements [11] so that the target detection probability and false alarm probability are given by

$$p_d = \exp\left(-\frac{\mathrm{Th}^2}{2(1+\mathrm{SNR_C})}\right) \tag{2.50}$$

and

$$p_{fa} = \exp\left(-\frac{\mathrm{Th}^2}{2}\right) \tag{2.51}$$

where Th is a suitable detection threshold. In the above, $\mathrm{SNR_C}$ means the SNR in one resolution cell.

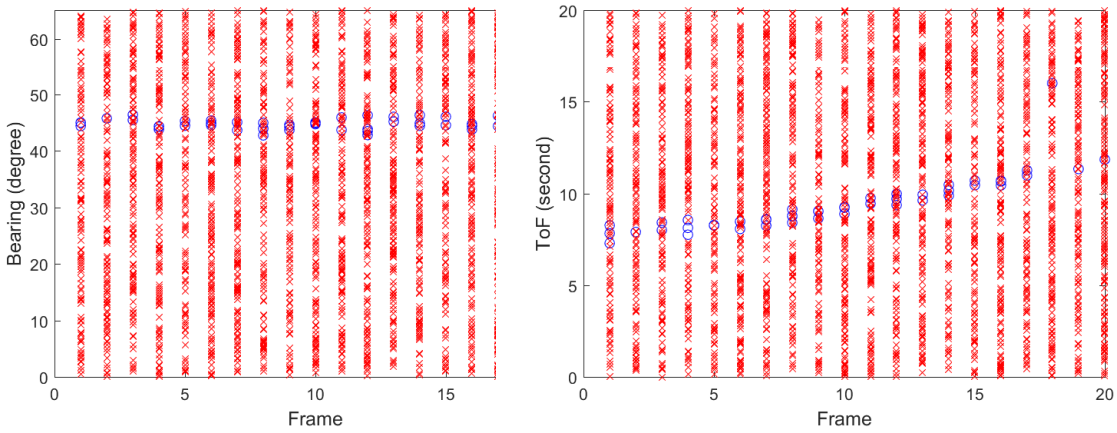

Figure 2.4: Bearing and ToF measurements in one batch. Green circles are target originated measurements, while red crosses are false alarms.

We assume that a high resolution active sonar is deployed here. The time resolution cell size, C_τ, is 0.1s and the azimuth cell size is 3.0°. Then the corresponding ToF and azimuth standard derivations are respectively given by [11]

$$\begin{aligned} \sigma_\tau &= 0.1/\sqrt{12} = 0.0289\text{s} \\ \sigma_\theta &= 3/\sqrt{12} = 0.866^\circ \end{aligned} \tag{2.52}$$

SNR_C in each cell is 6.1 dB and the detection probability p_d for each measurement model is 0.6. Due to the existence of multiple modes, the combined probability of at least one target-originated measurement being detected within one frame is very high. Then, Th = 2.64 and $p_{fa} = 0.0306$ from (2.50) and (2.51), respectively. The expected number of false alarms per frame is $N_{fa} = 132$. The parameters used in the simulations are given in Table 3.1. The simulated ToF and azimuth measurements from a single Monte Carlo run are shown in Figure 2.4.

Table 2.2: Scenario parameters

Parameter	Value
Number of Monte Carlo runs	50
Target initial state (in m and m/s)	[2000 10 2000 10 −4 5200]
Sonar platform state (in m and m/s)	[0 0 0 0 400 0]
Ocean depth (in m)	[0, 5500]
Number of frames N_w	20
Surveillance region volume V	$[0°, 65°] \times [0s, 20s]$
p_d for each propagation model	0.6
Sampling time T	20s
Range error standard deviation σ_τ	0.0289s
Azimuth error standard deviation σ_θ	0.866°
False alarm probability p_{fa}	0.0306
Expected number of false alarms per scan	132

In Table 2.3, the simulation results are summarized along with the average estimated standard deviation $\sqrt{\text{CRLB}}$. The normalized estimation error squared (NEES) [82] is adopted to evaluate the efficiency of the proposed algorithm. We can see that the average estimated target state is close to the ground truth, which demonstrates that the unbiasedness property of the proposed estimator. The estimates by the proposed algorithm in 48 runs are validated out of 50 runs. The corresponding NEES value is 6.77, which is within the 95% confidence region $[5.08, 6.99]$. Figure 2.5 shows the convergence of the objective function JLLR vs. iteration number of PSO. Note that the LLR value increase quickly in the first iteration, which demonstrates the

capability of PSO to find the solution space of interest. In the last generations, the LLR value remains relatively constant with an optimal solution.

Figures 2.6 and 2.7 show the JLLR surface with known SSP. From Figure 2.6 we can see that the azimuth ambiguity dominates in the x-y horizontal plane. Figure 2.7 depicts the localization uncertainty caused by the ToF noise in the y-ζ vertical plane. From both Figures 2.6 and 2.7, we can see that the maximum value of the JLLR surface matches the true target position, with much higher value at the peak than the JLLR values at other points. The existence of many ridges and local optima in these JLLR surfaces makes the global optimal estimate harder to find. To estimate the best-fitting parameters of the Gumbel distribution, an off-line method is adopted. Figure 2.8 shows the histogram statistics and its best-fitting pdf with 10,000 samples. The corresponding cumulative distribution function (cdf) and the selected threshold $\mathrm{Th_v} = -27.5$ with significance level $P_{FT} = 0.05$ is depicted in Figure 2.9.

Table 2.3: Results from 50 Monte Carlo Runs for IMP-ML-PDA with uncertain SSP

Unit	X_{true}	X_{initial}	Mean of $\hat{X}$	RMSE	$\sqrt{\text{CRLB}}$
m	2000	1500–2500	2011.4	104.6	93.5
m/s	10	5–15	10.1	0.31	0.3
m	2000	1500–2500	2013.2	105.3	93.5
m/s	10	5–15	10.1	0.32	0.3
m	5200	4500–5500	5194.9	69.7	61.6
m/s	−4	−10–0	−3.9	0.21	0.19

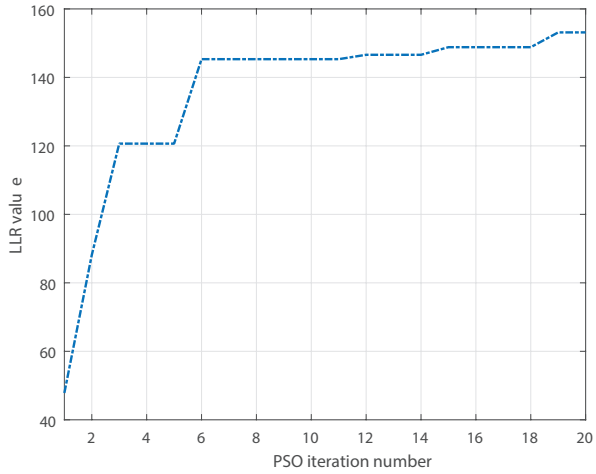

Figure 2.5: Convergence of objective function JLLR vs. iteration number of PSO

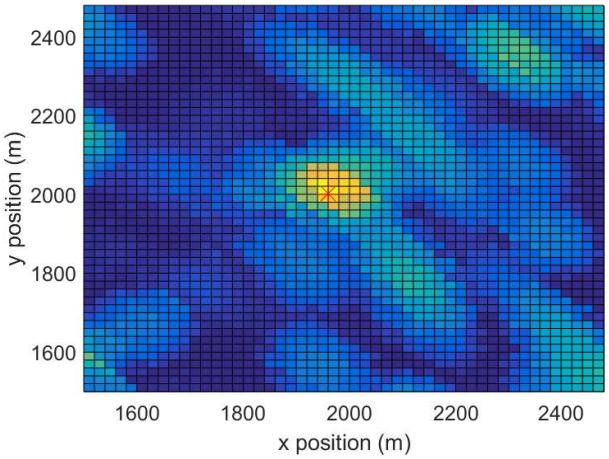

Figure 2.6: JLLR surface in x-y vertical plane

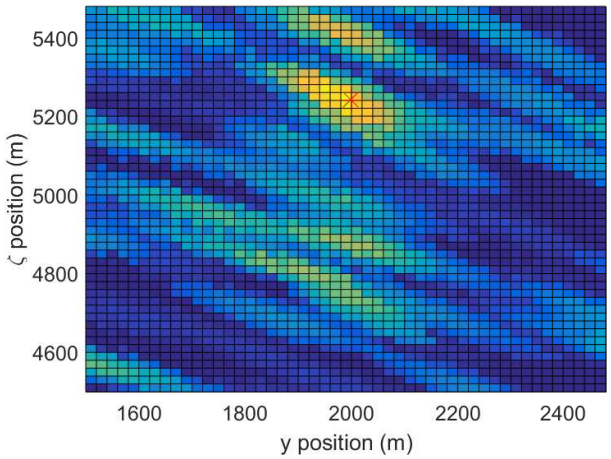

Figure 2.7: JLLR surface in y-ζ vertical plane

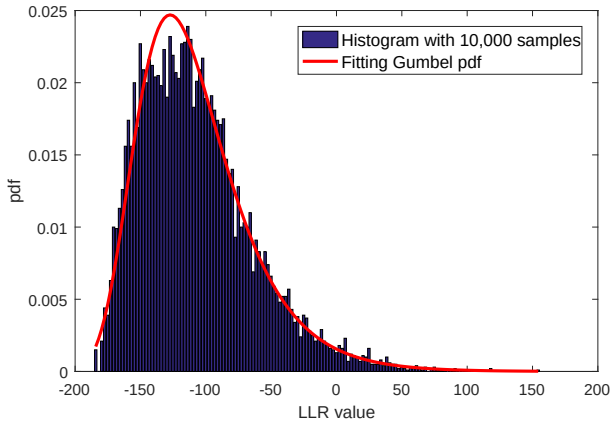

Figure 2.8: Histogram and best-fitting Gumbel pdf

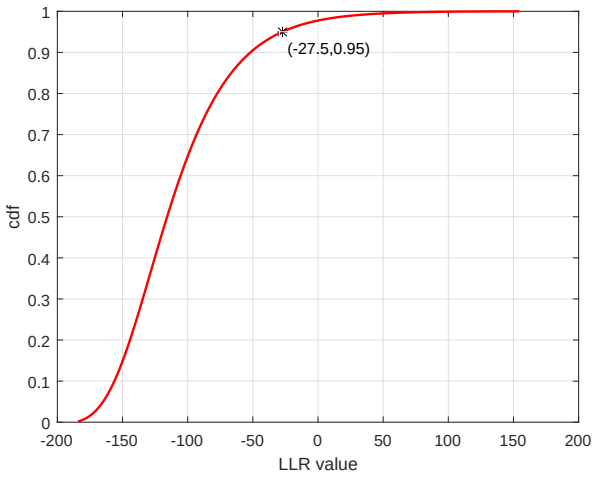

Figure 2.9: Gumbel cdf and threshold

In the conventional underwater target positioning and localization approaches [38][41][42][21], constant sound speed (CSS) and straight propagation model are mostly assumed, and range-based methods are applied instead of using the ToF-based model [31]. Numerical simulations with $c_{\text{CSS}} = 1500$ m/s are implemented and compared with our more realistic model with the target motion model, azimuth measurement model and the clutter model being same as before. The ToF measurement models for the direct path and the surface-reflected path with CSS are respectively given by

$$\tau_{dp} = s_{dp}/c_{\text{CSS}} \tag{2.53}$$

and

$$\tau_{sp} = s_{sp}/c_{\text{CSS}} \tag{2.54}$$

where

$$\begin{aligned} s_{dp} &= \sqrt{(\zeta_t - \zeta_s)^2 + (x_t - x_s)^2 + (y_t - y_s)^2} \\ s_{sp} &= \sqrt{(\zeta_t + \zeta_s)^2 + (x_t - x_s)^2 + (y_t - y_s)^2} \end{aligned} \tag{2.55}$$

The simulation results can be found in Table 2.4. By assuming the CSS model with mismatched SSP, the baseline estimator cannot match the performance of the proposed estimator assuming a realistic ocean environment. The RMSE of the baseline estimator is larger and only 35 track estimate out 50 runs are accepted and the corresponding NEES is 9.75, which is beyond its 95% confidence region. This shows that the simple CSS model cannot yield satisfactory estimates for underwater target tracking. In contrast, the proposed algorithm yields highly reliable estimates and is able to handle measurement origin and SSP uncertainties effectively.

Table 2.4: Results from 50 Monte Carlo Runs for IMP-ML-PDA with constant sound speed

Unit	X_{true}	X_{initial}	Mean of $\hat{X}$	RMSE	$\sqrt{\text{CRLB}}$
m	2000	1500–2500	1924.7	136.6	93.5
m/s	10	5–15	9.9	0.40	0.3
m	2000	1500–2500	1912.3	135.3	93.5
m/s	10	5–15	9.8	0.37	0.3
m	5200	4500–5500	5284.3	78.9	61.6
m/s	−4	−10–0	−4.2	0.26	0.19

In practical scenarios, the SNR of signals detected via Mode 4 is often suppressed to very low values due to its two-time contact with the ocean surface. One can see that Mode 2 and Mode 3 share the same path, and they cannot always be resolved by the sensor. Instead of using all four paths listed in Table 2.1, another case with only Mode 1 and Mode 2 is considered to evaluate the performance of the proposed estimator. Also, a deterministic sampling multipath-enabled ML-PDA (DS-MP-ML-PDA) estimator is adopted for comparison with the proposed IMP-ML-PDA algorithm with

$I_{\max} = 2$. From Table 2.5, one can see that the performance degrades due to fewer modes being used in the estimator. The NEES values for DS-MP-ML-PDA and IMP-ML-PDA are 10.3 and 8.9, respectively, and both of them are beyond the 95% confidence region bounds. Figures 2.10 and 2.11 show the best-fitting Gumbel pdf and the validation threshold for the case with Mode 1 and Mode 2. In addition, the average computing time to process the whole batch (20 frames) of data set for a single Monte Carlo run of DS-MP-ML-PDA and IMP-ML-PDA are 42.2 minutes and 72.4 minutes, respectively. The simulations are implemented in C on an Intel(R) Core(TM) i7 CPU with 32 GB of RAM, and an OpenMP [83] based parallel computing technique is used for loops.

Table 2.5: Results from 50 Monte Carlo Runs for DS-MP-ML-PDA and IMP-ML-PDA with mode 1 and mode 2

Unit	X_{true}	X_{initial}	Mean of $\hat{X}$(DS-MP-ML-PDA)	RMSE (DS-MP-ML-PDA)	Mean of $\hat{X}$(IMP-ML-PDA)	RMSE (IMP-ML-PDA)	$\sqrt{\text{CRLB}}$
m	2000	1500–2500	1977.9	152.2	2015.4	145.7	134.3
m/s	10	5–15	9.9	0.45	10.1	0.43	0.4
m	2000	1500–2500	1977.8	157.5	2015.3	144.3	135.9
m/s	10	5–15	10.0	0.47	10.1	0.41	0.4
m	5200	4500–5500	5230.8	117.3	5192.6	103.9	89.9
m/s	−4	−10–0	−4.1	0.35	−3.9	0.32	0.3

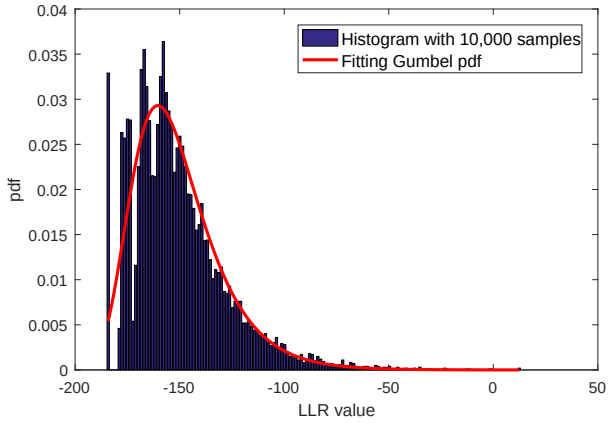

Figure 2.10: Histogram and best-fitting Gumbel pdf

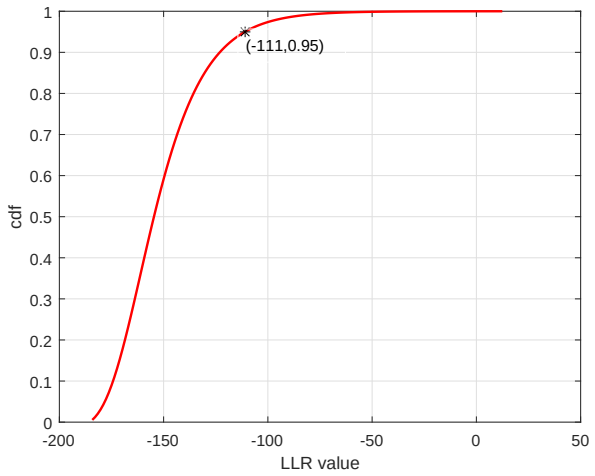

Figure 2.11: Gumbel cdf and threshold

2.7 Conclusions

In this paper, the problem of underwater target localization in practical scenarios was addressed and an improved ML-PDA framework was proposed as an effective solution. To incorporate the influence of SSP uncertainty into the tracker, a realistic

curvilinear acoustic propagation model with arbitrary noisy SSP was derived and deployed. Also, by taking advantage of the realistic SSP with multipath propagation from a single target, 3D target state can be obtained even with a 2D active sonar. The CRLB for this estimation problem was derived, and it was demonstrated that the proposed IMP-ML-PDA can meet the CRLB, i.e, it is efficient. Simulations showed that the CRLB values using all four propagation modes are significantly lower than those using only two propagation modes. Compared with the baseline DS-MP-ML-PDA, the proposed IMP-ML-PDA can yield a better performance, but at the cost of increased computational complexity.

2.8 Appendix

2.8.1 Derivation of $\partial \mathcal{M}^l / \partial X^*$

Assume that the position of the sonar platform given by $X_s = [0, 0, 0, 0, \zeta_s, 0]$ is known. With (2.16)–(2.20), we can get

$$\begin{aligned}
\frac{\partial s}{\partial \eta} &= \eta \int_{\zeta_s}^{\zeta_t} \frac{c^2(\zeta) d\zeta}{\sqrt{(1 - [\eta c(\zeta)]^2)^3}} \\
\frac{\partial \tau}{\partial \eta} &= \eta \int_{\zeta_s}^{\zeta_t} \frac{c(\zeta) d\zeta}{\sqrt{(1 - [\eta c(z)]^2)^3}} \\
\frac{\partial r}{\partial \eta} &= \int_{\zeta_s}^{\zeta_t} \frac{c(\zeta) dz}{\sqrt{(1 - [\eta c(\zeta)]^2)^3}} = \frac{1}{\eta} \frac{\partial \tau}{\partial \eta}
\end{aligned} \tag{2.56}$$

and

$$\begin{aligned}\frac{\partial r}{\partial x_t} &= \frac{x}{\sqrt{x_t^2 + y_t^2}} \\ \frac{\partial r}{\partial y_t} &= \frac{y}{\sqrt{x_t^2 + y_t^2}} \\ \frac{\partial \tau}{\partial \zeta_t} &= \frac{1}{c(\zeta_t)\sqrt{1 - [\eta c(\zeta_t)]^2}}\end{aligned} \tag{2.57}$$

Then,

$$\begin{aligned}\frac{\partial \tau}{\partial r} &= \frac{\partial \tau}{\partial \eta} \Big/ \frac{\partial r}{\partial \eta} = \eta \\ \frac{\partial s}{\partial r} &= \frac{\partial s}{\partial \eta} \Big/ \frac{\partial r}{\partial \eta} = \eta \int_{\zeta_s}^{\zeta_t} c(\zeta) d\zeta\end{aligned} \tag{2.58}$$

Therefore,

$$\begin{aligned}\frac{\partial \tau}{\partial x_t^{k^*}} &= \frac{\partial \tau}{\partial r}\frac{\partial r}{\partial x^{k^*}} \\ \frac{\partial \tau}{\partial \dot{x}_t^{k^*}} &= \frac{\partial \tau}{\partial x^k}\frac{\partial x_t^{k^*}}{\partial \dot{x}_t^k}; \\ \frac{\partial \tau}{\partial y_t^k} &= \frac{\partial \tau}{\partial r}\frac{\partial r}{\partial y_t^{k^*}} \\ \frac{\partial \tau}{\partial \dot{y}_t^{k^*}} &= \frac{\partial \tau}{\partial y_t}\frac{\partial y_t}{\partial \dot{y}_t^{k^*}}\end{aligned} \tag{2.59}$$

where $\partial x / \partial \dot{x}_t^{k^*} = \partial y / \partial \dot{y}_t^{k^*} = \partial \zeta / \partial \dot{\zeta}_t^{k^*} = (k - k^*)T$, T is the sampling period, and k^* denotes the reference frame.

For the environment state $X_e = [a_1, a_2]$, we have

$$\begin{aligned}\frac{\partial \tau}{\partial a_1} &= \frac{\partial \tau}{\partial c(z)}\frac{\partial c(z)}{\partial a_1} \\ &= \int_{\zeta_s}^{\zeta_t} \frac{2[\eta c(\zeta)]^2 - 1}{c^2(\zeta)\sqrt{(1 - [\eta c(\zeta)]^2)^3}} f_1 d\zeta \\ \frac{\partial \tau}{\partial a_2} &= \frac{\partial \tau}{\partial c(\zeta)}\frac{\partial c(\zeta)}{\partial a_2} \\ &= \int_{\zeta_s}^{\zeta_t} \frac{2[\eta c(\zeta)]^2 - 1}{c^2(\zeta)\sqrt{(1 - [\eta c(\zeta)]^2)^3}} f_2 d\zeta\end{aligned} \tag{2.60}$$

where f_1 and f_2 are the EOFs models. In this paper, we have $L = 4$ propagation models from two eigenrays each for the *dp*, *sp* paths between the target and the sensor.

For Mode 1 with $\mathbf{t}_1 = 2\tau_{dp}$, we have

$$\frac{\partial \mathbf{t}_1}{\partial X^*} = 2\frac{\partial \tau_{dp}}{\partial X^*} \tag{2.61}$$

For Mode 2 and Mode 3 with $\mathbf{t}_{2,3} = \tau_{dp} + \tau_{sp}$, we have

$$\frac{\partial \mathbf{t}_2}{\partial X^*} = \frac{\partial \tau_{dp}}{\partial X^*} + \frac{\partial \tau_{dp}}{\partial X^*} = \frac{\partial \mathbf{t}_3}{\partial X^*} \tag{2.62}$$

For Mode 4 with $\mathbf{t}_4 = 2\tau_{sp}$, we have

$$\frac{\partial \mathbf{t}_4}{\partial X^*} = 2\frac{\partial \tau_{sp}}{\partial X^*} \tag{2.63}$$

Since the azimuth measurement θ is only dependent on $[x_t, y_t]$, we get

$$\begin{aligned}
\frac{\partial \theta}{\partial x_t} &= \frac{-y_t}{x_t^2 + y_t^2} \\
\frac{\partial \theta}{\partial y_t} &= \frac{x_t}{x_t^2 + y_t^2} \\
\frac{\partial \theta}{\partial \dot{x}_t} &= T\frac{y_t}{x_t^2 + y_t^2} \\
\frac{\partial \theta}{\partial \dot{y}_t} &= T\frac{-x_t}{x_t^2 + y_t^2}
\end{aligned} \tag{2.64}$$

Chapter 3

Diver Tracking in Unknown Structured Clutter Background using a Force-based GM-PHD Filter

3.1 Abstract

This paper considers the problem of tracking multiple human divers using a high-resolution 2D active sonar. While conventional trackers assume the diver motion model to follow a constant velocity or acceleration, in many scenarios, the behavior of human divers is more complex due to being affected by external factors such as water current, activities of neighboring divers and the intent of the divers themselves. That is, not only are the kinematic states of divers correlated with each other but

they are also dependent on external factors. Another challenge in underwater diver target tracking is that the spatial distribution of false alarms is no longer a homogeneous Poisson point process (PPP) but location-dependent with unknown spatial non-homogeneous intensity due to the complex non-stationary underwater environment.

In this paper, a multitarget tracking solution based on the probability hypothesis density (PHD) that can deal with the challenges of a time-varying number of targets, inter-target interactions, and non-homogeneous structured clutter environment is proposed.A new social forced-based diver dynamic motion (DDM) is proposed to represent the complex inter-dependent behaviors of targets. To calculate the likelihood in the prediction step of the PHD filter with environmental dependencies, the proposed DDM model is integrated into the recursive Gaussian mixture (GM) Bayesian framework, and a new GM-DDM-PHD filter is proposed to track human divers in deep water. Further, to handle the structured clutter environment, a log-Gaussian Cox process (LGCP) model is integrated into the GM-DDM-PHD filter to estimate the clutter spatial intensity over the whole surveillance region.

In addition, the posterior Cramér-Rao lower bound (PCRLB), which quantifies the best possible accuracy in the presence of kinematic interactions among targets and in an uncertain underwater environment, is derived as the benchmark for performance evaluation. Simulation results demonstrate the improved performance of the proposed method over the standard PHD filter in the presence of interactions and unknown structured background clutter.

3.2 Introduction

The tracking of underwater divers using active sonar has applications in marine infrastructure security of ports, harbors and bridges [84, 85] and in search and rescue of humans. This paper presents an effective and robust multiple target tracking method to track a time-varying number of underwater divers in structured background clutter environments. The estimation of the unknown number of divers and their state along with adaptive clutter intensity estimation using an active sonar is considered. The two main challenges in multiple diver tracking in an underwater environment with an active sonar are: 1) complex motion models influenced by environmental factors and neighboring targets and 2) unknown structured background clutter. Those two challenges provide the motivation for this paper.

3.2.1 Dynamic Motion Model

In modeling the kinematics of multiple targets, there are two opinions: 1) macroscopic and microscopic [86]. Macroscopic models treat the overall motion of targets as an aggregated flow of the motions of individual targets with the interactions among targets being ignored. Microscopic models treat targets as a set of individuals with interrelated movements among neighboring divers and interactions with the surrounding environment being considered. In microscopic modeling, the SFM [47] can be utilized to represent the movement of divers by assuming that the motion of a diver is driven by social forces such as the diver's objective force, repulsion and attraction forces from other divers, and repulsion and attraction forces from the external environment. Compared with other microscopic models [87, 88], the SFM offers flexibility to be incorporated into a probabilistic Bayesian estimation framework [8].

The SFM has been used in pedestrian tracking to model the interactions among people and with static obstacles. In [86], the SFM is utilized to handle the complex inter-target interactions with occlusions. In [8, 89], the SFM is integrated with the framework of probability hypothesis density (PHD) filter. Using the SFM, the interactions among pedestrians and the goals of targets are incorporated into the PHD filter to track a varying number of targets. Further, a modified SFM is presented in [90] to model the movement of vehicles for ground target tracking.

In contrast to ground target tracking [8, 89, 90], one distinguishing feature in multiple diver tracking is that the kinematic behavior of each diver is subject not only to interactions with other divers but also to hydrodynamic forces arising from water flow. However such interactions among divers and with the environment are ignored in existing diver tracking algorithms [26, 27, 28].

To model how a diver reacts to the movement of other neighboring divers, and to model the effects of non-stationary water flow on a diver's motion, the concept of social force model is used in this paper to propose a novel diver dynamic motion (DDM) model to represent the complex movement of divers. With this novel diver motion model, one can rebuild the likelihood function in the prediction step of the recursive Bayesian estimation algorithm [6, 9, 10, 40, 91], such that the influences of the environment on an individual target can be factored in.

3.2.2 Structured Background Clutter

Another challenging problem in underwater target tracking is the existence of unknown structured background clutter arising from the noisy and non-stationary surrounding environment, for example, near ports or in shallow water.

The classic multitarget trackers [9, 10, 40] assume that the background clutter is homogeneously distributed over the surveillance region and that the clutter distribution is known a priori. However, in practical scenarios, false alarms are often non-uniformly distributed in the measurement space with an unknown distribution. The estimation of spatial clutter statistics from a number of scans in the presence of environment-induced caused noisy background is a crucial step in target tracking with measurement origin uncertainty [92]. In the literature, multiple algorithms are available to simultaneously estimate the unknown non-homogeneous spatial clutter distribution parameters along with target states [92, 93, 94, 95].

The clutter background estimation methods in the literature can be broadly divided into two categories: 1) track-oriented and 2) measurement-oriented. The track-oriented methods [93] assume that the clutter is homogeneously distributed spatially inside a certain region, e.g., a track validation gate. In track-oriented methods, the size of the area of interest is highly dependent on track parameters such as the innovation matrix and gate probability threshold, which may render clutter density estimation results unreliable. Furthermore, the estimated clutter densities for the same measurement location may differ for different tracks [96]. Also, the outputs of all these clutter map estimators may be discontinuous and block-structured due to the partitioning operation over the surveillance space [97].

The measurement-oriented methods estimate the clutter spatial intensity over the whole measurement space based on the measurement information. Clutter map is commonly used in clutter estimation algorithms [92, 98]. One solution is to average the number of detections over multiple frames, which results in a biased estimate of the inverse of the clutter intensity [92]. By taking advantage of the spatial and

temporal characteristics of the point process separately, both the spatial clutter map estimator and the temporal clutter map estimator can provide an unbiased estimate of the inverse of the clutter density [92, 99].

In [94, 95, 100, 101], the non-homogeneous spatial clutter intensity over the measurement space is estimated with an approximate Bayesian estimator based on the RFS theory [102]. By building a clutter generator set using the non-homogeneous Poisson process (NHPP) in addition to the sets of targets and measurements, the clutter density estimation problem is transformed into estimating the spatial intensity of the clutter generator [94, 95, 100, 101].

To represent the variation in the Poisson intensity function in space or time, another stochastic process called Cox process can be utilized. In this paper, the log-Gaussian Cox process (LGCP) [48], where the logarithm of the stochastic intensity function is a Gaussian process (GP), is utilized to estimate the environment-induced structured clutter spatial intensity over the whole measurement space. By integrating the clutter estimator with a multitarget tracker, the combination of target-originated detections and false alarms is handled properly under a data association mechanism.

Compared with the track-oriented clutter estimator [93], the LGCP-based estimation method can provide the clutter density over the whole measurement space. Further, a dynamic evolution model for the clutter generator as in [94, 95, 100, 101] need not be assumed here.

In this paper, we focus on tracking multiple divers with inter-target dependency and environmental influences. The paper is organized as follows: In Section 3.3, the modified force-based motion model for underwater divers that factors in the interactions between divers and the influence of non-stationary water flow is presented. In

Section 3.4, the basic framework of the GM-PHD filter and derivation of the GM-DDM-PHD filter are presented. In Section 3.5, we first review the concepts of the Gaussian process and the LGCP, and then present a combination of the proposed GM-DDM-PHD tracker with the LGCP-based clutter estimator to handle structured clutter. The PCRLB for the multiple diver tracking problem with inter-target interactions with non-stationary water flow is derived in Section 3.6. Simulation results are presented in Section 3.7, while conclusions are discussed in Section 3.8.

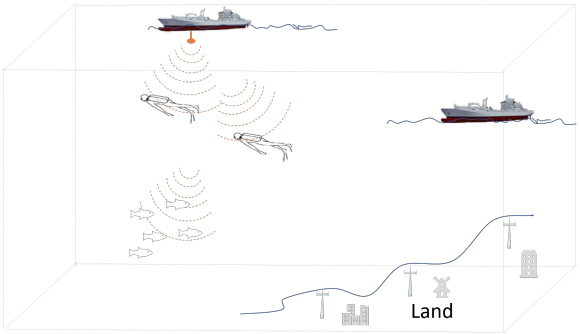

Figure 3.1: Diver tracking using a shipborne sonar

3.3 Force-Based Modeling of Diver Dynamics

In most existing diver trackers, it is assumed that the target motion model is linear and modeled by [26, 27, 28]

$$\boldsymbol{x}_k = F\boldsymbol{x}_{k-1} + G\boldsymbol{\omega}_{k-1} \tag{3.1}$$

where $\boldsymbol{x}_k = [x_k, \dot{x}_k, y_k, \dot{y}_k]'$ is a column vector with the diver's position and velocity at time instant k, F is the state transition matrix across two consecutive time instants, $\boldsymbol{\omega}_{k-1}$ is the process noise assumed to be the model input to control the evolution of

target state $\boldsymbol{x}_{k-1}$ and G is the noise gain. To model the uncertainties in the diver's motion caused by the external environment, the process noise is usually assumed to be Gaussian-distributed with zero mean and a known fixed covariance matrix [103]. However, in practical underwater scenarios, the kinematic state of divers is affected by external factors including fluid dynamics (e.g., flow speed and direction) and the movement of other neighboring divers.

To incorporate the influence of the surrounding environment on the process model, the DDM model is presented here based on the concept of SFM [47, 104]. The SFM can be used to describe the kinematic behavior of human targets [8, 86, 104]. In the social force models in [8, 86, 104], the interaction among targets and that between targets and obstacles in that environment are considered. However, the underwater diver tracking problem is more complex and challenging due to the existence of water flow. Even in a static underwater environment, the fluid drag force on a target moving through water is larger than that exerted by the air on an airborne target because of the higher water absolute viscosity [105]. The diver dynamic movements will be complex when the water around the target moves with a non-zero speed in a certain direction. Thus, the model input parameter should not only consider the forces from the neighboring targets but also the fluid force that is dependent on target size and the relative velocity between the diver and water flow around the diver. As shown in Figure 4.1, divers t_i and t_j are traveling against the water flow as a group at time $k-1$. For simplicity, the time index $k-1$ is omitted in the following unless explicitly needed. Let $\bar{\boldsymbol{v}}_i$ be the desired velocity of the target, $\boldsymbol{v}_w$ the velocity of water flow, $\boldsymbol{\mathcal{F}}_{ji}^{I}$ the interaction force exerted by t_j on t_i, which is related to the distance between targets. In contrast, $\boldsymbol{\mathcal{F}}_{i}^{w}$ is the fluid force dependent on both the relative velocity $\tilde{\boldsymbol{v}}_i$

between the target and the water flow and the target size.

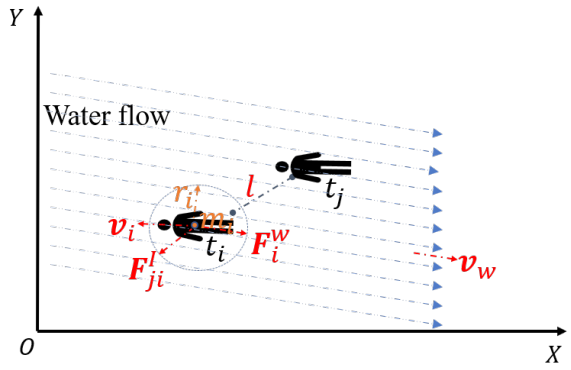

Figure 3.2: External forces on moving divers

In the proposed DDM, the main forces that influence the motion of a diver are given as follows: First, the model assumes that a human diver target t_i tends to travel through water with a certain desired velocity $\bar{\boldsymbol{v}}_i$ or to reach a certain destination. Therefore, the target has to adapt the actual velocity $\boldsymbol{v}_i$ to the desired one within a certain relaxation time τ_i. This personal motivation force $\boldsymbol{\mathcal{F}}_i^t$ can be represented by [104]

$$\boldsymbol{\mathcal{F}}_i^t = m_i \frac{\bar{\boldsymbol{v}}_i - \boldsymbol{v}_i}{\tau_i}, \tag{3.2}$$

where m_i is the mass of the target.

The divers in a group usually tend to follow one another but try to avoid collisions. The repulsion force $\boldsymbol{\mathcal{F}}_{ji}^r$ and the attraction force $\boldsymbol{\mathcal{F}}_{ji}^a$ are included in the interaction force $\boldsymbol{\mathcal{F}}_{ji}^I$. When two targets approach each other but to try to avoid collision, the repulsion force between them will become larger. The attraction force becomes smaller when two targets try to move apart in order to keep them as a group. The repulsion force is opposite to the attraction force and ensures that the targets maintain a safe distance in a group. The repulsion force and attraction force from t_j to t_i are

respectively given by [86]

$$\boldsymbol{\mathcal{F}}^{r}_{ji} = p_j \alpha_r \exp\left(\frac{r^l_{ji} - d^l_{ji}}{b}\right) \mathbf{n}_{ji}, \tag{3.3}$$

$$\boldsymbol{\mathcal{F}}^{a}_{ji} = p_j \alpha_a \exp\left(-\frac{r^l_{ji} - d^l_{ji}}{b}\right) \mathbf{n}_{ji}, \tag{3.4}$$

where p_j is the weight of the force from other targets, α_r and α_a are the magnitude parameters of the respectively exerted forces, b is the range boundary parameter of the social force, d^l_{ji} is the Euclidean distance between diver t_j and t_j along path l assuming that the radius of the influence of a diver is r^l_i, and $r^l_{ji} = r^l_i + r^l_j$. The unit vector depicting the force direction from t_j to t_i is defined as $\mathbf{n}_{ji}$. Also, the interaction force will act, if and only if d^l_{ji} is smaller than the empirically predefined threshold $\mathrm{Th_d}$. Otherwise, the diver will reach a non-interaction state, where only $\boldsymbol{\mathcal{F}}^t_i$ and $\boldsymbol{\mathcal{F}}^w_i$ exist.

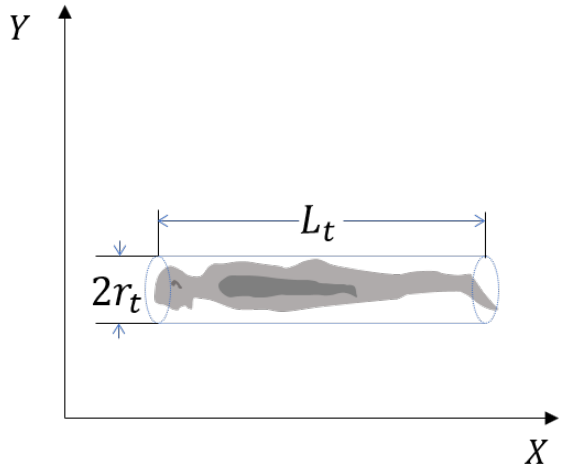

Figure 3.3: Cylindrical model of human body

In underwater environments, the fluid force on divers always exists. In contrast,

in air or space environment, the force exerted by air may or may not exist (or be significant) depending on the altitude and air density. When a diver moves against the water flow, the fluid force will act as a drag force to impede the movement of the diver. However, the water flow will accelerate a diver when the diver moves along the direction of the water flow. In addition, the water flow will divert the diver away from the intended course due to the lateral fluid force. The study of the fluid force on swimmers is, however, a very challenging subject area [106]. By taking advantage of computational fluid dynamics (CFD) and particle image velocimetry (PIV) techniques, a number of approaches have been proposed in the literature [106, 107, 108]. Also, 3D mapping of swimmers using a laser scanner has been carried out to obtain high-resolution images of the human body and to accurately simulate flow dynamics [109].

In this paper, we assume that divers move horizontally [28] in a slowly time-varying underwater environment. When the drivers try to speed through water, they will stretch out their bodies instead of rolling up to reduce the resistance due to water flow. This is because the total fluid force on the body is mainly affected by the body trunk. Consequently, a homogeneous cylindrical model of the human body that represents a flat-lying posture is adopted in this paper as depicted in Figure 3.3.

The hydrodynamic force may act as a drag force or drive force, which is dependent on the water with a magnitude proportional to water density ρ and the square of the target-to-flow relative velocity $\tilde{\boldsymbol{v}}_i$. The fluid force on a target is given by [110]

$$\boldsymbol{\mathcal{F}}_i^w = 0.5\rho C_D \tilde{v}_i^2 S \mathbf{n}_{\tilde{\boldsymbol{v}}_i} \quad \text{with} \quad \mathbf{n}_{\tilde{\boldsymbol{v}}_i} = \frac{1}{|\tilde{v}_i|}\tilde{\boldsymbol{v}}_i, \tag{3.5}$$

where C_D is referred to as the hydrodynamic force coefficient, $\tilde{v}_i$ is the relative speed

and the reference area S is defined as the maximum cross-sectional area normal to the direction of $\tilde{\boldsymbol{v}}_i$.

According to Newtonian dynamics, the motion change from all the above mentioned forces is given by

$$m_i \bar{\boldsymbol{w}}_{k-1,i} = \boldsymbol{\mathcal{F}}^t_{k-1,i} + \boldsymbol{\mathcal{F}}^w_{k-1,i} + \sum_{j=1, j\neq i}^{J} \boldsymbol{\mathcal{F}}^I_{k-1,ji}, \tag{3.6}$$

where $\bar{\boldsymbol{w}}_{k-1}$ is the exerted force induced acceleration matrix. In the presence of the external forces, it is impractical to use a simple Gaussian noise component to model the uncertainties due to neighboring divers and the water flow fluid force. Hence, the original dynamic model is expanded into a new DDM by incorporating the environmental forces as

$$\begin{aligned} \boldsymbol{x}_k &= F\boldsymbol{x}_{k-1} + G(\bar{\boldsymbol{w}}_{k-1} + \boldsymbol{\omega}_{k-1}) \\ &= f(x_{k-1}, \bar{\boldsymbol{w}}_{k-1}) + G\boldsymbol{\omega}_{k-1} \end{aligned} \tag{3.7}$$

.

One can note that the forces exerted on each target are integrated into (3.7) as an input component, and the new DDM can provide more accurate state prediction than the standard constant velocity motion model [82] in the presence of complex interactions. The DDM reduces to a standard constant velocity motion model when $\bar{\boldsymbol{w}}_{k-1} = 0$.

3.3.1 Measurement Model

An active sonar usually provides measurements in polar coordinates (i.e., in bearing and range). Coordinate conversion is required in most trackers because the kinematic states are better modeled in Cartesian space. For simplicity, we assume that the sonar sensor can provide the position of scattering points directly as

$$\boldsymbol{z}_k = \boldsymbol{H}\boldsymbol{x}_k^{\text{pos}} + \boldsymbol{v}_k, \tag{3.8}$$

where $\boldsymbol{H}$ is a 2×2 transition identity matrix, $\boldsymbol{x}_k^{\text{pos}} = [x_k, y_k]'$ is the position of the target, $\boldsymbol{v}_k$ is a 2×1 Gaussian noise vector denoted by $\boldsymbol{v}_k \sim N(0, R_k)$ and $R_k = \text{diag}([\sigma_x^2\ \sigma_y^2])$.

Assume that the probability of detection p_d of each target is less than unity. Then, the target-originated measurement vector is denoted by $\{z_k^i\}$ when the target is detected or $\varnothing$ when the target is missed. Also, false alarms are generated randomly over the surveillance area with their number being Poisson-distributed with a known parameter $\lambda(\boldsymbol{x}^{\text{pos}})$.

As mentioned before, $\boldsymbol{x}_k$ and $\boldsymbol{z}_k$ denote the target state vector and measurement vector that may consist of target-originated detections and/or false alarms. In a scenario with N_k targets in the k-th frame with states $\boldsymbol{x}_k^1$, $\boldsymbol{x}_k^2$, …,$\boldsymbol{x}_k^{N_k}$, we have M_k detections $\boldsymbol{z}_k^1$, $\boldsymbol{z}_k^2$,…, $\boldsymbol{z}_k^{M_k}$. The random finite sets for the collections of the unknown number of targets and observations at time k can therefore respectively be given by

$$\text{X}_k = \{\boldsymbol{x}_k^1, \boldsymbol{x}_k^2, \ldots, \boldsymbol{x}_k^{N_k}\} \tag{3.9}$$

and

$$\mathrm{Z}_k = \{\boldsymbol{z}_k^1, \boldsymbol{z}_k^2, \ldots, \boldsymbol{z}_k^{M_k}\}. \tag{3.10}$$

3.4 GM-DDM-PHD Filter

To track a variable number of unknown targets with clutter detections, the PHD filter can be used because of its low computational complexity and reliable tracking performance [9, 10].

In this Section, the standard PHD filter is reviewed first. Then, the proposed DDM is integrated into the PHD filter within the Gaussian-mixture implementation framework [10] to develop the GM-DDM-PHD tracker for divers.

3.4.1 PHD Filter

The classic Bayesian formulation within a fixed dimensional space cannot handle the case of the unknown time-varying number of targets. The random-set filtering approach using the Finite set statistics (FISST) theory, with a flexible set space can, however, estimate the frame-dependent number of targets. As an effective implementation of the RFS theory, the PHD filter has been applied to multitarget tracking problem because of the set integral-free calculations in the recursive propagation of the first moment of the multi-object posterior, which is called the intensity function of PHD [111].

Denote by $f_{k|k-1}(\mathrm{X}_k|\mathrm{X}_{k-1})$ and $g_k(\mathrm{Z}_k|\mathrm{X}_k)$ the multitarget transition density and the likelihood function, respectively. Thus, the optimal Bayesian recursive formulas

within the FISST framework are given by

$$p_{k|k-1}(\mathrm{X}_k|\mathrm{Z}_{1:k-1}) = \int f_{k|k-1}(\mathrm{X}_k|\mathrm{X}) p_{k-1}(\mathrm{X}|\mathrm{Z}_{1:k-1}) \mu_s(\delta \mathrm{X}) \tag{3.11}$$

and

$$p_k(\mathrm{X}_k|\mathrm{Z}_{1:k}) = \frac{g_k(\mathrm{Z}_k|\mathrm{X}_k) p_{k|k-1}(\mathrm{X}_k|\mathrm{Z}_{1:k})}{\int g_k(\mathrm{Z}_k|\mathrm{X}) p_{k|k-1}(\mathrm{X}|\mathrm{Z}_{1:k-1}) \mu_s(\delta \mathrm{X})}, \tag{3.12}$$

where $p_{k|k-1}(\mathrm{X}_k|\mathrm{Z}_{1:k-1})$ and $p_k(\mathrm{X}_k|\mathrm{Z}_{1:k})$ are the multi-target predicted and posterior distributions, respectively.

To avoid the intractable implementation of the set integral in (3.11) and (3.12) and to reduce the computational complexity, the PHD filter, a first moment approximation of the recursion is proposed in [111], and the general derivations of the PHD filter are summarized by

$$\begin{aligned} D_{k|k-1}(\boldsymbol{x}) &= \int p_s f_{k|k-1}(\boldsymbol{x}|\boldsymbol{\zeta}) D_{k-1}(\boldsymbol{\zeta}) d\boldsymbol{\zeta} \\ &\quad + \int \beta_{k|k-1}(\boldsymbol{x}|\boldsymbol{\zeta}) D_{k-1}(\boldsymbol{\zeta}) d\boldsymbol{\zeta} + \gamma_k(\boldsymbol{x}), \\ D_k(\boldsymbol{x}) &= [1 - p_d]\, D_{k|k-1}(\boldsymbol{x}) \\ &\quad + \sum_{\boldsymbol{z} \in \mathrm{Z}_k} \frac{p_d g_k(\boldsymbol{z}|\boldsymbol{x}) D_{k|k-1}(\boldsymbol{x})}{\lambda(\boldsymbol{z}) + \int p_d g_k(\boldsymbol{z}|\boldsymbol{\xi}) D_{k|k-1}(\boldsymbol{\xi})}, \end{aligned} \tag{3.13}$$

where the p_s is the survival probability of a target, $\beta_{k|k-1}(\cdot|\boldsymbol{\zeta})$ is the intensity function of the spawned RFS set $B_{k|k-1}(\boldsymbol{\zeta})$ from a target at time k, $\gamma_k(\cdot)$ is the intensity function of the possible RFS set Γ_k of newborn targets at time k, and $\lambda(\boldsymbol{z})$ is the clutter intensity. To focus on the external disturbances stimulating the targets and the influence of uncertain structured false alarms, we assume that p_d and p_s are constant and known a priori here. Since the number of target within the surveillance

is unknown and time-varying, the estimated cardinality of the targets of interests Ω is given by

$$\hat{N}_k = \int_{\Omega} D_k(\boldsymbol{x}_k|\mathrm{Z}^k)d\boldsymbol{x}_k. \tag{3.14}$$

The PHD filter recursion avoids the combinational complexity of explicit data association between measurements and tracks that is carried out in explicit association based methods such as the MHT [4] and the JPDA [40]. However, no closed-form for the PHD filter can be obtained due to the multiple integrals. Solutions for the PHD filter based on Sequential Monte Carlo (SMC) and Gaussian-mixture techniques are available, resulting in the SMC-PHD filter [9] and the GM-PHD filter [10], respectively. In SMC-PHD filter, the posterior intensity is represented by a number of particles with various weights. The state estimates are extracted from those particles using specially designed clustering techniques. The SMC-PHD filter suffers from high computational complexity and unstable state extraction performance when the number of clusters within the posterior intensity differs from the cardinality of targets [9, 10]. To reduce of effects of particle degeneracy [112], resampling is an essential component in SMC techniques [113]. For the tracking problem here, the GM-PHD is adopted because of its relatively low computational load and the flexibility to incorporate the new DDM and the proposed online non-homogeneous clutter estimator to improve the robustness of the modified PHD filter in the presence of unknown but non-homogeneous clutter.

3.4.2 GM-PHD Filter with Diver Dynamic Model

Similar to Gaussian sum filter [114], the GM-PHD filter is derived by approximating the posterior PHD intensity with Gaussian components under certain linear Gaussian

assumptions [10]. By integrating the DDM (3.7) into the GM-PHD predictive step, uncertain disturbances from other targets and water flow are incorporated into the Bayesian framework. The resulting GM-DDM-PHD filter does not natively maintain target identity over time. To maintain track identity, a Gaussian tag approach is utilized and the label of each Gaussian component is propagated with associated mean and covariance. Denote by $\{\mathcal{T}^i_{k-1}, w^i_{k-1}, \bar{\boldsymbol{x}}^i_{k-1}, \boldsymbol{P}^i_{k-1}\}$ the set of Gaussian components at time $k-1$, where $\mathcal{T}^i_{k-1}$ is tag of i-th Gaussian component while $\bar{\boldsymbol{x}}^i_{k-1}$, $\boldsymbol{P}^i_{k-1}$ are the mean and covariance matrix for the i-th Gaussian component, respectively. Also, w^i_{k-1} is the corresponding weight of each Gaussian component. The posterior intensity $D_{k-1}(\boldsymbol{x})$ of PHD filter at time $k-1$ is represented by a mixture of Gaussian components as

$$D_{k-1}(\boldsymbol{x}) = \sum_{i=1}^{I_{k-1}} w^i_{k-1}\mathcal{N}(\boldsymbol{x}; \bar{\boldsymbol{x}}^i_{k-1}, \boldsymbol{P}^i_{k-1}), \tag{3.15}$$

where $\mathcal{N}(\cdot; \bar{\boldsymbol{x}}, \boldsymbol{P})$ is Gaussian distribution with mean $\bar{\boldsymbol{x}}$ and covariance $\boldsymbol{P}$.

For the diver tracking problem here, we assume that no new targets can be spawned by existing ones, which is a reasonable assumption in diver tracking problems. With the new DDM presented in (3.7), the predicted intensity at time k is written as

$$D_{k|k-1}(\boldsymbol{x}) = D_{s,k|k-1}(\boldsymbol{x}) + \gamma_k(\boldsymbol{x}), \tag{3.16}$$

where

$$D_{s,k|k-1}(\boldsymbol{x}) = \sum_{j=1}^{J_{k-1}} w^{(j)}_{k|k-1}\mathcal{N}(\boldsymbol{x}; \bar{\boldsymbol{x}}^{(j)}_{s,k|k-1}, \boldsymbol{P}^{(j)}_{s,k|k-1}), \tag{3.17}$$

$$\gamma_k(\boldsymbol{x}) = \sum_{j=1}^{J_{\gamma,k}} w^{(j)}_{\gamma,k}\mathcal{N}(\boldsymbol{x}; \bar{\boldsymbol{x}}^{(j)}_{\gamma,k}, \boldsymbol{P}^{(j)}_{\gamma,k}) \tag{3.18}$$

with $w_{k|k-1} = p_s w_{k-1}$. Since the target states are not independent of one another and are influenced by the fluid force, the above force-based model is adopted in the prediction step of the GM-PHD filter instead of using the standard model in [10]. Thus, the predicted mean and the covariance of each Gaussian component with tag $\mathcal{T}_{k-1}$ are calculated and propagated based on the proposed DDM (3.7).

Consider a representative scenario where two divers traveling underwater at the k-th frame with two Gaussian components $\{\mathcal{T}^i_{k-1}, w^i_{k-1}, \bar{\boldsymbol{x}}^i_{k-1}, \boldsymbol{P}^i_{k-1}\}$, $i = 1, 2$ being used to represent their states. Before the target states can be predicted, all the forces on each component need to be calculated separately based on the force models. If the distance d^l_{12}, $l = 1$ between these two tagged components is greater than the empirically found threshold $\mathrm{Th_d}$, these two components with $\mathcal{T}_1$ and $\mathcal{T}_2$ are free of the interaction force. On the other hand, their states will be affected by the distance-dependent attraction and repulsion forces between each other. Also, the fluid force from the water flow on each tagged component must be taken into account. The relative velocity between the water flow and the Gaussian component with $\mathcal{T}_i$, $i = 1, 2$ is a vital factor because the hydrodynamic force is proportional to the square of the local speed. Then taking those forces as inputs, the states of all the Gaussian components are predicted to the next time step based on the new dynamic model (3.7).

Since the kinematic behaviors of divers are correlated with each other, a stacked vector [115, 116] is adopted here to implement the joint evolution of the Gaussian components. Assume that there are N_{k-1} targets working in the surveillance area at time $k-1$, and let X_{k-1} denote the stacked state set containing the state $\boldsymbol{x}^{i,n}_{k-1}$, which represents the state vector of the i-th Gaussian component of target n, where

$i = 1, \ldots, I_{k-1}$ and $n = 1, \ldots, N_{k-1}$. Given by (3.7), the propagation of X_{k-1} can be written as

$$\mathrm{X}_k = \boldsymbol{F}\mathrm{X}_{k-1} + \boldsymbol{G}(\bar{\boldsymbol{W}}_{k-1} + \boldsymbol{W}_{\boldsymbol{k-1}}) \tag{3.19}$$

where

$$\boldsymbol{F} = \mathrm{diag}\{F^{1,1}, \ldots, F^{1,N_{k-1}}, \ldots, F^{I_{k-1},1}, \ldots, F^{I_{k-1},N_{k-1}}\}, \tag{3.20}$$

$$\boldsymbol{G} = \mathrm{diag}\{G^{1,1}, \ldots, G^{1,N_{k-1}}, \ldots, G^{I_{k-1},1}, \ldots, G^{I_{k-1},N_{k-1}}\}, \tag{3.21}$$

$$\bar{\boldsymbol{W}}_k = [\bar{\boldsymbol{w}}_{k-1}^{1,1}, \ldots, \bar{\boldsymbol{w}}_{k-1}^{1,N_{k-1}}, \ldots, \bar{\boldsymbol{w}}_{k-1}^{I_{k-1},1}, \ldots, \bar{\boldsymbol{w}}_{k-1}^{I_{k-1},N_{k-1}}]', \tag{3.22}$$

$$\boldsymbol{W}_{k-1} = [\boldsymbol{w}_{k-1}^{1,1}, \ldots, \boldsymbol{w}_{k-1}^{1,N_{k-1}}, \ldots, \boldsymbol{w}_{k-1}^{I_{k-1},1}, \ldots, \boldsymbol{w}_{k-1}^{I_{k-1},N_{k-1}}]'. \tag{3.23}$$

With ΔT denoting the sampling interval of sonar sensor, one has

$$F^{i,n} = \begin{bmatrix} 1 & \Delta T & 0 & 0 \\ 0 & 1 & 0 & 0 \\ 0 & 0 & 1 & \Delta T \\ 0 & 0 & 0 & 1 \end{bmatrix}, \quad G^{i,n} = \begin{bmatrix} \Delta T^2/2 & 0 \\ \Delta T & 0 \\ 0 & \Delta T^2/2 \\ 0 & \Delta T \end{bmatrix}, \tag{3.24}$$

where $\boldsymbol{w}_{k-1}^{i,n}$ is the Gaussian process noise with zero mean and covariance matrix $Q_{k-1}^{i,n}$. The stacked set of covariance is given by

$$\boldsymbol{Q}_{k-1} = \mathrm{diag}(Q_{k-1}^{1,1}, \ldots, Q_{k-1}^{1,N_{k-1}}, \ldots, Q_{k-1}^{I_{k-1},1}, \ldots, Q_{k-1}^{I_{k-1},N_{k-1}}). \tag{3.25}$$

To handle the target state evolution and the corresponding covariance matrix propagation within the GM framework, the unscented transform (UT) [62, 117] is utilized due to the high nonlinearity of the new diver motion model. The implementation of the PHD filter with UT technique is detailed in [10].

Therefore, the stacked sets of predicted and updated covariances can be respectively written as

$$\boldsymbol{P}_{k|k-1} = \text{diag}(P_{k|k-1}^{1,1}, \ldots, P_{k|k-1}^{1,N_{k-1}}, \ldots, P_{k|k-1}^{I_{k-1},1}, \ldots, P_{k|k-1}^{I_{k-1},N_{k-1}}) \tag{3.26}$$

and

$$\boldsymbol{P}_{k} = \text{diag}(P_{k}^{1,1}, \ldots, P_{k}^{1,N_{k}}, \ldots, P_{k}^{I_{k},1}, \ldots, P_{k}^{I_{k},N_{k}}). \tag{3.27}$$

To maintain the track ID within the proposed GM-DDM-PHD algorithm, the stacked ID set is written as

$$\boldsymbol{\mathcal{T}}_{k-1} = \left\{ \mathcal{T}_{k-1}^{*,1}, \ldots, \mathcal{T}_{k-1}^{*,N_{k-1}}, \ldots, \mathcal{T}_{k-1}^{*,1}, \ldots, \mathcal{T}_{k-1}^{*,N_{k-1}} \right\}, \tag{3.28}$$

where $\mathcal{T}_{k-1}^{*,n}$ is the tag of the n-th target. Multiple Gaussian components may be needed to represent one target state in (3.28). In the GM-DDM-PHD filter, the forces between the Gaussian components with the same ID are zero. Also, the weight $p_{k,ji}$ of the forces between the Gaussian components tagged with different IDs in (4.1) and (4.2) is required due to the uncertainty in target existence. In addition, the forces between two divers are inversely proportional to the distance between them [8]. Thus, we define

$$p_{k,ji} = \frac{w_k^{(j)}/d_{ji}}{\sum_{j=1}^{J} w_k^{(j)}/d_{ji}}, \tag{3.29}$$

where the weight $w_k^{(j)}$ of each Gaussian component in (3.15) is utilized to represent the intensity of target existence, which represents the expected number of targets originating from $\bar{\boldsymbol{x}}_k^{(j)}$ at time k.

Thus, the predicted intensity can be calculated according to (3.16) and the label

set is updated as

$$\boldsymbol{\mathcal{T}}_k = \boldsymbol{\mathcal{T}}_{k-1} \cup (\mathcal{T}_{\gamma,k}^1, \ldots, \mathcal{T}_{\gamma,k}^{J_{\gamma,k}}). \tag{3.30}$$

The posterior intensity at time k is given by

$$D_k(\boldsymbol{x}) = (1 - p_d) D_{k|k-1}(\boldsymbol{x}) + \sum_{\boldsymbol{z}^i \in \mathrm{Z}_k} D_{v,k}(\boldsymbol{x}; \boldsymbol{z}), \tag{3.31}$$

where

$$D_{v,k}(\boldsymbol{x}; \boldsymbol{z}) = \sum_{j=1}^{J_{k|k-1}} w_k^{(j)} \mathcal{N}(\boldsymbol{x}; \bar{\boldsymbol{x}}_k^{(j)}, \boldsymbol{P}_k^{(j)}), \tag{3.32}$$

$$w_k^{(j)} = \frac{p_d w_{k|k-1}^{(j)} q_{k|k-1}^{(j)}}{\lambda(\boldsymbol{z}) + p_d \sum_{l=1}^{J_{k|k-1}} w_{k|k-1}^{(j)} q_k^{(j)}}. \tag{3.33}$$

The updated state and the covariance can be calculated according to the equations in [10].

3.5 Non-homogeneous Clutter Estimation with GM-DDM-PHD Filter

In practical underwater surveillance scenarios, the false alarms are not necessarily uniformly distributed over the region of interest as assumed in the literature, because of the existence of non-stationary water flow, mammals and rough boundaries (e.g., ocean surface or bottom). As mentioned previously, LGCP is a Cox process using the Gaussian process to describe the variation in the intensity surface of the spatial point process. As an effective non-parametric approach to learn the regression function from training data, LCGP has the advantages of modeling flexibility and

relatively tractable moment properties [118]. To enhance the robustness of the proposed tracker in realistic underwater environments, a new LGCP-based method [48] is proposed and integrated with the GM-DDM-PHD filter in this paper to estimate the unknown structured spatial density distribution of clutter, which is assumed to be a non-homogeneous spatial Point point process here.

In this section, the Gaussian process is reviewed first. Then the LGCP with geo-distributed points and the combination of the GM-DDM-PHD filter and LGCP-based clutter background estimator are presented.

3.5.1 Review of Gaussian Process

A Gaussian process is commonly used to describe a distribution over functions [119]. To learn the variation in the intensity function of the Poisson point process over the surveillance area, the Gaussian process model is applied here.

A Gaussian process can be represented as a function $f(\mathrm{p})$ with random variables at input p with an arbitrary finite number of such $f(\mathrm{p_i})$, $i = 1, ..., n$ having a multidimensional Gaussian distribution [119]. A Gaussian process can be specified in terms of a mean $m(\mathrm{p})$ and the covariance function $k(\mathrm{p}, \mathrm{p}')$ of a practical process $f(\mathrm{p})$ given by

$$\begin{aligned} m(\mathrm{p}) &= \mathrm{E}[f(\mathrm{p})], \\ k(\mathrm{p}, \mathrm{p}') &= \mathrm{E}[(f(\mathrm{p}) - m(\mathrm{p}))(f(\mathrm{p}') - m(\mathrm{p}'))]. \end{aligned} \tag{3.34}$$

The joint distribution of a random finite collection of variables $f(\mathrm{p}_1), \cdots, f(\mathrm{p}_n)$ is

given by

$$\begin{pmatrix} f(\mathrm{p}_1) \\ \vdots \\ f(\mathrm{p}_n) \end{pmatrix} \sim \mathcal{N}\left(\begin{pmatrix} m(\mathrm{p}_1) \\ \vdots \\ m(\mathrm{p}_n) \end{pmatrix}, \begin{pmatrix} k(\mathrm{p}_1,\mathrm{p}_1) & \cdots & k(\mathrm{p}_1,\mathrm{p}_n) \\ \vdots & \ddots & \\ k(\mathrm{p}_n,\mathrm{p}_1) & & k(\mathrm{p}_n,\mathrm{p}_n) \end{pmatrix} \right). \tag{3.35}$$

In our case of spatial Gaussian processes, we have $\mathrm{p} = [x, y]'$ that corresponds to a spatial location [120].

3.5.2 Log-Gaussian Cox Model with Geo-distributed Sensor Detections

To model the non-homogenous spatial Poisson intensity of sensor detection points, a doubly-stochastic Poisson process called log-Gaussian Cox process is utilized here by assuming that the intensity function $\lambda(\mathrm{p})$ is a transformation of a random realization from a Gaussian process, i.e., $f(\mathrm{p}) = \log\lambda(\mathrm{p})$ [48, 121].

With a realization of such a process being a spatial point pattern $s = (s_1, ..., s_n)$, the corresponding likelihood of the unknown function f within a sonar surveillance region bounded by $S \subset \mathbb{R}^2$ is given by

$$p(s|f) = \exp \int_S \exp(f(s))ds + \sum_{i=1}^{n} f(s_i). \tag{3.36}$$

Note that the above likelihood function is computationally intractable because it involves the nontrivial integration over the exponential of a GP in (3.36). A computationally tractable grid-based approximation method assuming a locally constant intensity over each sub-region is proposed in [48]. The likelihood after discretizaion

is then given by

$$p(s|f) = \prod_{k=1}^{K} \text{Poisson}(n_k|\exp(f(\bar{\text{p}}_k))), \tag{3.37}$$

where $\bar{\text{p}}_k$ is the coordinate of the k-th sub-region of S and n_k is the number of data points falling in it.

3.5.3 GM-DDM-PHD with LGCP Structured Clutter Density Estimator

The log-Gaussian Cox model for sonar detections is proposed here. As previously mentioned, a single sensor detection is assumed to be disturbed by Gaussian noise, resulting location uncertainty over the corresponding sub-region s_k. The set of measurements are assumed to represent a GM distribution, so the number $\hat{n}_k$ of data points in sub-region s_k can be rewritten as

$$\hat{n}_k = \int_{s_k} \sum_{m=1}^{M_k} \varpi_m \mathcal{N}(\bar{\text{p}}_k, z_m, \hat{R}) ds. \tag{3.38}$$

In clutter intensity estimation, one challenge is to distinguish clutter detections from target-originated detections to avoid over-fitting to the intensity functions [6, 94]. In contrast to the classic clutter density estimators where target-originated detections incorrectly inflate the estimates, the estimator proposed here tries to statistically exclude target-originated detections with seamless integration into the GM-DDM-PHD filter.

GM-PHD is effective in tracking an unknown and time-varying number of targets in the presence of data association uncertainty, non-zero clutter, and non-unity detection probability. In GM-PHD, the weights $W = w_i, i = 1, ..., J_k$ of target state set

at time k are updated based on the sensor measurements set $Z = z_m, m = 1, ..., M_k$. Likewise, we can also derive the corresponding probability (weight) $\varpi_m, m = 1, ..., M_k$ that a measurement is a false alarm instead of arising from a real target. Note that there are two parts in the weight set of W, namely, predicted weights assuming no measurements and updated weights based on measurements. Letting $\tilde{w}_{dm}$ be the d-th updated weight from the m-th measurement, we have $\tilde{W} = \tilde{w}_{dm}, D = 1, ..., J_k - \bar{J}, m = 1, ..., M_k$, where $\bar{J}$ is the prior number of Gaussian birth terms.

The derivation of ϖ_i is then given by

$$\varpi_m = 1 - \sum_{m=1}^{M_k} \tilde{w}_{\cdot,m}. \tag{3.39}$$

Using (3.39) with (3.38), we get

$$\hat{n}_k = \int_{s_i} \sum_{m=1}^{M_k} \varpi_m \mathcal{N}(\bar{\mathrm{p}}_k, z_m, \hat{R}) ds. \tag{3.40}$$

Note that measurement origin ambiguity and sensor noise uncertainty are both considered and included in the derivation of $\hat{n}_k$.

3.6 PCRLB for Diver state Estimation

In this section, the PCRLB is derived to quantify the achievable estimation accuracy in a multi-driver tracking problem in the presence of false alarms, missed target-originated measurements and external forces exerted on the targets. The CRLB, given by the inverse of the Fisher information matrix (FIM), quantifies the achievable accuracy of any unbiased estimator for a specific parameter estimation problem

[82]. The PCRLB is used to evaluate the performance in dynamic state estimation problems.

Let $\hat{\mathrm{X}}_k(\mathrm{Z}_k)$ denote an unbiased estimate of X_k, which is a function of the measurement set Z_k. The lower bound on the mean square error (MSE) matrix is given by

$$\mathrm{E}\{[\hat{\mathrm{X}}_k(\mathrm{Z}_k)-\mathrm{X}_k][\hat{\mathrm{X}}_k(\mathrm{Z}_k)-\mathrm{X}_k]'\}\geq J(k)^{-1}, \tag{3.41}$$

where E represents the expectation operation and $'$ denotes transposition. The FIM at time k is given by

$$\begin{aligned} J(k+1) =&\mathrm{E}\{\Delta^{\mathrm{X}}_{\mathrm{X}}\ln\, p(\mathrm{Z},\mathrm{X})\}\\ =&J_{\mathrm{X}}(k+1)+J_{\mathrm{Z}}(k+1)\\ =&\Omega_k^{22}-\Omega_k^{12\prime}/(J_k+\Omega_k^{11})\Omega_k^{12}+J_{\mathrm{Z}}(k+1), \end{aligned} \tag{3.42}$$

where

$$\Omega_k^{11} =\mathrm{E}\left\{-\Delta^{\mathrm{X}_k}_{\mathrm{X}_k}\ln p(\mathrm{X}_{k+1}|\mathrm{X}_k)\right\}, \tag{3.43}$$

$$\Omega_k^{12} =\mathrm{E}\left\{-\Delta^{\mathrm{X}_{k+1}}_{\mathrm{X}_k}\ln p(\mathrm{X}_{k+1}|\mathrm{X}_k)\right\}, \tag{3.44}$$

$$\Omega_k^{22} =\mathrm{E}\left\{-\Delta^{\mathrm{X}_k}_{\mathrm{X}_{k+1}}\ln p(\mathrm{X}_{k+1}|\mathrm{X}_{k+1})\right\}, \tag{3.45}$$

$$J_{\mathrm{Z}}(k+1) =\mathrm{E}\left\{-\Delta^{\mathrm{X}_{k+1}}_{\mathrm{X}_{k+1}}\ln p(\mathrm{Z}_{k+1}|\mathrm{X}_{k+1})\right\}. \tag{3.46}$$

with the $\Delta^{\epsilon}_{\varrho}$ denoting partial derivative operation over ϵ and ϱ.

Substituting the new DDM model (3.19) for multiple divers into (3.43)–(4.61) and

after some manipulations, one has

$$J_X(k+1) = \left[\boldsymbol{Q}(k) + \boldsymbol{\Gamma}(k)J(k)\boldsymbol{\Gamma}(k)'\right]^{-1}, \tag{3.47}$$

where

$$\boldsymbol{\Gamma} = \begin{bmatrix} F_k^1 + G\frac{\partial \bar{\boldsymbol{w}}_k^1}{\partial \boldsymbol{x}_k^1} & G\frac{\partial \bar{\boldsymbol{w}}_k^1}{\partial \boldsymbol{x}_k^2} & \cdots & \cdots & G\frac{\partial \bar{\boldsymbol{w}}_k^1}{\partial \boldsymbol{x}_k^{N_k}} \\ G\frac{\partial \bar{\boldsymbol{w}}_k^2}{\partial \boldsymbol{x}_k^1} & F_k^2 + G\frac{\partial \bar{\boldsymbol{w}}_k^2}{\partial \boldsymbol{x}_k^2} & \cdots & \cdots & \cdots \\ \cdots & \cdots & \cdots & \cdots & \cdots \\ \cdots & \cdots & \cdots & \cdots & \cdots \\ G\frac{\partial \bar{\boldsymbol{w}}_k^{N_k}}{\partial \boldsymbol{x}_k^1} & \cdots & \cdots & \cdots & F_k^{N_k} + G\frac{\partial \bar{\boldsymbol{w}}_k^{N_k}}{\partial \boldsymbol{x}_k^{N_k}} \end{bmatrix}.$$

Note that the off-diagonal elements of $\boldsymbol{\Gamma}$ are not necessarily zero because of mutual dependence among targets and the target-environment interaction in the new force-based diver motion model.

3.7 Simulations

In this section, Monte Carlo simulation experiments with 100 trials are used to evaluate the performance of the proposed algorithm in two different scenarios with interactions, structured background clutter and a varying number of targets. To quantify performance, the root mean squared error (RMSE) of targets' position and velocity estimates, the optimal sub-pattern assignment (OSPA) metric and the PCRLB are used as performance metrics. The standard PHD filter [10] and the GM-SF-PHD filter [8] are used as the benchmark algorithms. Target-originated detections and false

alarms are independently generated over 100 Monte Carlo runs on the same target trajectories.

Table 3.1: Scenario parameters

Parameter	Value
Number of Monte Carlo runs	100
Number of frames	50
Sampling time ΔT (s)	1
Process noise (m^2/s^4)	2.5E−4
Target mass (kg)	80
Target size (m)	1.8 (Length)×0.15 (Radius)
Relaxation time τ (s)	$10\Delta T$
Intended destination (m)	[−405, 160]
Desired Speed $\bar{v}$ (m/s)	1.8
Force magnitude parameters α_a, α_r (N)	(10, 20)
Range parameter b of the force (m)	15
Radii influence parameter r of divers (m)	3
Water flow direction (degree)	30
Water flow speed (m/s)	0.5
Hydrodynamic force coefficient C_D	0.05
Water density ρ (kg/m^3)	997
Survival probability of target p_s	0.99

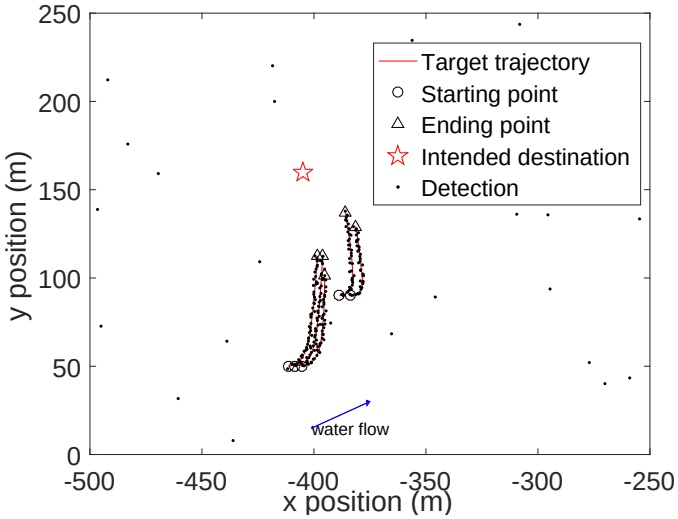

Figure 3.4: Target trajectories and measurements from one Monte Carlo trial

Scenario I: The surveillance region is $[-500, -250]$m and $[0, 250]$m in x and y directions, respectively. A stationary linear position-only sensor at $[0, 0]$m, generates the measurements. Five motion-dependent divers are within this area of interest, but with different starting and ending times. All these targets intend to move to a predefined location $[-405, 160]$m with the same desired speed at 1.8 m/s. Note that the velocities of the targets are actually different from each other and cannot be maintained at exactly 1.8 m/s due to the disturbances from the external environmental factors and the process noise. The two-dimensional homogeneous, isotropic water flow field is assumed with fixed known flow direction 30° at flow speed 0.5 m/s. The target detection probability is 0.98 and the false alarms are uniformly distributed in the surveillance region with a priori intensity 10^{-5} m^{-2}. The sensor measurement noise in the x and y directions are $\sigma_x = 0.667$m and $\sigma_y = 0.667$m, respectively. The other parameters are summarized in Table 3.1. Figure 3.4 shows the scenario including the true target trajectories, intended destination, water flow direction and the

sensor detections from one Monte Carlo trial.

Figures 3.5 and 3.6 show the RMSE of position and velocity estimates, respectively. The proposed GM-DDM-PHD filter outperforms the standard GM-PHD filter [10] and the GM-SFM-PHD filter [8]. By considering the complex interactions among targets and with water flow, an improved prediction model is utilized to calculate the likelihood function and a consistent covariance can be calculated based on the proposed DDM model for the better measurement-target association, which results in the better performance of the proposed GM-DDM-PHD filter compared with the standard GM-PHD. Further, the GM-SFM-PHD filter only considers the dependencies between targets without addressing the hydrodynamic forces. Thus, the GM-SFM-PHD performs well initially when targets appear and there is a maneuver to adjust the target's initial velocity to the intended velocity. However, after the targets' motions stabilize with a nearly constant velocity motion, the performance of the standard GM-PHD filter surpasses that of the GM-SFM-PHD due to the mismatch in the motion model in the prediction stage. In contrast, the proposed GM-DDM-PHD filter performs uniformly better at all times. The PCRLB for underwater divers tracking problem with inter-target and environmental dependencies is utilized to verify the performance of the proposed GM-DDM-PHD filter. It is noticed that the RMSE values obtained by the GM-DDM-PHD filter follow the trend of the PCRLB, demonstrating efficiency of the proposed tracker.

The Monte Carlo average of the OSPA distance is given in Figure 3.8, which shows that the proposed algorithm yields the smallest OSPA metric. Figure 3.7 shows the Monte Carlo average of the estimated number of targets and one can see that the proposed GM-DDM-PHD filter is almost free of false tracks except at the beginning

of the scenario. The other two filters yield lower expected averages of the estimated target cardinality, which is due to the improper target-measurement association based on the erroneous dependency-free covariance calculation. Table 3.2 shows the Monte Carlo average of the execution times for a single run in this simulation. One can see that the standard GM-PHD has the lowest computational load because of ignoring the external force calculations that are part of the other two algorithms. The GM-SFM-PHD filter, however, runs slower than the proposed GM-DDM-PHD algorithm due to inaccurate data association that results in additional false tracks.

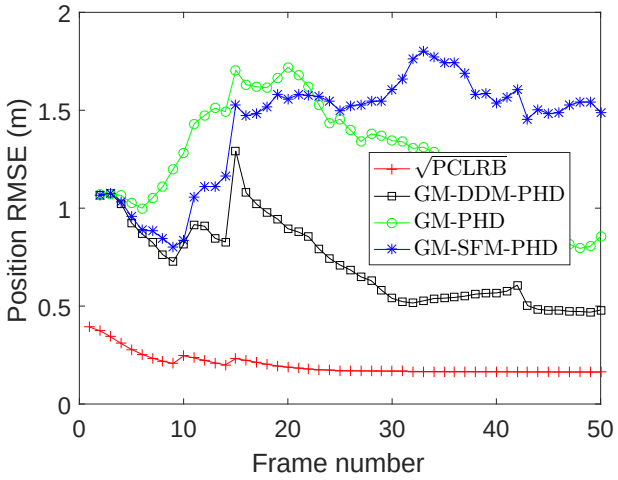

Figure 3.5: RMS position errors

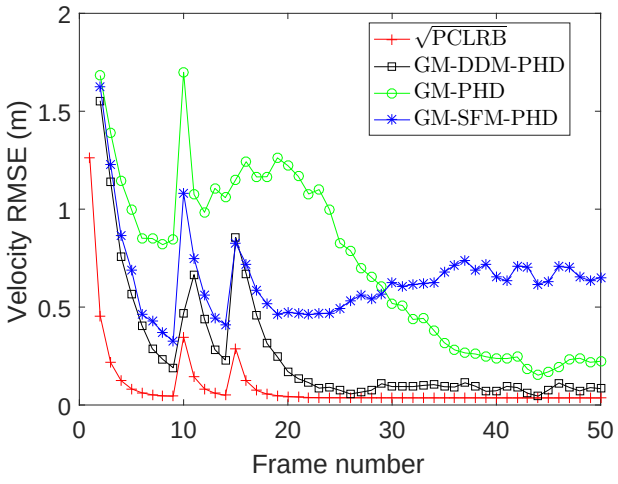

Figure 3.6: RMS velocity errors

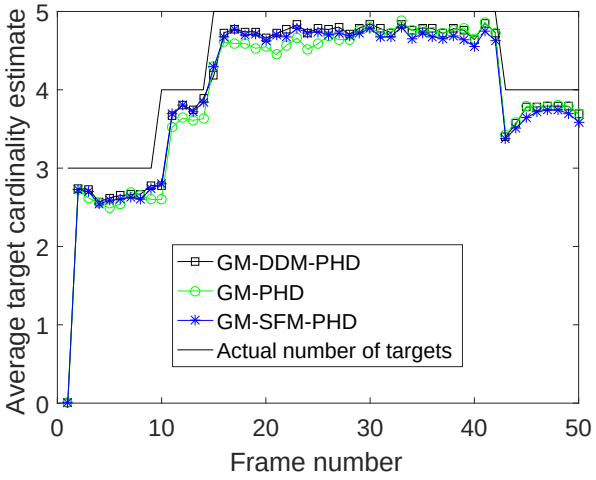

Figure 3.7: Number of targets

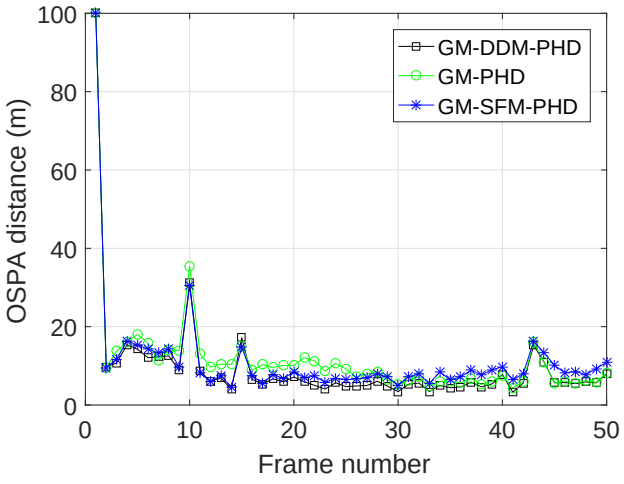

Figure 3.8: OSPA distance

Table 3.2: Average computation times from 100 Monte Carlo trials

Method	Time (s)
GM-PHD	0.22
GM-SFM-PHD	1.54
GM-DDM-PHD	0.95

Scenario II: To validate the performance of the GM-DDM-PHD filter with LGCP clutter density estimator, another simulation is implemented here. All the parameters are the same as in Scenario I except for the assumption about the clutter distribution. Here, a structured clutter background is considered with four additional dense clutter regions over the surveillance region. The false alarm rate in those dense clutter regions is 5E−3 m^{-2}. In addition, there is a background clutter generator over the whole area of interest with a clutter rate of 1E−5 m^{-2}. Figure 3.9 shows the scenario including the true target trajectories, the intended destination, the water flow direction, and

the sensor detections from one Monte Carlo trial. Note that three of the targets go through at least one of the dense clutter areas during the surveillance interval.

The results produced by the GM-DDM-PHD filter using the true spatial intensity of false alarms is used as the benchmark for comparison with the proposed method. Also, the Kernel density estimation (KDE) method proposed in [97] and the GM-DDM-PHD filter with a hypothesized spatial intensity of 1E−5 m^{-2} are implemented for comparison. As can be seen in Figures 3.10 and 3.11, all these methods yield almost the same performance in the terms of the position and velocity estimates RMSE values, which is in accordance with the observation that RMSE improvement due to clutter estimation is usually negligible [98]. This is because the RMSE is calculated only for those tracks that match actual targets trajectories.

From Figures 3.12 and 3.13, which show the cardinality estimates and the OSPA metrics, respectively, it can be observed that the LCGP-based method is superior to the KDE method and nearly matches value of the results obtained assuming true clutter spatial intensity, which shows the superiority and robustness of the proposed method in an underwater environment with state-dependent external forces on divers and unknown non-homogenous clutter background. Using the LGCP method, the proposed tracker can initialize tracks without any substantial delay and significantly reduce the number of false tracks. The clutter spatial intensity estimates obtained in different frames by the LGCP method and the KDE method from a single Monte Carlo run are shown in Figures 3.14 and 3.15, respectively. One can see that although those two methods can cluster the structured clutter background satisfactorily, the LGCP method provides better accuracy than the KDE method, resulting in better

target cardinality estimates. As a trade-off, the LGCP method has a higher computational complexity than the KDE method, as listed in Table 3.3. However, with the computational resources available today, the computational complexity is not a bottleneck and the improved estimation accuracy and reduced false track rate make the additional computational complexity worthwhile.

The simulations are implemented in MATLAB® 2016a on an Intel(R) Core(TM) i7 CPU with 32 GB RAM with parallel computing techniques being used for loops.

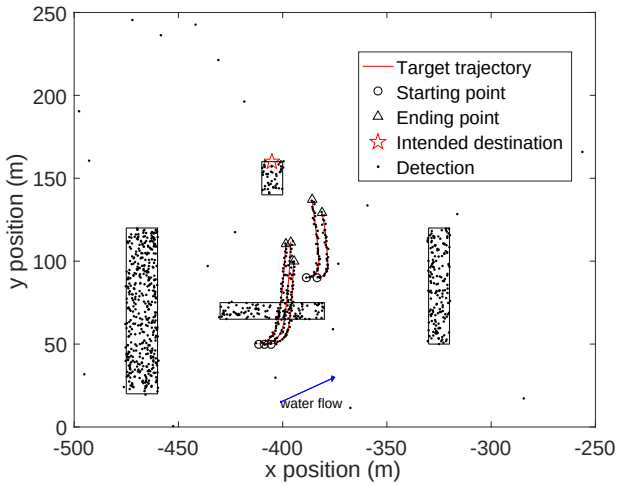

Figure 3.9: Target trajectories and all measurements from one Mont Carlo trial

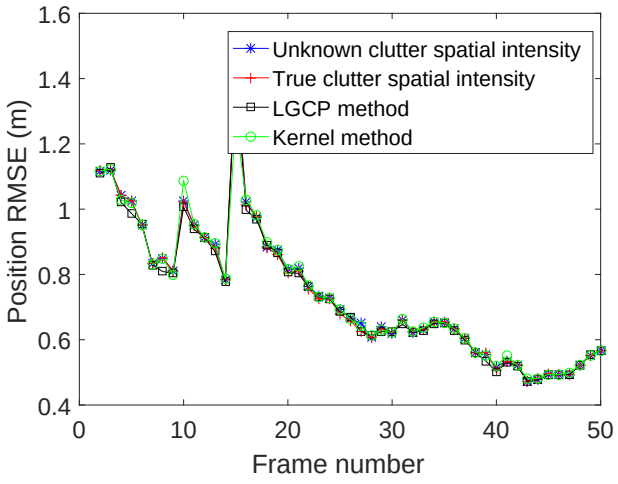

Figure 3.10: RMS position errors

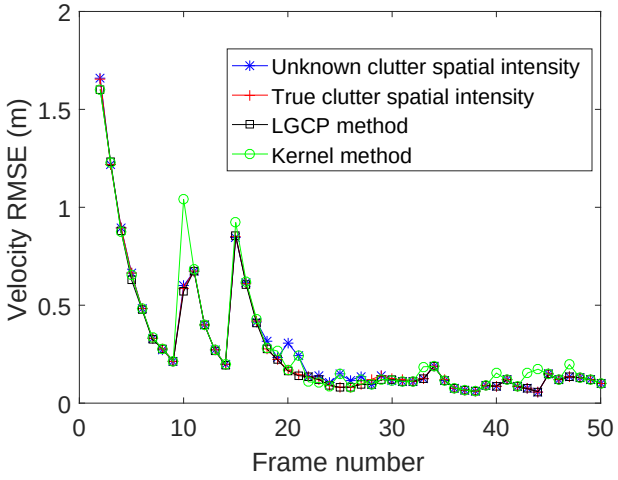

Figure 3.11: RMS velocity errors

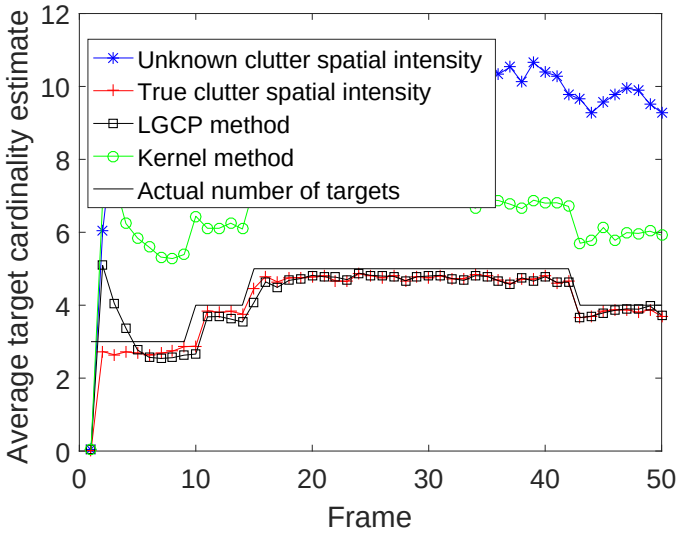

Figure 3.12: Number of targets

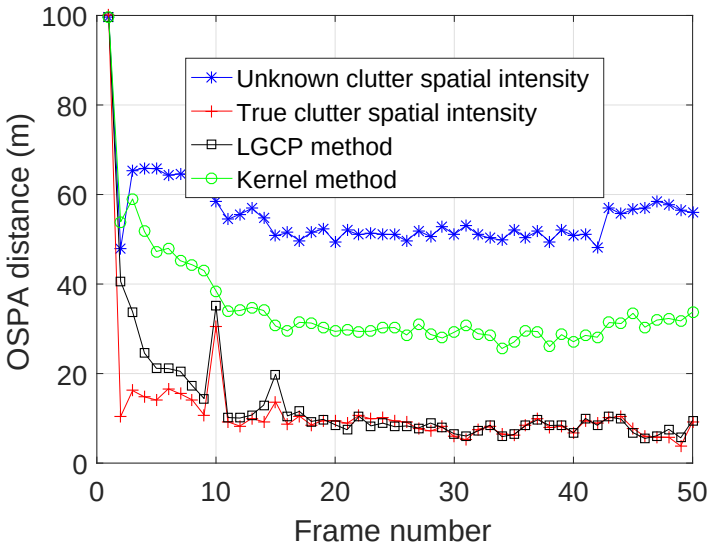

Figure 3.13: OSPA distance

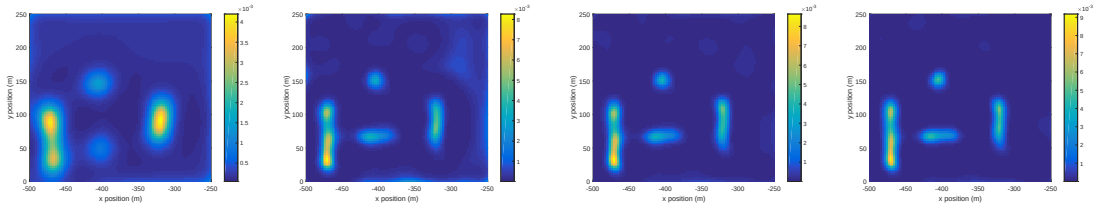

(a) 4th frame (b) 19th frame (c) 25th frame (d) 36th frame

Figure 3.14: Clutter intensity estimates from one Monte Carlo trial of LGCP method

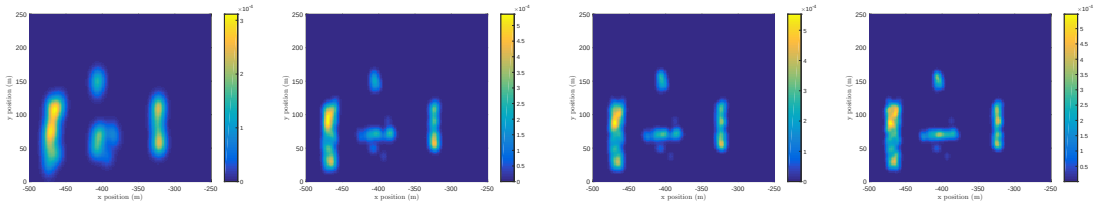

(e) 4th frame (f) 19th frame (g) 25th frame (h) 36th frame

Figure 3.15: Clutter intensity estimates from one Mont Carlo trial of KDE method

Table 3.3: Average computational time from 100 Monte Carlo trials

Method	Time (in s)
Unknown clutter background	65.95
Known clutter background	3.98
LGCP method	52.07
KDE method	34.62

3.8 Conclusions

A log-Gaussian Cox process clutter estimator and a force-based motion model were proposed in this paper for multiple diver tracking with motion dependencies among neighboring targets and interaction between targets and the underwater current in unknown structured clutter background. In the proposed DDM motion model, the

external forces exerted on a target by other targets and the environment are correctly factored in while building the likelihood function in the prediction step of the recursive filter. The LGCP method was integrated with the proposed GM-DDM-PHD filter to handle the practical problem of unknown non-homogenous clutter background with measurement-origin ambiguity, improving the performance of the algorithms. Simulations were carried out to evaluate the performance of the proposed method relative to the performance of existing algorithms and the theoretic PCRLB.

Chapter 4

Extended Target Tracking with Multipath Detections, Terrain-Constrained Motion Model and Clutter

4.1 Abstract

To address the problem of extended target tracking (ETT) with measurement-origin uncertainty in a multipath environment with clutter, a new generalized version of the standard probabilistic data association (PDA) filter, called MP-ET-PDA, based on random matrices (RM) is proposed in this paper. In the MP-ET-PDA filter, we assume that multipath detections and clutter are possible in the extended target tracking problem, which are prevalent in practical systems but barely addressed in

the literature. Further, a clustering-aided MP-ET-PDA algorithm with reduced computational complexity that makes use of the Variational Bayesian technique, called MP-ET-PDA-VB, is presented to provide near real-time processing capability in ETT problems with an uncertain multipath environment. In addition to using a constant velocity motion model, a new terrain-constrained motion model is presented for scenarios where terrain-following is required by motion-constrained autonomous vehicles.

The PCRLB, which quantifies the best possible accuracy in realistic ETT problems with multipath detections and measurement-origin uncertainty, is derived as the benchmark for performance evaluation. Simulations results demonstrate the improved performance of the proposed algorithms.

4.2 Introduction

With the increasing availability of high-resolution sensors (e.g., video camera, phased array radar, synthetic aperture sonar and LiDAR), the ETT problem, which involves the tracking of a target occupying more than one measurement resolution cell, has received attention recently [49, 50, 59, 122]. In the ETT literature, it is usually assumed that the detections are generated from the exterior of a target, and the models of rectangular, circular and other simple shapes are used to represent the appearance of a two-dimensional target [50, 123, 124]. The random matrices (RM) model for modeling extended target is introduced in [123] and used to approximate the contour of an ellipsoidal target [50, 51, 52, 53, 54, 55, 56] because of its ability to estimate both the kinematic state and the extent state simultaneously but independently [50, 59]. The multiple RM model is derived in [125, 126] to handle non-ellipsoidal targets. Further, the star-convex shaped target tracking is studied in [122, 127]. The GP, a

statistical model, is integrated into trackers to estimate and learn the boundary of an unknown target by defining the target extent as generating GP-based measurements [59, 128, 129]. The main contribution of the GP probabilistic model is that the algorithm can learn the locally observable part of the target extent without updating the shape estimate in a global manner [59]. However, the improved modeling capability of the GP method requires more parameters than those using simpler shape models (e.g., RM) [49]. The ETT problem becomes even more complex and challenging with measurement-origin uncertainty caused by false alarms and missed detections. In [51, 57, 58], the PHD algorithm is modified to track multiple extended targets in clutter. A generalized RM-based PDA filter is presented in [55] to handle ETT. The GP-PDA filter can jointly estimate the kinematic state and the physical extent state while suppressing the effects of false alarms.

However, in some ETT scenarios, the sensor may receive target-originated detections via multiple propagation modes (e.g., non-line-of-sight vs. line-of-sight) in constrained environments such as underwater, indoor and tunnels that are prone to generating indirect multipath measurements. Such multipath detections may render the above ET trackers that assume only a single propagation path ineffective. Point target (PT) trackers in the presence of multipath detections are presented in [37, 38, 130]. However, the trackers in [37, 38, 130] assume that at most one measurement can be generated by a target via each propagation path and thus cannot handle ETT scenarios with multiple target-originated detections via the same propagation path. To the best of our knowledge, the ETT problem with multipath detections has been discussed only in [43], where a two-level approach deals separately with measurement-origin uncertainty and multipath detections from extended targets. In

[43], such detections are treated as measurements from multiple pseudo-targets, which are then fed into the ET-PHD filter [131], which may result in loss of information between the two steps and thus degrade tracking performance. Also, the method in [43] does not yield target shape information, which may be crucial for accurate data association in ETT problems with measurement-origin uncertainty [59] as well as for target typing or classification.

In this paper, an RM-based PDA algorithm called MP-ET-PDA that estimates both the kinematic state and the target extent by explicitly handling MP-ET detections in clutter is developed to take advantage of the additional information in multi-path measurements. Due to the time-varying number of target-originated detections corresponding to different points on the target via the same path, the measurement-origin uncertainty and the complexity of the algorithm increase, but the performance of the tracker in terms of estimation accuracy and rejection of duplicate tracks are significantly improved by processing all measurements under the more general MD-ET assumption. In the proposed MP-ET-PDA tracker, the assumptions that a point target can only generate at most one detection via each propagation path [37, 38, 130] and that an extended target can generate multiple measurements through only one propagation path [51, 55, 57, 58, 128] are replaced with the assumption that MP-ET detections may be received by a high-resolution sensor. In MP-ET-PDA, all possible association events are enumerated to handle the possible MP-ET measurements from a single target. The maximum number of propagation paths and the expected number of target-originated detections from each path are assumed to be known as prior scenario parameters, which is incorporated into the recursive Bayesian framework. The MP-ET-PDA is a generalization of the PDA filter and reduces to the conventional

PDA algorithm with RM theory [125] when only one single path (SP) exists.

The computational complexity of MP-ET-PDA is higher than that of other extended target trackers due to the larger number of association events accounting for the uncertainty arising from a time-varying number of MP-ET detections and the measurement-origin uncertainty due to clutter. To mitigate this, a VB clustering-based MP-ET-PDA filter, called MP-ET-PDA-VB, is proposed in this paper as an extension of MP-ET-PDA that can satisfactorily maintain the accuracy in MD-ET tracking problems with a lower computational complexity. A clustering-aided algorithm is introduced in [132, 133] to deal with target occlusions in video tracking problems. Using this clustering technique, the measurements are labelled and divided into different groups that correspond to different targets. The key to the clustering-aided method is the assumption that the measurements generated by the same target are spatially close to one another [49]. In our paper, we assume that the MP-ET detections are independent of one another and that multiple measurements from the same target via a certain propagation path are spatially close to one another with a Gaussian distribution. Therefore, a GM can be utilized to model an MP-ET measurement set in this paper.

The proposed work is intended to track autonomous vehicles with obstacle avoidance (OA) [134, 135, 136, 137] that move in a confined space or follow the local terrain [138, 139]. In scenarios where the target is constrained by the surrounding environment, modifying the target dynamic model to take advantage of the local terrain information can improve the performance of the tracker [140]. This provides the motivation for the next contribution of this paper, namely terrain-constrained MD-ETT.

The SFM is often used to model the inter-target interactions or the interactions between targets and the environment. In [8, 104, 132], pedestrian motion is modeled using an SFM that considers the interactions between neighboring targets and the influence by the surrounding environment (e.g., obstacles, boundaries). In [90], a modified SFM is presented to model the movement of vehicles in ground target tracking scenarios. To deal with target motion constrained by the terrain, an SFM-based terrain constrained motion model (TCMM) is proposed and integrated into MD-ETT algorithms in this paper.

The paper is organized as follows: Section 4.3 presents the terrain constrained motion model by considering the interaction between the target and the terrain. In Section 4.4, the basic framework of the RM-PDA filter is introduced first and then the proposed MP-ET-PDA filter is derived for MP-ET. In Section 4.5, the clustering algorithm for computational complexity reduction is presented. The PCRLB for the ellipsoidal extended target tracking problem with multipath detections in clutter is derived in Section 4.6. Simulation results are presented in Section 4.7 while conclusions are discussed in Section 4.8.

4.3 Problem Formulation

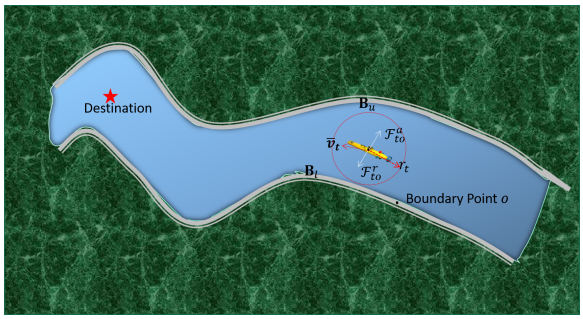

Figure 4.1: An illustrative scenario with an underwater vehicle traveling through confined space.

4.3.1 Terrain Constrained Motion Model

The basic idea behind the terrain constrained motion model is that the targets usually intend to reach a destination and try to avoid collision with obstacles in their way and the boundary of terrain [135, 136, 137]. The SFM is modified and applied here to model the interactions between an autonomous vehicle and the local terrain.

As shown in Figure 4.1, an autonomous vehicle is traveling through a confined space. For simplicity, the time index $k-1$ is omitted in the following unless explicitly needed. Let $\bar{\boldsymbol{v}}_t$ be the desired velocity of target t, $\boldsymbol{\mathcal{F}}^I_{to}$ the interaction force exerted on target t by an arbitrary point o located on terrain boundaries $(\mathbf{B_l}, \mathbf{B_u})$, which is determined by the distance between the target centroid and the boundary. As components of the interaction force, the repulsion and attraction forces by an arbitrary point o on the obstacle boundary are respectively given by

$$\boldsymbol{\mathcal{F}}^r_{to} = w_o \varrho_r \exp\left(\frac{r_t - d^l_{to}}{b}\right) \mathbf{n}_{to}, \tag{4.1}$$

$$\boldsymbol{\mathcal{F}}_{to}^{a} = w_o \varrho_a \exp\left(-\frac{r_t - d_{to}^{l}}{b}\right) \mathbf{n}_{to}, \tag{4.2}$$

where w_o is the weight of the force from single point o, ϱ_r and ϱ_a are the respective magnitude parameters of the exerted force, b is the range boundary parameter of the force, d_{to}^{l} is the Euclidean distance between target t and boundary point o and r_t is the minimum safety radius distance of a target. The unit vector depicting the force direction from a boundary point o to the target t is defined as $\mathbf{n}_{to}$.

Assume that autonomous vehicles usually intend to move with a certain speed $\bar{\boldsymbol{v}}_t$. Therefore, the motivation force $\boldsymbol{\mathcal{F}}^{t}$ is given by [104]

$$\boldsymbol{\mathcal{F}}^{t} = m_t \frac{\bar{\boldsymbol{v}}_t - \boldsymbol{v}_t}{\tau_t}. \tag{4.3}$$

where $\boldsymbol{v}_t$ is the actual speed of the target and τ_t is the relaxation time.

According to Newtonian dynamics, the motion change from all the above mentioned forces is given by

$$m\bar{\boldsymbol{w}}_{k-1} = \boldsymbol{\mathcal{F}}_{k-1}^{t} + \int_{\mathbf{B}_l + \mathbf{B}_u} \boldsymbol{\mathcal{F}}_{k-1,\mathbf{b}}^{I} d\mathbf{b}. \tag{4.4}$$

with m denoting the mass of the target. Note that $\bar{\boldsymbol{w}}_{k-1}$ reduces to zero if no force is exerted on a target.

4.3.2 Extended Target Model

The extended target state $\boldsymbol{x}_k$ in this paper is defined by

$$\boldsymbol{x}_k = (\xi_k, X_k), \tag{4.5}$$

where $\xi_k = [x_k, \dot{x}_k, y_k, \dot{y}_k]'$ is a column vector with the position and velocity information in 2D Cartesian space at time k. The extent state $X_k \in \mathbb{S}^2_{++}$ is a random $d \times d$ symmetric positive definite matrix, which represents the appearance of the target. The random matrix model [50, 123] is utilized here because of its ability to model ellipsoidal objects with low computational complexity [141].

Therefore, the dynamic model of an extended target is given by [141]

$$\xi_k = \mathcal{F}\xi_{k-1} + G(\bar{\boldsymbol{w}}_{k-1} + \boldsymbol{\omega}_{k-1}), \tag{4.6}$$

where $\mathcal{F} = F \otimes \mathrm{I}_d$, I_d is an identity matrix of dimension d, $\bar{\boldsymbol{w}}_{k-1}$ is the force input to model the TCMM from (4.4) and $\boldsymbol{\omega}_{k-1}$ is the zero mean Gaussian process noise with covariance Q_{k-1}. Note that (4.6) will reduce to the commonly used CV model [82] when $\bar{\boldsymbol{w}}_{k-1} = \mathbf{0}$, in which case the target is free of any terrain constraints. In the above, $A \otimes B$ denotes the Kronecker product [142] of two matrices A and B. The transition matrix F and the covariance matrix Q are given by

$$F = \begin{bmatrix} 1 & \delta T \\ 0 & 1 \end{bmatrix}, \; Q = G \begin{bmatrix} \sigma_x^2 & 0 \\ 0 & \sigma_y^2 \end{bmatrix} G^{\mathrm{T}}, \; G = \begin{bmatrix} \frac{\delta T^2}{2} & 0 \\ \delta T & 0 \\ 0 & \frac{\delta T^2}{2} \\ 0 & \delta T \end{bmatrix} \tag{4.7}$$

where δT is the sampling time and σ_x and σ_y are the acceleration standard deviations in the x and y directions, respectively.

According to the RM model in [50], the model for the target physical extent state

is given by

$$X_k = X_{k-1}. \tag{4.8}$$

The Wishart transition density for the extent state can be calculated by [50, 141, 143]

$$p\left(X_k|X_{k-1}\right) = \mathcal{W}_d\left(X_{k+1}, n, n^{-1}X_k\right). \tag{4.9}$$

Defining $\text{etr}(\cdot) = \exp(\text{tr}(\cdot))$ as the exponential of the trace of matrix given by $\text{tr}(\cdot)$, the notation

$$\begin{aligned}\mathcal{W}_d(X; w, W) = \\ \frac{|X|^{\frac{w-d-1}{2}}}{2^{\frac{wd}{2}}\Gamma_d\left(\frac{w}{2}\right)|X|^{\frac{w}{2}}}\text{etr}\left(-\frac{1}{2}W^{-1}X\right)\end{aligned} \tag{4.10}$$

defines a Wishart distribution over the symmetric positive definite (SPD) matrix X with scalar degree of freedom $w \geq d$ and SPD parameter matrix W [142].

4.3.3 Measurement Model

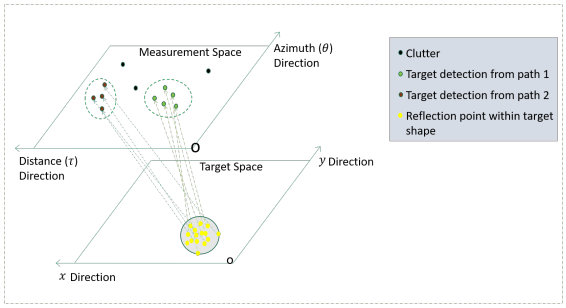

Figure 4.2: An illustrative example with an extended target and sensor measurements via two multiple propagation.

As illustrated in Figure 4.2, one can first note that a target has a time-varying number of reflection points, which are nonstationary and unknown. For each reflection point,

there exist two different propagation paths in this example, which may lead to multiple target-originated detections. The points can arise from not only the target contour but also from the target surface. To make the system model more realistic, measurement-origin uncertainty caused by false alarms and missed detections is also considered here.

In conventional sonar or radar systems, a received measurement signal consists of the distance ℓ and the azimuth θ. Assume that J_k number of measurements are received by the sensor at time k and denote the measurement vector by

$$\mathcal{Z}_{J_k}^k = [\zeta_1^k, \zeta_2^k, ..., \zeta_{J_k}^k], \tag{4.11}$$

where $\zeta_j^k = [\ell_j^k, \theta_j^k]'$, $j = 1, \cdots, J_k$. Assume that the measurement rate γ_l is Poisson distributed and the detections are independent of one another over time. Measurement ζ_i^k can be target-originated or from clutter (false alarm). The corresponding measurement equation is given by

$$\zeta_j^k = \begin{cases} \mathcal{H}^l(\mathrm{p}_t^{j_l}, \mathrm{p}_s, \widehat{\mathrm{env}}) + v_l^k & \text{Mode } l,\ j_l = 1, \ldots, J_k^l, \\ \text{clutter} & \text{otherwise}, \end{cases} \tag{4.12}$$

where $v_l^k = [\bar{v}_{l,\ell}^k, \bar{v}_{l,\theta}^k]'$ is zero-mean white Gaussian noise of model l with covariance $R_l = \mathrm{diag}([\sigma_\ell, \sigma_\theta])$, J_k^l denotes the number of target-originated detections through the l-th path, $\mathrm{p} = [x, y, \nu]$ is the position in 3D Cartesian state space, $x - y$ denotes a horizontal plane and ν represents the altitude/depth information while $\mathrm{p}_t^{j_l}$ and p_s denote the 3D positions of the target scattering point and sensor, respectively and $\widehat{\mathrm{env}}$ denotes the potential environmental factors.

The measurement equation is defined by

$$\mathcal{H}^l(\mathrm{p}_t, \mathrm{p}_s, \widehat{\mathrm{env}}) = \begin{bmatrix} \ell \\ \theta \end{bmatrix} = \begin{bmatrix} h^l(\mathrm{p}_t^{j_l}, \mathrm{p}_s, \widehat{\mathrm{env}}) \\ \arctan\left(\frac{y_k - \mathrm{p}_s(y)}{x_k - \mathrm{p}_s(x)}\right) \end{bmatrix}, \tag{4.13}$$

where $\mathrm{p}_s(x)$ and $\mathrm{p}_s(y)$ represent the position of the sensor in $x-y$ plane, respectively.

Assuming that the polar measurements are independent of one another, the polar detections can be converted into Cartesian space using the standard conversion method [82], which is given by

$$z_k^{l,j} = \begin{bmatrix} \mathcal{IH}^l(\ell_k^{l,j}, \mathrm{p}_s, \widehat{\mathrm{env}}) \cos(\theta_k^{l,j}) \\ \mathcal{IH}^l(\ell_k^{l,j}, \mathrm{p}_s, \widehat{\mathrm{env}}) \sin(\theta_k^{l,j}) \end{bmatrix}, \tag{4.14}$$

where $\mathcal{IH}(\cdot)$ is the inverse operation of the mapping in (4.13) at time step k and $z_k^{l,j}$ is the Cartesian detection of j-th detected point via the l-th path. Note that during the conversion from sensor space to Cartesian coordinates, the Gaussian noise in target space becomes related to the distance traveled by the signal. To calculate the covariance of the Cartesian measurement uncertainty, a first-order Taylor-series approximation of the conversion in (4.14) can be used, and the modified covariance matrix is given by

$$\hat{R}_k^{l,j} = \mathrm{IH}_l(\zeta_k)\mathrm{diag}([\sigma_\ell, \sigma_\theta])\mathrm{IH}_l'(\zeta_k) \tag{4.15}$$

where $\hat{R}_k^l$ is the converted covariance of the l-th path in Cartesian space and

$$\mathrm{IH}_l(\xi_k) = \begin{bmatrix} \frac{\partial \mathcal{IH}^l(\cdot)}{\partial \ell_k} \cos(\theta_k) & -\mathcal{IH}(\cdot) \sin(\theta_k) \\ \frac{\partial \mathcal{IH}^l(\cdot)}{\partial \ell_k} \sin(\theta_k) & \mathcal{IH}(\cdot) \cos(\theta_k) \end{bmatrix} \tag{4.16}$$

is the Jacobian matrix. To simplify the representation, the measurement model (4.14) is simplified to $z_k^{l,j} = h(\zeta_k^{l,j})$. Also, the unscented transformation (UT) [62, 117] can be used to perform the covariance transformation [55].

Since the sensor measurements also include clutter (false alarms) arising from the noisy environment, the union set of the sensor detections in Cartesian space is defined as

$$Z_k = Z_k^{\mathrm{c}} \cup Z_k^t \tag{4.17}$$

with target-originated measurements

$$Z_k^t = \left(\bigcup_{l=1}^{L} \bigcup_{j_l=1}^{J_k^l} z_k^{l,j_l} \right), \tag{4.18}$$

where Z_k^{c} is the set of clutter measurements that appear within the surveillance area in frame k, L is the total number of signal propagation modes, which is assumed to be known a priori, and J_k^l is a random integer indicating the number of possible target-originated detections via path l modeled as a Poisson distribution with a known measurement rate [51, 141].

The clutter measurements are assumed to be distributed uniformly and independently over the whole area of interest and the corresponding number of clutter measurement is assumed to follow a Poisson distribution with a known rate [11].

4.4 MP-ET-PDA Filter

4.4.1 SP-ETT Filter

The objective of RM-based extended target tracking approaches within the Bayesian framework is to jointly estimate both the kinematic state and the physical extent of target interest simultaneously and independently. Here we assume that only a single path exists and J_k number of ET measurements $Z_k = Z_k^c \cup Z_k^t = [z_1^k, z_2^k, ..., z_{J_k}^k]$ are captured by the sensor. By taking advantage of the framework of sensor measurement update for the random matrix model in [52], the posterior density function using Bayes' update can be written as

$$\begin{aligned} & p(\xi_k, X_k|Z_k) \\ & = \frac{p\left(Z_k\,|\xi_k, X_k\right) p(\xi_k, X_k|Z_{1:k-1})}{\iint p\left(Z_k\,|\xi_k, X_k\right) p(\xi_k, X_k|Z_{1:k-1})\,\mathrm{d}\xi_k \mathrm{d}X_k}, \end{aligned} \tag{4.19}$$

where $p(\xi_k, X_k|Z_{1:k-1})$ denotes the prior distribution. The likelihood of a set of measurements conditioned on both the kinematic state and the target extent as well as the number of measurements is given by

$$\begin{aligned} & p\left(Z_k\,|J_k, \xi_k, X_k\right) \\ & \quad = p\left(Z_k\,|\xi_k, X_k, J_k\right) p\left(J_k|\,\xi_k, X_k\right), \end{aligned}$$

where $p(J_k|\xi_k, X_k)$ and $p(Z_k|\xi_k, X_k, J_k)$ indicate the cardinality density and the spatial distribution of the measurements, respectively. Using the models presented in Section

4.3, the measurement likelihood can be computed as

$$p(Z_k|J_k,\ \xi_k,\ X_k) = \prod_{j=1}^{J_k} \mathcal{N}(z_k^j; h(\xi_k), \rho X_k + \hat{R}_k^j), \tag{4.20}$$

where ρ is a scaling parameter to define the extent of the target and $\hat{R}$ denotes the Cartesian measurement covariance.

The prior and posterior densities for a single path in the presence of non-negligible sensor errors can be respectively approximated as [50, 52, 53]

$$\begin{aligned} p(\xi_k, X_k|Z_{1:k-1}) \approx & p(\xi_k|Z_{1:k-1})p(X_k|Z_{1:k-1}) \\ = & \mathcal{N}\left(\xi_k\,;\, m_{k|k-1}, P_{k|k-1}\right) \\ & \times \mathcal{IW}_d\left(X_k\,;\, v_{k|k-1}, V_{k|k-1}\right), \\ p(\xi_k, X_k|Z_{1:k}) \approx & p(\xi_k|Z_{1:k})p(X_k|Z_{1:k}) \\ = & \mathcal{N}\left(\xi_k\,;\, m_{k|k}, P_{k|k}\right) \\ & \times \mathcal{IW}_d\left(X_k\,;\, v_{k|k}, V_{k|k}\right), \end{aligned} \tag{4.21}$$

where

$$\begin{aligned} &\mathcal{IW}_d(X\,;\, v, V) = \\ &\frac{|V|^{\frac{v}{2}}}{2^{\frac{vd}{2}}\Gamma_d\left(\frac{v}{2}\right)|X|^{\frac{v+d+1}{2}}}\mathrm{etr}\left(-\frac{1}{2}VX^{-1}\right) \end{aligned} \tag{4.22}$$

indicates an Inverse-Wishart distribution [142] over the SPD matrix X with scalar degrees of freedom $v > 2d$ and SPD parameter matrix V. Here, $\Gamma_d(\cdot)$ denotes the multivariate gamma density.

The mean measurement and the measurement spread are respectively defined as

$$\begin{aligned} \bar{z}_k &= \frac{1}{n}\sum_{j=1}^{J_k} z_k^j, \\ \bar{S}_k &= \sum_{j=1}^{J_k} (z_k^j - \bar{z}_k)(z_k^j - \bar{z}_k)'. \end{aligned} \tag{4.23}$$

Then, we can rewrite (4.20) as [50]

$$\begin{aligned} p(Z_k|J_k,\ \xi_k, X_k) \propto \\ \mathcal{N}(\bar{z}_k; h(\xi_k), X_k/J_k) \times \mathcal{W}_d(\bar{S}; J_k - 1, X_k). \end{aligned} \tag{4.24}$$

With the above, the update of the predicted state can be performed using the following steps [50]:

- Kinematic state update: Define the predicted kinematic state $\xi_{k|k-1}$ and the corresponding covariance $P_{k|k-1}$. Then,

$$\begin{aligned} \xi_{k|k} &= \xi_{k|k-1} + \bar{K}_{k|k-1}(\bar{z}_k - h(\xi_{k|k-1})), \\ P_{k|k} &= P_{k|k-1} - \bar{K}_{k|k-1} S_{k|k-1} \bar{K}'_{k|k-1} \end{aligned} \tag{4.25}$$

  with

$$\begin{aligned} \bar{S}_{k|k-1} &= \rho X_{k|k-1} + R, \\ \bar{K}_{k|k-1} &= P_{k|k-1} {H_k}' S^{-1}_{k|k-1}, \\ S_{k|k-1} &= H_k P_{k|k-1} {H_k}' + \frac{\bar{S}_{k|k-1}}{J_k}, \end{aligned} \tag{4.26}$$

  where $H_k = \partial h(\cdot)/\partial \xi_k$.

- Extent state update: Define predicted extent state $X_{k|k-1}$. Then,

$$X_{k|k} = \frac{1}{\alpha_{k|k}}(\alpha_{k|k-1}X_{k|k-1} + \widehat{N}_{k|k-1} + \widehat{\bar{S}}_{k|k-1}) \tag{4.27}$$

with

$$\alpha_{k|k} = \alpha_{k|k-1} + J_k, \tag{4.28}$$

and

$$\begin{aligned} \widehat{N}_{k|k-1} &= X_{k|k-1}^{1/2} S_{k|k-1}^{-1/2} N_{k|k-1} \left(S_{k|k-1}^{-1/2}\right)' \left(X_{k|k-1}^{1/2}\right)', \\ \widehat{\bar{S}}_{k|k-1} &= X_{k|k-1}^{1/2} \bar{S}_{k|k-1}^{-1/2} \bar{S}_k \left(\bar{S}_{k|k-1}^{-1/2}\right)' \left(X_{k|k-1}^{1/2}\right)'. \end{aligned} \tag{4.29}$$

Since the kinematic state and the target extent state are independent of each other, the prediction step here, which is the same as that in the standard Kalman filter [82], is given by

- Kinematic state prediction: According to model (4.6)

$$\begin{aligned} \xi_{k|k-1} &= \mathcal{F}\xi_{k-1} \\ P_{k|k-1} &= \breve{F} P_{k-1|k-1} \breve{F}' + Q \end{aligned} \tag{4.30}$$

- Extent state prediction: According to model (4.8)

$$\begin{aligned} \alpha_{k|k-1} &= 2 + \exp^{\frac{-\delta T}{\delta t}(\alpha_{k-1|k-1}-2)}, \\ X_{k|k-1} &= X_{k-1}, \end{aligned} \tag{4.31}$$

where δt indicates the time-related constant that controls the change in target extent over time [54] and $\alpha = v - d - 1$.

With the above derivations, note that the SP-ETT filter assumes not only no

measurement-origin uncertainty but also only one propagation path, which is, however, unrealistic in many practical scenarios.

4.4.2 Data Association with Uncertain MP-ET Pattern

This paper not only focuses on the ETT problem with measurement-origin uncertainty, but also considers the challenging multipath environment. Inspired by the standard PDA [144], to deal with the measurement-origin uncertainty, association events are calculated based on the assumptions in Section 4.3. Let $\mathcal{A}_k^{\phi,J_k}, (\phi = 0, 1, \cdots, J_k)$ be the mutually exclusive and exhaustive measurement set-to-track association events that ϕ out of J_k measurements are from target with $\mathcal{A}_k^{0,J_k}$ denoting the event that no target is detected. Under $\mathcal{A}_k^{\phi,J_k}$, further consider $\mathcal{B}_k^{\{\varphi^l\}_{l=1}^L,\phi}$ to indicate the measurement set-to-path events that the number of target-originated detections from various propagation models is $\sum_{l=1}^{L} \varphi^l = \phi$. Define $\mathrm{P}_m^n = m!/(m-n)!$, $\mathrm{C}_m^n = \mathrm{P}_m^n/m!$. Then, the total number of events $\mathcal{A}_k^{\phi,J_k}$ is given by $n_\phi = \mathrm{C}_{J_k}^{\phi}$ and the total number of events $\mathcal{B}_k^{\{\varphi^l\}_{l=1}^L,\phi}$ is given by $n_\phi^L = \underbrace{L \times L \times \cdots \times L}_{\phi}$. We can also get the total number $n_\phi n_\phi^L$ of the association events that ϕ target-originated detection from J_k measurements via L different paths.

To make the problem clear, one example is illustrated here. Assume that we have $J_k = 3$ measurements (z_k^1, z_k^2, z_k^3) from $L = 2$ propagation modes (p_1, p_2). Then, we get events $\mathcal{A}_k^{0,3}$,$\mathcal{A}_k^{1,3}$, $\mathcal{A}_k^{2,3}$, $\mathcal{A}_k^{3,3}$. Under each association event $\mathcal{A}_k^{\phi,J_k}$, the possible measurement set-to-path events can be enumerated.

Let $\Omega_k^{(\phi,\kappa)}$ indicate the association event including ϕ target-originated measurements combining the κ-th measurement set-to-track event at time k. All association events are listed below:

- None of the measurements is target-originated (event $\mathcal{A}_k^{0,3}$)

  That is, $\phi = 0$, $n_0 = 1$, $n_0^2 = 1$, $n_0 n_0^2 = 1$.

- One of the measurements is target-originated (event $\mathcal{A}_k^{1,3}$)

  That is, $\phi = 1$, $n_1 = 3$, $n_1^2 = 2$, $n_1 n_1^2 = 6$.

  Three measurement set-to-track association events, which indicate z_1 or z_2 or z_3 is generated by a target.

  Under each measurement set-to-track association event, two measurement set-to-path association events exist, which indicates l_1 or l_2 is used by the detections. Then,

$$\begin{aligned}
\Omega_k^{(1,1)} &= \{z_k^{1,l_1}\},\ \{\varphi^1 = 1, \varphi^2 = 0\},\\
\Omega_k^{(1,2)} &= \{z_k^{1,l_2}\},\ \{\varphi^1 = 0, \varphi^2 = 1\},\\
\Omega_k^{(1,3)} &= \{z_k^{2,l_1}\},\ \{\varphi^1 = 1, \varphi^2 = 0\},\\
\Omega_k^{(1,4)} &= \{z_k^{2,l_2}\},\ \{\varphi^1 = 0, \varphi^2 = 1\},\\
\Omega_k^{(1,5)} &= \{z_k^{3,l_1}\},\ \{\varphi^1 = 1, \varphi^2 = 0\},\\
\Omega_k^{(1,6)} &= \{z_k^{3,l_2}\},\ \{\varphi^1 = 0, \varphi^2 = 1\}.
\end{aligned} \tag{4.32}$$

- Two of the measurements are target-originated (event $\mathcal{A}_k^{2,3}$)

  That is, $\phi = 2$, $n_2 = 3$, $n_2^2 = 4$, $n_2 n_2^2 = 12$.

  Three measurement set-to-track association events, which indicate z_1 and z_2 or z_1 and z_3 or z_2 and z_3 are generated by a target.

  Under each measurement set-to-track association event, four measurement set-to-path association events exist, which indicate l_1 and l_1 or l_1 and l_2 or l_2 and

l_1 or l_1 and l_2 are used by the detections. Then,

$$\begin{aligned}
\Omega_k^{(2,1)} &= \{z_k^{1,l_1}, z_k^{1,l_1}\},\ \{\varphi^1 = 2, \varphi^2 = 0\},\\
\Omega_k^{(2,2)} &= \{z_k^{1,l_1}, z_k^{2,l_2}\},\ \{\varphi^1 = 1, \varphi^2 = 1\},\\
\Omega_k^{(2,3)} &= \{z_k^{1,l_2}, z_k^{1,l_1}\},\ \{\varphi^1 = 1, \varphi^2 = 1\},\\
\Omega_k^{(2,4)} &= \{z_k^{1,l_2}, z_k^{2,l_2}\},\ \{\varphi^1 = 0, \varphi^2 = 2\},\\
\Omega_k^{(2,5)} &= \{z_k^{1,l_1}, z_k^{3,l_1}\},\ \{\varphi^1 = 2, \varphi^2 = 0\},\\
\Omega_k^{(2,6)} &= \{z_k^{1,l_1}, z_k^{3,l_2}\},\ \{\varphi^1 = 1, \varphi^2 = 1\},\\
\Omega_k^{(2,7)} &= \{z_k^{1,l_2}, z_k^{3,l_1}\},\ \{\varphi^1 = 1, \varphi^2 = 1\},\\
\Omega_k^{(2,8)} &= \{z_k^{1,l_2}, z_k^{3,l_2}\},\ \{\varphi^1 = 0, \varphi^2 = 2\},\\
\Omega_k^{(2,9)} &= \{z_k^{2,l_1}, z_k^{3,l_1}\},\ \{\varphi^1 = 2, \varphi^2 = 0\},\\
\Omega_k^{(2,10)} &= \{z_k^{2,l_1}, z_k^{3,l_2}\},\ \{\varphi^1 = 1, \varphi^2 = 1\},\\
\Omega_k^{(2,11)} &= \{z_k^{2,l_2}, z_k^{3,l_1}\},\ \{\varphi^1 = 1, \varphi^2 = 1\},\\
\Omega_k^{(2,12)} &= \{z_k^{2,l_2}, z_k^{3,l_2}\},\ \{\varphi^1 = 0.\varphi^2 = 2\},
\end{aligned} \tag{4.33}$$

- Three of the measurements are target-originated (event $\mathcal{A}_k^{0,3}$)

  That is, $\phi = 1$, $n_3 = 1$, $n_3^2 = 8$, $n_3 n_3^2 = 8$.

  One measurement set-to-track association event, which indicates z_1, z_2 and z_3 generated by a target,

  Under each measurement set-to-track association event, eight measurement set-to-path association events exist, which indicates l_1, l_1 and l_1 or l_1, l_1 and l_2 or l_1, l_2 and l_1 or l_1, l_2 and l_2 or l_2, l_1 and l_1 or l_2, l_1 and l_2 or l_2, l_2 and l_1 or l_2, l_2

and l_2 are used by the detections. Then,

$$\begin{aligned}
\Omega_k^{(3,1)} &= \{z_k^{1,l_1}, z_k^{2,l_1}, z_k^{3,l_1}\},\ \{\varphi^1 = 3, \varphi^2 = 0\},\\
\Omega_k^{(3,2)} &= \{z_k^{1,l_1}, z_k^{2,l_1}, z_k^{3,l_2}\},\ \{\varphi^1 = 2, \varphi^2 = 1\},\\
\Omega_k^{(3,3)} &= \{z_k^{1,l_1}, z_k^{2,l_2}, z_k^{3,l_1}\},\ \{\varphi^1 = 2, \varphi^2 = 1\},\\
\Omega_k^{(3,4)} &= \{z_k^{1,l_1}, z_k^{2,l_2}, z_k^{3,l_2}\},\ \{\varphi^1 = 1, \varphi^2 = 2\},\\
\Omega_k^{(3,5)} &= \{z_k^{1,l_2}, z_k^{2,l_1}, z_k^{3,l_1}\},\ \{\varphi^1 = 2, \varphi^2 = 1\},\\
\Omega_k^{(3,6)} &= \{z_k^{1,l_2}, z_k^{2,l_1}, z_k^{3,l_2}\},\ \{\varphi^1 = 1, \varphi^2 = 2\},\\
\Omega_k^{(3,7)} &= \{z_k^{1,l_2}, z_k^{2,l_2}, z_k^{3,l_1}\},\ \{\varphi^1 = 1, \varphi^2 = 2\},\\
\Omega_k^{(3,8)} &= \{z_k^{1,l_2}, z_k^{2,l_2}, z_k^{3,l_2}\},\ \{\varphi^1 = 0, \varphi^2 = 3\}.
\end{aligned} \tag{4.34}$$

Accordingly, we have the joint association event set conditioned on J_k measurements from a single target through L multipath denoted by

$$\Theta_k = \bigcup_{\phi=0}^{J_k} \bigcup_{\kappa=1}^{n_\phi n_\phi^L} \Omega_k^{(\phi,\kappa)}. \tag{4.35}$$

For simplicity, let $\Omega^{(\phi,\kappa)} = \Omega_k^{(\phi,\kappa)}$. Then, the target-originated measurement equation under one arbitrary event $\Omega^{(\phi,\kappa)}$ becomes

$$Z_k^{\Omega^{(\phi,\kappa)}} = h^{\Omega^{(\phi,\kappa)}}(\cdot) + v \tag{4.36}$$

where

$$\begin{aligned} Z_k^{\Omega^{(\phi,\kappa)}} &= \bigoplus_{z_k^j \in \Omega^{(\phi,\kappa)}} z_k^j \\ h^{\Omega^{(\phi,\kappa)}}(\cdot) &= \bigoplus_{l \in \Omega^{(\phi,\kappa)}} h^l(\cdot) \end{aligned} \tag{4.37}$$

with $\bigoplus$ indicating vertical concatenation.

The likelihood for the batch measurement set of a single event therefore becomes

$$p(Z_k^{\Omega^{(\phi,\kappa)}}|\cdot) = \mathcal{N}(Z_k^{\Omega^{(\phi,\kappa)}}; h^{\Omega^{(\phi,\kappa)}}(\cdot), R_k^{\Omega^{(\phi,\kappa)}}). \tag{4.38}$$

4.4.3 Derivation of MP-ET-PDA using Random Matrices

In this Section, a new extension of the PDA, called MP-ET-PDA, is proposed to estimate both the kinetic state and the physical extent of a target in the presence of multipath and measurement origin uncertainty. Compared with the standard PDA [144], the MP-ET-PDA makes the following assumptions:

- The extended target shape can be modeled as an ellipse in 2D Cartesian coordinates.
- Each random scattering point within one target may generate at most one measurement through the l-th known propagation mode (measurement model).
- The target is detected from each propagation mode with a known probability.
- Within the validated measurement set Z_k, a random number of measurements can be independently generated by one target through various propagation modes.

- The number of measurements via path l follows a Poisson distribution with a known measurement rate.
- The false alarms are uniformly distributed over the region of interest and the cardinality of false alarms is assumed to follow a Poisson distribution [145].
- MP-ET-PDA is applied to tracks that are initialized using the one-point or two-point initialization methods [82] based on the measurements that are not associated with any existing tracks by MP-ET-PDA.

Within the recursive Bayesian framework, the prediction step of the proposed algorithm can be computed by (4.30) and (4.31).

Inspired by the standard PDA filter [144], the conditional mean $\boldsymbol{x}_k$ in MP-ET-PDA is given by

$$\begin{aligned}\boldsymbol{x}_k &= E(\boldsymbol{x}_k|Z_k) \\ &= \sum_{\phi=1}^{J_k}\sum_{\kappa=1}^{n_\phi n_\phi^L} E(\boldsymbol{x}_k|\Omega^{(\phi,\kappa)},\{\varphi^l\}_{l=1}^L,Z_k) \\ &\qquad\qquad \times p((\Omega^{(\phi,\kappa)},\{\varphi^l\}_{l=1}^L|Z_k) \\ &= \sum_{\phi=1}^{J_k}\sum_{\kappa=1}^{n_\phi n_\phi^L} \hat{\boldsymbol{x}}_{k|k}^{\Omega^{(\phi,\kappa)}} \times \beta_{k|k}^{\Omega^{(\phi,\kappa)}},\end{aligned} \tag{4.39}$$

where $\hat{\boldsymbol{x}}_{k|k}^{\Omega^{(\phi,\kappa)}}$ is the update of the predicted kinematic and extent states conditioned on a hypothesized association event $\Omega^{(\phi,\kappa)}$ and a set of measurements Z_k at time k. One can note that $\hat{\boldsymbol{x}}_{k|k}^{\Omega^{(\phi,\kappa)}}$ can be determined by performing the filter steps, i.e., (4.25) and (4.26), mentioned in Section 4.4.1.

The second term of $\beta_{k|k}^{\Omega^{(\phi,\kappa)}}$ refers to the probability of the association event conditioned on the measurement set. That is,

$$\begin{aligned}\beta_{k|k}^{\Omega^{(\phi,\kappa)}} =& p(\Omega^{(\phi,\kappa)}, \{\varphi^l\}_{l=1}^{L}|Z_k, J_k, Z_{k-1}) \\ =& \frac{1}{c} p(Z_k|J_k, Z_{k-1}) \times p(\Omega^{(\phi,\kappa)}, \{\varphi^l\}_{l=1}^{L}|J_k, \phi, Z_{k-1}) \\ =& \frac{1}{c} p(Z_k|J_k, Z_{k-1}) \times p(\Omega^{(\phi,\kappa)}, \{\varphi^l\}_{l=1}^{L}|J_k, \phi),\end{aligned} \tag{4.40}$$

where c is the normalization factor. Since the false detections and the target-originated measurements are both independent of each other, the likelihood in (4.40) becomes

$$\begin{aligned}& p(Z_k|(\Omega^{(\phi,\kappa)}, Z_{k-1}) \\ &= p(Z_k^x|\Omega^{(\phi,\kappa)}, Z_{k-1}) \times p(Z_k^c|\Omega^{(\phi,\kappa)}, Z_{k-1}) \\ &= \begin{cases} \frac{\mathcal{N}(Z_k^{\Omega^{(\phi,\kappa)}}; h^{\Omega^{(\phi,\kappa)}}(\cdot), \boldsymbol{R}_k^{\Omega^{(\phi,\kappa)}})}{(V_k)^{(J_k-\phi)}}, & \\ \qquad\qquad \phi = 1, \cdots, J_k, & \\ (V_k)^{-J_k}, & \\ \qquad\qquad \phi = 0. & \end{cases}\end{aligned} \tag{4.41}$$

Then, the prior probability of a single event presented above conditioned on measurement cardinality J_k is given by

$$\begin{aligned}
&p(\Omega^{(\phi,\kappa)}, \{\varphi^l\}_{l=1}^L | J_k, \phi) \\
&\quad = p(\Omega^{(\phi,\kappa)}, \{\varphi^l\}_{l=1}^L | J_k - \phi, J_k) \times p(J_k - \phi | J_k) \\
&\quad = \begin{cases} \frac{\prod_{l=1}^L [p_d(\varphi^l)]^{D(\varphi^l)} [(1-p_d(\varphi^l))]^{1-D(\varphi^l)} \mu_x^l(\varphi^l)}{(\sum_{\phi=0}^{J_k} n_\phi n_\phi^L) \Pr(\cdot)} \mu_c(J_k - \phi), \\ \qquad\qquad\qquad\qquad \phi = 1, \cdots, J_k, \\ \frac{1-p_d}{(\sum_{\phi=0}^{J_k} n_\phi n_\phi^L) \Pr(\cdot)} \mu_c(J_k), \\ \qquad\qquad\qquad\qquad \phi = 0, \end{cases}
\end{aligned} \tag{4.42}$$

with

$$\Pr(\cdot) = (1 - p_d)\mu_c(J_k) + \sum_{\phi=1}^{J_k} \sum_{\kappa=1}^{n_\phi n_\phi^L} \lambda\left(\{\varphi^l\}_{l=1}^L\right), \tag{4.43}$$

where the probability that $\phi = \sum_{l=1}^L \varphi^l$ out of total J_k measurements are generated by the target with L paths is given by

$$\begin{aligned}
&\lambda\left(\{\varphi^l\}_{l=1}^L\right) = \\
&\quad \mu_c(J_k - \phi) \prod_{l=1}^L [p_d(\varphi^l)]^{D(\varphi^l)} [(1 - p_d(\varphi^l))]^{1-D(\varphi^l)} \mu_x^l(\varphi^l),
\end{aligned} \tag{4.44}$$

and $D(\varphi^l)$ is a binary indicator. Here, $D(\varphi^l)$ is equal to zero or unity determined by whether or not there exist φ^l ToDs arising via path l, $p_d(\varphi^l)$ means the superposition probability of φ^l target-originated measurements being captured through path l, p_d is the probability that the target is detected while $\mu_x^l(\cdot)$ and $\mu_c(\cdot)$ are the probability mass functions of the number of l-th path target-originated measurements and of the number of clutter measurements over the whole surveillance area, respectively

[128, 144].

4.4.4 Computational Complexity of the MP-ET-PDA

The major computational complexity of the proposed MP-ET-PDA filter arises from the measurement-update step (4.39), where the conditional state estimate over different association events and the corresponding weights are calculated. Note that the computational complexity in manipulating all these association events is determined by the number $\sum_{\phi=0}^{J_k} n_\phi n_\phi^L$ of possible association events detailed in Section 4.4.2. For example, with $J_k = 6$ and $L = 3$ in one scan, there are 4,096 association events. The total event number increases to 1,048,576 if J_k goes to 10. Thus, in ETT scenarios with both multipath detections and measurement-origin uncertainty, approximation techniques must be utilized to reduce the computational load of the algorithm. Therefore, another clustering-aided algorithm is proposed in Section 4.5 to simplify the data association problem while maintaining reasonable performance. Average computer execution times over one frame are illustrated and compared in Section 4.7.

4.5 Clustering-aided Data Association Algorithm

As mentioned before, the MP-ET-PDA is computationally expensive, especially when there are more than two propagation paths at high measurement rates . With target detections via various propagation paths, it is reasonable to assume that the measurements from different measurement paths are spatially clustered. In this Section,

a new Variational Bayesian clustering-aided data association technique is presented to scenarios with dense multipath detections, reducing the computational burden significantly while maintaining tracking accuracy compared with the MP-ET-PDA approach proposed in Section 4.4. Since one cannot distinguish which path is used by a certain detection before data association, we have to use original sensor measurements $\mathcal{Z}_{J_k}^k = [\zeta_1^k, \zeta_2^k, ..., \zeta_{J_k}^k]$ in the clustering algorithm rather than their Cartesian counterparts.

4.5.1 Gaussian Mixture Model

The basic idea behind the clustering method is to subdivide the detections set $\mathcal{Z}_k$ into Ψ_k mutually exclusive subsets in the measurement space. We assume that each clustered subset follows a certain Gaussian distribution $\mathcal{N}(\bar{m}_k^\psi, \Lambda_\psi)$ where $\bar{m}_k^\psi$ and Λ_k^ψ denote the mean and the covariance, respectively. The sensor detections can be modeled as a mixture of Gaussian distributions, i.e.,

$$p(z_k^j) = \sum_{\psi=1}^{\Psi_k} \varpi_k^\psi \mathcal{N}(\xi_k^j | \bar{m}_k^\psi, \Lambda_k^\psi), \tag{4.45}$$

where Ψ_k is the total number of Gaussian component and ϖ_ψ denotes the mixing coefficients representing the probability that the detection point z^j belongs to the ψ-th cluster while $0 \leq \varpi_k^\psi \leq 1$ and $\sum_{\psi=1}^{\Psi_k} \varpi_k^\psi = 1$.

As introduced in Section 4.4.3, the sensor detections within one frame are all independent from one another. Then,

$$\log p(\mathcal{Z}_k) = \sum_{j=1}^{J_k} \log \left\{ \sum_{\psi=1}^{\Psi_k} \varpi_k^\psi \mathcal{N}(\xi_k^j | \bar{m}_k^\psi, \Lambda_k^\psi) \right\}. \tag{4.46}$$

Each detection point is assigned into one cluster, and we define a 1-of-Ψ_k binary indicator vector (latent variables) as

$$\emptyset_k^j = [\phi_k^{j,1}, \phi_k^{j,2}, \ldots, \phi_k^{j,\Psi_k}] \tag{4.47}$$

to denote the corresponding assignment modes of the j-th sensor measurement. In (4.47), $\phi_k^{j,\psi}$ equals to zero or unity, determined by whether the j-th measurement belongs to the ψ-th cluster. The marginal distribution over $\emptyset_k^j$ is $\varpi_k^\psi = p(\phi_k^{j,\psi} = 1)$ with $\sum \emptyset_k^j = 1$.

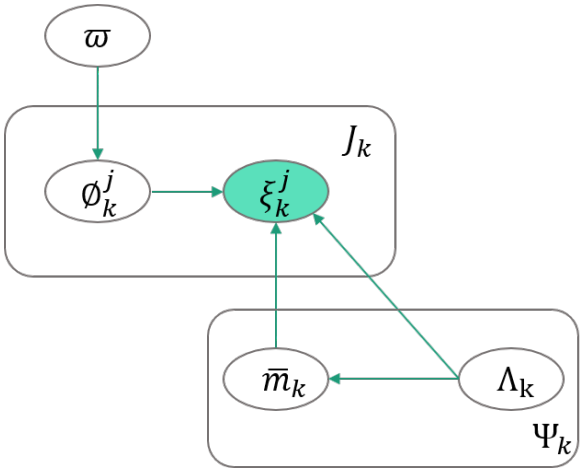

Figure 4.3: Graph model illustration of the Gaussian mixture model.

As assumed before, only one element of the indicator vector can be 1 while all other elements are zero. Thus, the conditional probability of O_k given the mixing coefficients, ϖ, is given by

$$p(\emptyset_k|\varpi) = \prod_{j=1}^{J_k} \prod_{\psi=1}^{\Psi_k} (\varpi_k^\psi)^{\phi_k^{j,\psi}}. \tag{4.48}$$

Let $\bar{m}_k = \{\bar{m}_k^\psi\}_{\psi=1}^{\Psi_k}$, $\Lambda_k = \{\Lambda_k^\psi\}_{\psi=1}^{\Psi_k}$. Then, the conditional probability of z_k^j given

a specified latent variable $\emptyset_k^j$ is

$$p(z_k^j|\emptyset_k^j, \bar{m}_k, \Lambda_k) = \prod_{\psi=1}^{\Psi_k} \mathcal{N}(\xi_k^j|\bar{m}_k^\psi, \Lambda_k^\psi)^{\varrho_k^{j,\psi}}. \tag{4.49}$$

Following the idea in [146], conjugate prior distributions over $\bar{m}$, Λ and ϖ are introduced to simplify the analysis. Assuming that the mixing coefficient ϖ follows a Dirichlet distribution, one can therefore obtain

$$p(\varpi) = \mathrm{Dir}(\varpi|\epsilon_0) = \frac{1}{\mathcal{V}(\epsilon_0)} \prod_{\psi=1}^{\Psi_k} (\varpi_k^\psi)^{(\epsilon_0-1)}, \tag{4.50}$$

where $\mathcal{V}(\epsilon_0)$ is the normalization variable for the Dirichlet distribution and ϵ_0 denotes the prior number of measurements assigned into each Gaussian mixture component (cluster) [146]. Further, the independent Gauss-Wishart distribution is assumed to constrain the mean $\bar{m}_k$ and the covariance matrix Λ_k. Thus, we have

$$\begin{aligned} p(\bar{m}_k, \Lambda_k) =& p(\bar{m}_k^\psi|\Lambda_k^\psi)p(\Lambda_k^\psi) \\ =& \prod_{\psi=1}^{\Psi} \mathcal{N}\left(\bar{m}_k^\psi|\bar{m}_0, (\pi_0\Lambda_k^\psi)^{-1}\right) \mathcal{W}_d(\Lambda_k^\psi|w_0, W_0), \end{aligned} \tag{4.51}$$

where $\bar{m}_0$, π_0, w_0 and W_0 are the parameters used as priors.

From the above derivations, one can note that parameter $\Pi_k = \{\varpi_k, \emptyset_k, \bar{m}_k, \Lambda_k\}$ governs the performance of clustering results leading to the objective conditional distribution $p(\Pi_k|Z_k)$, which is however intractable to evaluate directly.

4.5.2 Gaussian Variational Approximation

The joint distribution of all the random variables including sensor detections (observations), hidden parameters and latent variables can be written as [146]

$$\begin{aligned} p(Z_k,&\emptyset_k, \varpi, \bar{m}_k, \Lambda_k) = \\ &p(Z_k|\emptyset_k, \bar{m}_k, \Lambda_k)p(\emptyset_k|\varpi)p(\varpi)p(\bar{m}_k|\Lambda_k)p(\Lambda_k). \end{aligned} \tag{4.52}$$

Define distribution $q(\emptyset_k)$ over all latent variable and hidden parameters for any arbitrary function of $q(\Pi_k)$. Then, the log marginal probability $p(\Pi_k)$ can be written again as [146]

$$\log p(Z_k) = \mathbb{L}(q) + \mathbb{KL}(q||p). \tag{4.53}$$

The idea behind the VB-clustering is to obtain $q(\Pi_k)$ by maximizing the Variational lower bound

$$\mathbb{L}(q) = \int q(\emptyset_k) \log \left\{ \frac{p(Z_k, \emptyset_k)}{q(\emptyset_k)} \right\} d\Pi_k, \tag{4.54}$$

or by minimizing the Kullback-Leibler (KL) divergence

$$\mathbb{KL}(q||p) = -\int \int q(\Pi_k) \log \left\{ \frac{p(\Pi_k|Z_k)}{q(\Pi_k)} \right\} d\Pi_k, \tag{4.55}$$

where $\mathbb{KL}(q||p)$ denotes the KL divergence between $q(\Pi_k)$ and posterior $p(Z_k|\Pi)$ [146], which implies that the maximum of $\mathbb{L}(q)$ can be obtained when $\mathbb{KL}(q||p) = 0$.

Assume that the objective distribution can be factorized as

$$q(\Pi_k) = q(\varpi_k, \emptyset_k, \bar{m}_k, \Lambda_k) = q(\emptyset_k)q(\varpi_k, \bar{m}_k, \Lambda_k). \tag{4.56}$$

We can further factorize $q(\varpi_k, \bar{m}_k, \Lambda_k)$ from the objective distribution as [146]

$$q(\varpi_k, \bar{m}_k, \Lambda_k) = q(\varpi_k) q(\bar{m}_k, \Lambda_k). \tag{4.57}$$

Note that $q(\emptyset_k)$, $q(\varpi_k)$ and $q(\bar{m}_k, \Lambda_k)$ can be determined after the VB distribution $q(\Pi_k)$ is optimized. The log-optimal distributions are then written as

$$\begin{aligned} \log q^*(\emptyset_k) &= E_{\varpi_k, \bar{m}_k, \Lambda_k} \left\{ \log p(\mathcal{Z}_k, \emptyset_k, \varpi, \bar{m}_k, \Lambda_k) \right\} + \mathcal{V}_1, \\ \log q^*(\varpi_k, \bar{m}_k, \Lambda_k) &= E_{\emptyset_k} \left\{ \log p(\mathcal{Z}_k, \emptyset_k, \varpi, \bar{m}_k, \Lambda_k) \right\} + \mathcal{V}_2, \end{aligned} \tag{4.58}$$

where $\mathcal{V}_1$, and $\mathcal{V}_2$ denote normalization constants.

With the above probabilistic derivations, the parameter set $\Pi_k = \{\varpi_k, \emptyset_k, \bar{m}_k, \Lambda_k\}$ needs to be estimated by optimizing $q(\emptyset_k)$, $q(\varpi_k)$, and $q(\bar{m}_k, \Lambda_k)$ given by the observed data set. A recursive VB-EM approach from [146] is used to solve the above Variational Bayesian problem. After clustering the measurement into groups with labels, we can assume that the detections with the same label share the same source (e.g., clutter, ToDs from the same path), leading to a much lower number of association events compared with the one in the MP-ET-PDA filter presented in Section 4.4.

4.6 Posterior Cramér-Rao Lower Bound

In this Section, the PCRLB [147] is derived for the ETT problem with false alarms, missed detections and multiple signal prorogation modes. The CRLB, calculated by the inverse of the FIM, qualifies the achievable accuracy of any unbiased estimator for a specific parameter estimation problem [82]. The PCRLB is used to evaluate the

performance of dynamic state estimators in target tracking applications.

Let $\mathcal{X}_k^*(Z_k)$ denote an unbiased estimate of state vector of interest $\mathcal{X}_k$, which is a function of the measurement set Z_k. Then, the lower bound of the MSE matrix is expressed as [82]

$$\mathrm{E}\{[\mathcal{X}_k^*(Z_k) - \mathcal{X}_k][\mathcal{X}_k(Z_k) - \mathcal{X}_k]'\} \geq J_k(\mathcal{X}), \tag{4.59}$$

where E represents the expectation operation, $[\cdot]'$ denotes transposition and the lower bound $J_k(\mathcal{X}) = \mathcal{I}_k^{-1}(\mathcal{X})$ with the FIM being denoted by $\mathcal{I}_k(\mathcal{X})$. The PCRLB and FIM can be calculated with the following recursions [82]:

$$\begin{aligned}
\mathcal{I}_{k+1}(\mathcal{X}) =& \mathrm{E}\{\Delta_{\mathcal{X}_k}^{\mathcal{X}_k} \ln\, p(Z_k, \mathcal{X}_k)\} \\
=& J_{\mathrm{X}}(k+1) + J_{\mathrm{Z}}(k+1) \\
=& \Omega_k^{22} - \Omega_k^{12\prime}/(\mathcal{I}_k(\mathcal{X}) + \Omega_k^{11})\Omega_k^{12} + \mathcal{I}_{Z,k}(\mathcal{X}),
\end{aligned} \tag{4.60}$$

where

$$\begin{aligned}
\Omega_k^{11}(\mathcal{X}) =& \mathrm{E}\left\{-\Delta_{\mathcal{X}_k}^{\mathcal{X}_k} \ln p(\mathcal{X}_{k+1}|\mathcal{X}_k)\right\}, \\
\Omega_k^{12}(\mathcal{X}) =& \mathrm{E}\left\{-\Delta_{\mathcal{X}_k}^{\mathcal{X}_{k+1}} \ln p(\mathcal{X}_{k+1}|\mathcal{X}_k)\right\}, \\
\Omega_k^{22}(\mathcal{X}) =& \mathrm{E}\left\{-\Delta_{\mathcal{X}_{k+1}}^{\mathcal{X}_k} \ln p(\mathcal{X}_{k+1}|\mathcal{X}_{k+1})\right\}, \\
\mathcal{I}_{Z,k}(\mathcal{X}) =& \mathrm{E}\left\{-\Delta_{\mathcal{X}_{k+1}}^{\mathcal{X}_{k+1}} \ln p(Z_{k+1}|\mathcal{X}_{k+1})\right\},
\end{aligned} \tag{4.61}$$

where $\Delta_{\mathcal{B}}^{\mathcal{A}}$ denotes the partial derivative operation over $\mathcal{A}$ and $\mathcal{B}$.

As we assumed in Section 4.4.3, the detections arising from the multiple propagation paths are independent of one another. Then,

$$\mathcal{I}_{Z,k}(\mathcal{X}) = \sum_{l=1}^{L} q^* \mathcal{I}_{Z,k}^{l}(\mathcal{X}), \tag{4.62}$$

where $\mathcal{I}_{Z,k}^{l}(\mathcal{X})$ is the FIM representing the l-th measurement mode's contribution to the PCRLB and q^* is the IRF qualifying the loss in information due to measurement origin uncertainty. In RM theory, the extent state X_k is assumed to be independent of the kinematic state x_k. Therefore, we can follow the derivations in [56, 148] and calculate the PCRLB over the target states, separately.

- Recursive calculation of the kinematic state FIM

  Using the assumed motion model with zero-mean Gaussian process noise (4.6) and letting $\mathcal{X}_k = \xi_k$, we obtain

$$\Omega_k^{11}(\xi) = \breve{F}' Q^{-1} \breve{F},\ \Omega_k^{12}(\xi) = -\breve{F} Q^{-1},\ \Omega_k^{22}(\xi) = Q^{-1}. \tag{4.63}$$

  For terrain-constrained motion model (4.6), we have

$$\breve{F} = \mathcal{F} + G \frac{\partial \bar{\boldsymbol{w}}_k^1}{\partial \xi_k^1}, \tag{4.64}$$

  If only a CV motion model is used, we have $\breve{F} = \mathcal{F}$. Further, $\mathcal{I}_{Z,k}^{l}(\xi)$ can be calculated as [56]

$$\mathcal{I}_{Z,k}^{l}(\xi) = \bar{\gamma}_l H' (\rho X_k + \hat{R}_k^l)^{-1} H, \tag{4.65}$$

where $H = \begin{bmatrix} 1 & 0 & 0 & 0 \\ 0 & 0 & 1 & 0 \end{bmatrix}$, and $\hat{R}_k^l$ is the Cartesian coordinate errors transformed from sonar's measurement noise using the UT technique [117].

- Recursion calculation of the extent state FIM

  As in the kinetic state FIM derivations, letting $\mathcal{X}_k = X_k$, we can get [56, 148]

$$\Omega_k^{ab}(X) = \begin{bmatrix} c_{11,11}^{ab} & c_{11,12}^{ab} + c_{11,21}^{ab} & c_{11,22}^{ab} \\ c_{12,11}^{ab} & c_{12,12}^{ab} + c_{12,21}^{ab} & c_{12,22}^{ab} \\ +c_{21,11}^{ab} & +c_{21,12}^{ab} + c_{21,21}^{ab} & +c_{21,22}^{ab} \\ c_{22,11}^{ab} & c_{22,12}^{ab} + c_{22,21}^{ab} & c_{22)22}^{ab} \end{bmatrix}, \tag{4.66}$$

where

$$\begin{aligned} c_{ij,sm}^{11} &= \frac{\bar{n}}{4}\left(X_{k,il}^{-1}X_{k,jm}^{-1} + X_{k,im}^{-1}X_{k,sj}^{-1}\right), \\ c_{ij,sm}^{21} &= -\frac{\bar{n}}{4}\left(X_{k,ij}^{-1}X_{k,sm}^{-1} + X_{k,js}^{-1}X_{k,im}^{-1}\right), \\ c_{ij,sm}^{12} &= c_{sm,ij}^{21}, \\ c_{ij,sm}^{22} &= \frac{\bar{n}^2}{4}\left(c_1(\bar{n}-d-1)^2 - 1\right)X_{k,ij}^{-1}X_{k,sm}^{-1} \\ &\quad + c_2\frac{\bar{n}^2}{4}(\bar{n}-d-1)^2 X_{k,is}^{-1}X_{k,jm}^{-1} \\ &\quad + c_2\frac{\bar{n}^2}{4}(\bar{n}-d-1)^2 X_{k,sj}^{-1}X_{k,im}^{-1}, \end{aligned} \tag{4.67}$$

and

$$\mathcal{I}_{Z,k}^l(X) = \begin{bmatrix} c_{11,11}^l & c_{11,12}^l + c_{11,21}^l & c_{11,22}^l \\ c_{12,11}^l & c_{12,12}^l + c_{12,21}^l & c_{12,22}^l \\ +c_{21,11}^l & +c_{21,12}^l + c_{21,22}^l & +c_{21,21}^l \\ c_{22,11}^l & c_{22,12}^l + c_{22,21}^l & c_{22,22}^l \end{bmatrix}, \tag{4.68}$$

where $\widehat{\text{cov}} = (\rho X_k + \hat{R}_k^l)^{-1}$, and

$$c_{ij,sm}^{l} = \bar{\gamma}_l \frac{\rho^2}{4} \left(\widehat{\text{cov}}_{is} \widehat{\text{cov}}_{jm} + \widehat{\text{cov}}_{im} \widehat{\text{cov}}_{sj} \right). \tag{4.69}$$

In the above, the subscripts i, j, s, m are integer variables from 1 to 2.

Define a_{major} and a_{minor} as the semi-major and semi-minor axes of the ellipsoidal target, respectively. Then, the PCRLB for the ellipse axes is given by [56]

$$\begin{aligned} J_k(a_{\text{major}}) &= \text{E}^{'} \left[\partial_{X_k} a_{\text{major}}(X_k) \right] J_k(X) \text{E} \left[\partial_{X_k} a_{\text{major}}(X_k) \right] \\ J_k(a_{\text{minor}}) &= \text{E}^{'} \left[\partial_{X_k} a_{\text{minor}}(X_k) \right] J_k(X) \text{E} \left[\partial_{X_k} a_{\text{minor}}(X_k) \right] \end{aligned} \tag{4.70}$$

where $\partial_{X_k} a_{\text{major}}(X_k)$ and $\partial_{X_k} a_{\text{minor}}(X_k)$ denote the gradients of a_{major} and a_{minor} over the elements of target extent state X_k, respectively.

4.7 Numerical Simulations

In this Section, Monte Carlo simulation experiments with 100 trials are used to evaluate the performances of the proposed MP-ET-PDA and MP-ET-PDA-VB-cluster methods with an active 2D sonar in an uncertain multipath environment. The baseline algorithm is the SP-RM-PDA [55] that assumes only a single direct path. Also, the PCRLB provides the benchmark for quantifying the accuracy achievable by any estimator. Two scenarios with the CV and the terrain-constrained motion models are used to validate the proposed algorithms. The sensor detections are independently generated over 100 Monte Carlo runs performed on the same target trajectories. Here, a scenario with underwater extended target tracking using a high-resolution

2D sonar with only two linear propagation paths is simulated. A more complex SSP model as in [39, 63, 149] with multipath environment can be used with the proposed algorithms, but only with additional a priori information. The proposed approaches can also be used for ground ETT problem in a confined space.

The sensor-to-target geometry is illustrated in Figure 4.4. A flat surface is used and the multipath phenomenon is common with an acoustic sensor due to ocean boundary. The direct path p_1 and the single-surface-hop path p_2 are assumed here. Using a zero-gradient SSP with constant speed C, the sonar measurements can be calculated as

$$\begin{aligned} \theta &= \text{atan}(\frac{y_{\text{Tx}} - y_{\text{Rx}}}{x_{\text{Tx}} - x_{\text{Rx}}}) + \bar{v}_\theta, \\ \ell_{\text{path-1}} &= \sqrt{r^2 + (\nu_{\text{Tx}} - \nu_{\text{Rx}})^2} + \bar{v}_{1,\ell}, \\ \ell_{\text{path-2}} &= \sqrt{r^2 + (\nu_{\text{Tx}} + \nu_{\text{Rx}})^2} + \bar{v}_{2,\ell} \end{aligned} \tag{4.71}$$

with $r = \sqrt{(y_{\text{Tx}} - y_{\text{Rx}})^2 + (x_{\text{Tx}} + x_{\text{Rx}})^2}$.

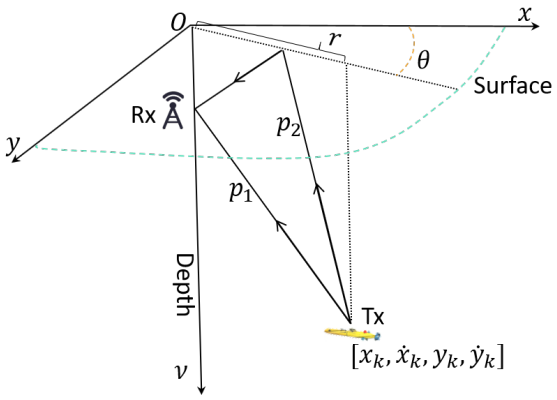

Figure 4.4: Geometry of target and sensor locations.

Scenario I: The surveillance region is limited to $[0, 500]$m in range and $[0°, 180°]$ in azimuth. The sensor Rx stays at $\text{p}_s = [0, 0, -10]$m. Sensor standard errors in

distance and azimuth are $\sigma_\ell = 0.1$m and $\sigma_\theta = 0.05°$, respectively. Assume one target Tx moves at a fixed depth -100m with a constant velocity but disturbed by a zero-mean Gaussian process noise. Also, $P_0 = \text{diag}([30, 0.1, 30, , 0.1])$ is used to initialize the kinematic state. The degree of the Wishart model and the initial degree of freedom are respectively selected as $v_0 = 10$ and $\alpha_{1|0} = 10$ for target extent state initialization. The extent changing time is $\delta t = 10$s and the other parameters are detailed in Table 4.1. Figures 4.5 and 4.6 show the scenario including the true target trajectories and the sensor detections from one Monte Carlo trial.

Table 4.1: Parameters in Scenario I

Parameter	Value
Number of Monte Carlo runs	100
Number of frames	50
Sampling time ΔT (s)	1
Process noise σ (m/s^2)	1E$-$2
Target depth (m)	-100
Ocean surface depth (m)	0
Sensor location $\mathrm{p_s}$ (m)	[0, 0, -10]
Range error standard deviation σ_ℓ (m)	0.1
Azimuth error standard deviation σ_θ (degree)	0.05
Number of paths L	2
Target-originated measurement rate γ_l	[2, 2]
Surveillance region volume V	$[0°, 180°] \times [0\mathrm{m}, 500\mathrm{m}]$
Expected number of false alarms per scan	10
p_d^l for each propagation model	[0.98, 0.98]
Semi-major and semi-minor axes of target (m)	[3, 1.5]

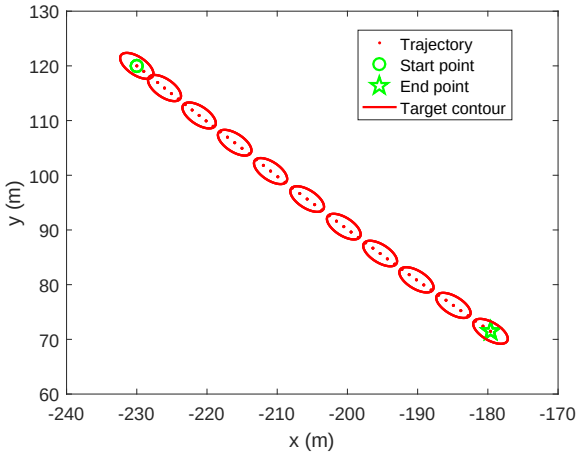

Figure 4.5: Target trajectory (Scenario I).

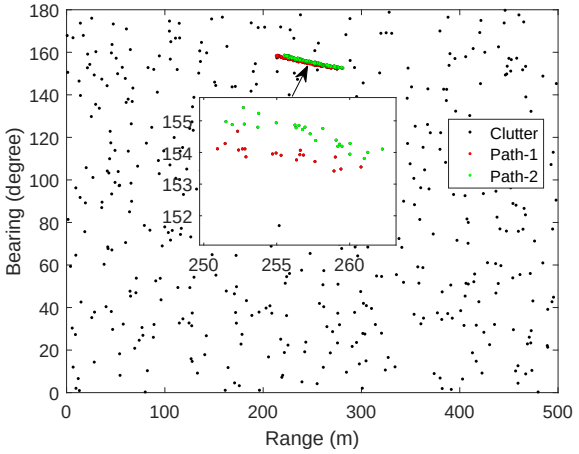

Figure 4.6: Sensor detections with multipath ET phenomenon (Scenario I).

Figures 4.7–4.8 show the Root Mean Square Error (RMSE) of the state estimates in position and target extent, respectively. The proposed MP-ET-PDA filter and the MP-ET-PDA-VB algorithms both outperform the standard SP-RM-PDA [55]. Instead of treating the multipath detections as false alarms or ignoring them as in conventional trackers, the correct likelihood function and a consistent covariance are calculated in the proposed algorithms by taking advantage of the potential

information in the multipath detections, which results in the better performance by the proposed algorithm. In contrast, by assuming only a single path (p_1), the SP-RM-PDA algorithm implies that the detections arising from the other path (p_2) are state-dependent clutter, which degrades the performance of that tracker. Thus, the SP-RM-PDA algorithm cannot counter the effects of the detections via path p_2. The PCRLB for the extended target tracking problem with multipath detections is used to verify the performance of the proposed algorithms. Note in Figures 4.7–4.8 that the RMSE values obtained by the MP-ETT-PDA filter follow the PCRLB well, demonstrating the efficiency of the proposed tracker. Also, the percentage of broken tracks by the MP-ETT-PDA filter is less than 1.5% (see Table 4.4). One can also note the gap between the RMSE values of the MP-ET-PDA-VB algorithm and those of the MP-ETT-PDA filter because of potential information loss due to clustering, which is a trade-off in trying to reduce the combinational complexity. As can be seen from Table 4.4, the percentage of validated tracks by the MP-ET-PDA-VB is only 3% percent higher than that of SP-RM-PDA, but the RMSE values of the MP-ET-PDA-VB algorithm is at least 80% less that that of the SP-RM-PDA method.

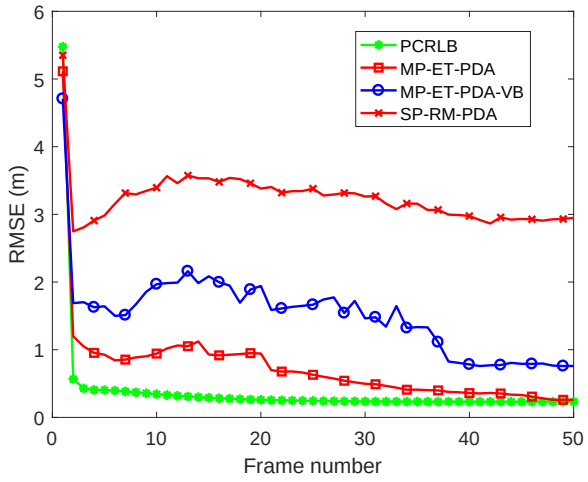

Figure 4.7: Position RMS errors (Scenario I).

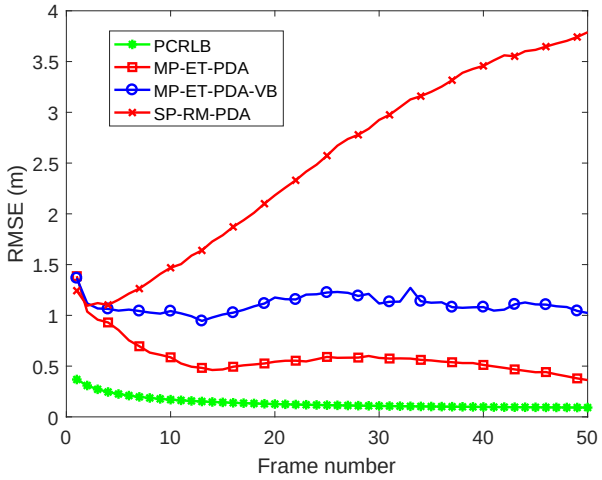

Figure 4.8: RMS errors in ellipse semi-axes (Scenario I).

Scenario II: The surveillance region is $[90°, 270°] \times [0, 500]$m in polar coordinates, and the sensor is deployed at $\mathrm{p}_s = [-70, 55, -3]$m. One target moves at a fixed depth of -100m but constrained by the river banks towards a certain destination along the terrain and avoids colliding with the boundaries. The same covariance matrix P_0 from Scenario I and the newly-added terrain information are used in the track initialization.

The parameters used in the scenario are listed in Table 4.2, and the other parameters are the same as those in Scenario I. Figures 4.9–4.10 show the scenario including the river influenced terrain, target's destination, ground truth and the sensor detections from one Monte Carlo trial.

Table 4.2: Parameters in Scenario II

Parameter	Value
Process noise σ (m/s^2)	1E−3
Sensor location p$_s$ (m)	[−70, 55, −3]
Surveillance region volume V	$[90°, 270°] \times [0\text{m}, 500\text{m}]$
Target mass (kg)	80
Relaxation time τ (s)	$1\Delta T$
Intended destination (m)	[−70, 55]
Desired Speed $\bar{v}$ (m/s)	2.25
Force magnitude parameters ϱ_a, ϱ_r (N)	[75, 75]
Range parameter b of the force (m)	10
Radius influence parameter r of target (m)	3

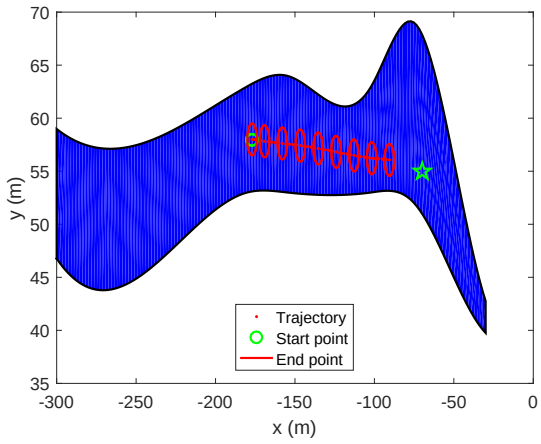

Figure 4.9: Target trajectory (Scenario II).

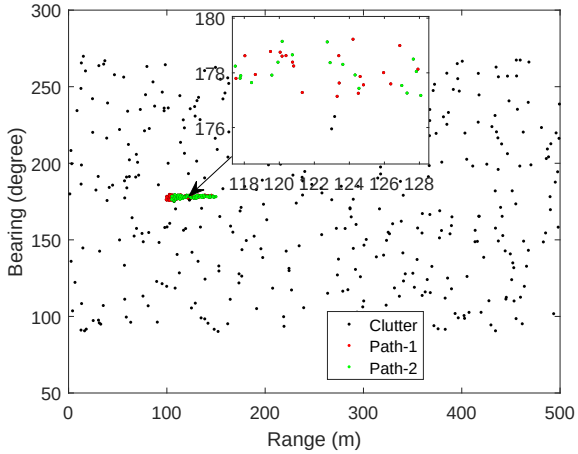

Figure 4.10: Sensor detections with multipath ET phenomenon (Scenario II).

Figures 4.11–4.12 show the RMSE of position and target extent state estimates, respectively. Note that MP-ET-PDA and MP-ET-PDA-VB perform better than the standard SP-RM-PDA [55] as in Scenario I by incorporating multipath detections from an extended target. Due to including the local terrain information in these filters, the performances of MP-ET-PDA, MP-ET-PDA-VB and SP-RM-PDA are better

than those of MP-ET-PDA-CV and MP-ET-PDA-VB-CV that assume a constant velocity model. In Table 4.4, one can note that the broken track rate of MP-ET-PDA is less than 1% while that of MP-ET-PDA-VB is also reduced to 3.5%. Due to using a mismatched motion model, although the extent estimates of MP-ET-PDA-CV are very poor, it yields reasonable position estimates. The MP-ET-PDA-VB-CV performs poorly both in terms of RMSE and rate of broken tracks.

The simulations are implemented in MATLAB® 2016b on an Intel(R) Core(TM) i7 CPU with 32 GB RAM with parallel computing techniques being used for loops in implementing both SP-RM-PDA and the proposed MP-ET-PDA algorithms. By using a clustering-aided data association technique, the computational load of MP-ET-PDA-VB is reduced compared with that of MP-ET-PDA while maintaining acceptable tracking performance in both two scenarios. Also, note that the computational complexities of all three algorithms (namely, MP-ET-PDA, MP-ET-PDA-VB and SP-RM-PDA) in Scenario II are higher than the corresponding values in Scenario I due to the cost of processing the new terrain-constrained model. Compared with the original MP-ET-PDA, the MP-ET-PDA-VB algorithm is able to provide significantly faster processing capability with application to practical scenarios. Also note that the proposed MP-ET-PDA-VB beats the SP-RM-PDA not only in terms of RMSE and rejection of broken track rate but also in terms of computing times. By comparing the RMSE values of position estimates and physical extent estimates in both scenarios, one can see that the RMSE values of target extent do not follow the trend of the PCRLB (cf. position estimates and corresponding PCRLB values), which is in accordance with the observation that a better estimator is required for extent state estimates [56].

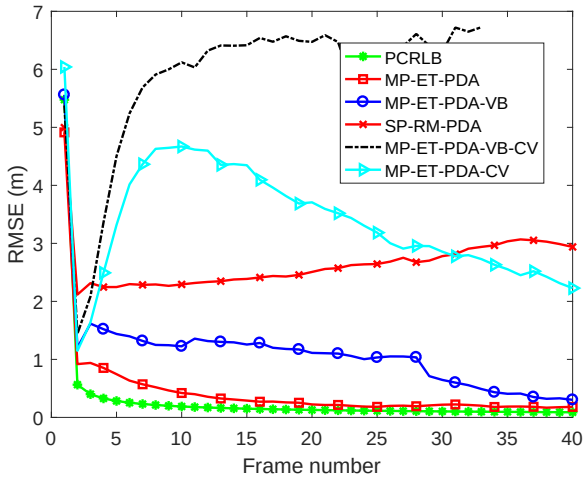

Figure 4.11: Position RMS errors (Scenario II).

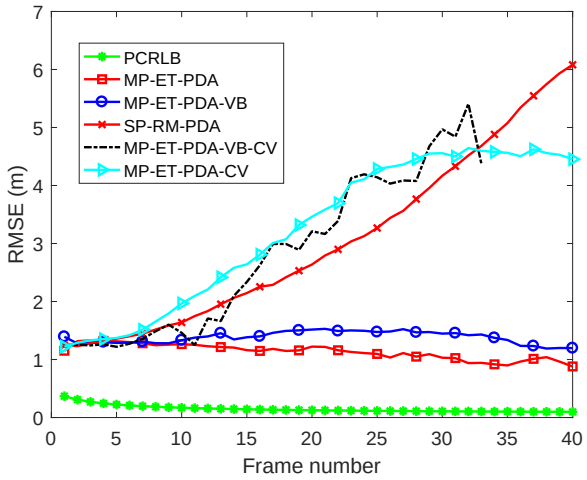

Figure 4.12: RMS errors ellipse semi-axes (Scenario II).

Table 4.3: Average processing times over one scan from 100 Monte Carlo trials

Method	Scenario I	Scenario II
MP-ET-PDA	2.52s	2.77s
MP-ET-PDA-VB	0.014s	0.027s
SP-RM-PDA	0.03s	0.07s
MP-ET-PDA-VB-CV	–	0.008s
MP-ET-PDA-CV	–	0.918s

Table 4.4: Percentages of validated tracks from 100 Monte Carlo trials

Method	Scenario I	Scenario II
MP-ET-PDA	98%	99%
MP-ET-PDA-VB	87%	96%
SP-RM-PDA	84%	96%
MP-ET-PDA-CV	–	65%
MP-ET-PDA-VB-CV	–	21%

4.8 Conclusions

In this paper, a new algorithm (MP-ET-PDA) was proposed to track elliptical extended targets in a multipath environment with measurement-origin uncertainty. To handle the combinatorial complexity in the MP-ET-PDA filter, a simplified real-time capable algorithm (MP-ET-PDA-VB) aided by a clustering method was also presented. In both MP-ET-PDA and MP-ET-PDA-VB, the association events were formed considering the existence of multipath detections from an extended target and

measurement-origin uncertainty, and the conditional target state was updated based on all the state estimates given by each event and the corresponding probability. For the scenarios with terrain information, a new social force-based motion model, named TCMM, was presented to calculate the likelihood function in the prediction step of the recursive filter by including the interactions between the target and the terrain boundary. The proposed algorithms were validated and evaluated through simulations and compared with the benchmark PCRLB.

Chapter 5

Conclusions

5.1 Research Summary

5.1.1 List of Contributions

The contributions of this thesis are listed as follows:

1) Developing an iterated underwater target detection method that can handle acoustic bending channel affected by uncertain oceanographical factors (i.e., sound speed profile), multipath detection and heavy clutter using active sonar.

2) Developing a computationally efficient optimization solution combining the grid search and particle swarm optimization to deal with the high computational cost optimization problem with many local optima.

3) Deriving the CRLB for the underwater target detection problem in an uncertain multipath environment.

4) Formulating a novel dynamic motion model for a diver affected by closed divers and water flow.

5) Developing an algorithm to solve the multiple divers tracking problem with complex motion model and unknown structured clutter density.

6) Deriving the PCRLB for the multiple divers tracking problem with independent motion model in a clutter environment.

7) Developing an algorithm to solve the extended target tracking problem in multipath clutter environment that can jointly estimate the target state and target extent.

8) Deriving the PCRLB for the extended target tracking problem with multipath detections in a clutter environment.

5.2 Future Work

There are few open problems that can be considered for future research as extensions to the work in this thesis. In Chapter 2, the proposed IMP-ML-PDA handles the target detection problem in a complex environment at the expense of high computational load. Parallel implementations of the IMP-ML-PDA can be a developed to reduce the computing time in future work. In Chapters 2 and 3, the uncertainty arising from the environment are considered. A deep learning method can be utilized to extract the features of the environment in advance to help improve the performance of the existing trackers dealing with the complex environment. In Chapter 4, instead of assuming a target with a simple elliptical shape in 2D, a more complex model can

be used and integrated into the trackers to track targets of complex shapes in 3D.

Bibliography

[1] Y. Bar-Shalom, *Tracking and Data Association*. Academic Press Professional, Inc., 1987.

[2] Y. Bar-Shalom and X.-R. Li, *Multitarget-Multisensor Tracking: Principles and Techniques*. YBs Storrs, CT, 1995, vol. 19.

[3] Y. Bar-Shalom, *Multitarget-Multisensor Tracking: Applications and Advances (Artech House Radar Library)*, 2000.

[4] D. Reid, "An algorithm for tracking multiple targets," *IEEE transactions on Automatic Control*, vol. 24, no. 6, pp. 843–854, December 1979.

[5] Y. Wang, Z. Jing, and S. Hu, "Data association for phd filter based on MHT," in *2008 11th International Conference on Information Fusion*. IEEE, 2008, pp. 1–8.

[6] X. Chen, R. Tharmarasa, M. Pelletier, and T. Kirubarajan, "Integrated Bayesian clutter estimation with JIPDA/MHT trackers," *IEEE Transactions on Aerospace and Electronic Systems*, vol. 49, no. 1, pp. 395–414, January 2013.

[7] R. P. Mahler, "Random-set approach to data fusion," in *Automatic Object Recognition IV*, vol. 2234. International Society for Optics and Photonics, 1994, pp. 287–296.

[8] K. Krishanth, X. Chen, R. Tharmarasa, T. Kirubarajan, and M. McDonald, "The social force PHD filter for tracking pedestrians," *IEEE Transactions on Aerospace and Electronic Systems*, vol. 53, no. 4, pp. 2045–2059, March 2017.

[9] B.-N. Vo, S. Singh, and A. Doucet, "Sequential Monte Carlo methods for multitarget filtering with Random Finite Sets," *IEEE Transactions on Aerospace and electronic systems*, vol. 41, no. 4, pp. 1224–1245, 2005.

[10] B. N. Vo and W. K. Ma, "The Gaussian mixture probability hypothesis density filter," *IEEE Transactions on Signal Processing*, vol. 54, no. 11, pp. 4091–4104, November 2006.

[11] T. Kirubarajan and Y. Bar-Shalom, "Low observable target motion analysis using amplitude information," *IEEE Transactions on Aerospace and Electronic Systems*, vol. 32, no. 4, pp. 1367–1384, October 1996.

[12] D. Avitzour, "A maximum likelihood approach to data association," vol. 28, no. 2, April 1992, pp. 560–566.

[13] P. Willett, Y. Ruan, and R. Streit, "PMHT: Problems and some solutions," *IEEE Transactions on Aerospace and Electronic Systems*, vol. 38, no. 3, pp. 738–754, July 2002.

[14] W. Blanding, P. Willett, and Y. Bar-Shalom, "ML-PDA: Advances and a new

multitarget approach," *EURASIP Journal on Advances in Signal Processing*, vol. 2008, Nov 2007.

[15] Y. T. Chan and F. L. Jardine, "Target localization and tracking from Doppler-shift measurements," *IEEE Journal of Oceanic Engineering*, vol. 15, no. 3, pp. 251–257, July 1990.

[16] Y. T. Chan and S. W. Rudnicki, "Bearings-only and Doppler-bearing tracking using instrumental variables," *IEEE Transactions on Aerospace and Electronic Systems*, vol. 28, no. 4, pp. 1076–1083, October 1992.

[17] S. C. Nardone and V. J. Aidala, "Observability criteria for bearings-only target motion analysis," *IEEE Transactions on Aerospace and Electronic Systems*, vol. 17, no. 2, pp. 162–166, March 1981.

[18] Y. Guo, R. Tharmarasa, S. Rajan, T. L. Song, and T. Kirubarajan, "Passive tracking in heavy clutter with sensor location uncertainty," *IEEE Transactions on Aerospace and Electronic Systems*, vol. 52, no. 4, pp. 1536–1554, August 2016.

[19] W. Cheng, A. Y. Teymorian, L. Ma, X. Cheng, X. Lu, and Z. Lu, "Underwater localization in sparse 3D acoustic sensor networks," in *IEEE INFOCOM 2008 - The 27th Conference on Computer Communications*, Phoenix, AZ, USA, April 2008, pp. 798–806.

[20] M. Erol, L. F. Vieira, and M. Gerla, "Localization with Dive'N'Rise (DNR) beacons for underwater acoustic sensor networks," in *Proceedings of the Second*

Workshop on Underwater Networks, Montreal, Quebec, Canada, September 2007, pp. 97–100.

[21] M. T. Isik and O. B. Akan, "A three dimensional localization algorithm for underwater acoustic sensor networks," *IEEE Transactions on Wireless Communications*, vol. 8, no. 9, pp. 4457–4463, September 2009.

[22] Y. Song, J. Wen, D. Yu, Y. Liu, and X. Wen, "Reduction of vibration and noise radiation of an underwater vehicle due to propeller forces using periodically layered isolators," *Journal of Sound and Vibration*, vol. 333, no. 14, pp. 3031–3043, July 2014.

[23] Z. Wang and Y. Sun, "Experimental research on active vibration control of pipe by inertial actuator and adaptive control," in *Proc. 21st International Congress on Sound and Vibration*, Beijing, China, July 2014, pp. 97–100.

[24] W. R. Blanding, P. K. Willett, Y. Bar-Shalom, and R. S. Lynch, "Directed subspace search ML-PDA with application to active sonar tracking," *IEEE Transactions on Aerospace and Electronic Systems*, vol. 44, no. 1, pp. 201–216, January 2008.

[25] D. Musicki, X. Wang, R. Ellem, and F. Fletcher, "Efficient active sonar multi-target tracking," in *OCEANS 2006 - Asia Pacific*, Singapore, Singapore, May 2006, pp. 1–8.

[26] E. Brekke, O. Hallingstad, and J. Glattetre, "Target tracking in state dependent wake clutter," in *OCEANS 2010 - Sydney*, Sydney, NSW, Australia, May 2010, pp. 1–10.

[27] A. Rodningsby, Y. Bar-Shalom, O. Hallingstad, and J. Glattetre, "Multitarget tracking in the presence of wakes," in *2008 11th International Conference on Information Fusion*, Cologne, Germany, July 2008, pp. 1–8.

[28] E. Brekke, O. Hallingstad, and J. Glattetre, "Tracking small targets in heavy-tailed clutter using amplitude information," *IEEE Journal of Oceanic Engineering*, vol. 35, no. 2, pp. 314–329, April 2010.

[29] D. E. Clark, J. Bell, Y. de Saint-Pern, and Y. Petillot, "PHD filter multi-target tracking in 3D sonar," in *Europe Oceans 2005*, vol. 1, Brest, France, June 2005, pp. 265–270.

[30] A. Mours, C. Ioana, J. I. Mars, N. F. Josso, and Y. Doisy, "Target-depth estimation in active sonar: Cramer–Rao bounds for a bilinear sound-speed profile," *Journal of the Acoustical Society of America*, vol. 140, no. 3, pp. 1771–1782, September 2016.

[31] M. Erol-Kantarci, H. T. Mouftah, and S. Oktug, "A survey of architectures and localization techniques for underwater acoustic sensor networks," *IEEE Communications Surveys Tutorials*, vol. 13, no. 3, pp. 487–502, March 2011.

[32] G. Isbitiren and O. B. Akan, "Three-dimensional underwater target tracking with acoustic sensor networks," *IEEE Transactions on Vehicular Technology*, vol. 60, no. 8, pp. 3897–3906, October 2011.

[33] J. Chen, H. Ma, C. Liang, and Y. Zhang, "OTHR multipath tracking using the Bernoulli filter," *IEEE Transactions on Aerospace and Electronic Systems*, vol. 50, no. 3, pp. 1974–1990, July 2014.

[34] H. Liu, Y. Liang, Q. Pan, and Y. Cheng, "A multipath Viterbi data association algorithm for OTHR," in *2006 CIE International Conference on Radar*, Shanghai, China, October 2006, pp. 1–4.

[35] R. Moose and T. Dailey, "Adaptive underwater target tracking using passive multipath time-delay measurements," *IEEE Transactions on Acoustics, Speech, and Signal Processing*, vol. 33, no. 4, pp. 778–787, August 1985.

[36] T. Sathyan, T. J. Chin, S. Arulampalam, and D. Suter, "A multiple hypothesis tracker for multitarget tracking with multiple simultaneous measurements," *IEEE Journal of Selected Topics in Signal Processing*, vol. 7, no. 3, pp. 448–460, June 2013.

[37] X. Tang, X. Chen, M. McDonald, R. Mahler, R. Tharmarasa, and T. Kirubarajan, "A multiple-detection probability hypothesis density filter," *IEEE Transactions on Signal Processing*, vol. 63, no. 8, pp. 2007–2019, April 2015.

[38] X. Tang, R. Tharmarasa, M. McDonald, and T. Kirubarajan, "Multiple detection-aided low-observable track initialization using ML-PDA," *IEEE Transactions on Aerospace and Electronic Systems*, vol. 53, no. 2, pp. 722–735, April 2017.

[39] H. Ramezani, H. Jamali-Rad, and G. Leus, "Target localization and tracking for an isogradient sound speed profile," *IEEE Transactions on Signal Processing*, vol. 61, no. 6, pp. 1434–1446, March 2013.

[40] D. Musicki and R. Evans, "Joint integrated probabilistic data association: JIPDA," *IEEE transactions on Aerospace and Electronic Systems*, vol. 40, no. 3, pp. 1093–1099, September 2004.

[41] H. Luo, Z. Guo, W. Dong, F. Hong, and Y. Zhao, "LDB: Localization with directional beacons for sparse 3D underwater acoustic sensor networks," *Journal of Networks*, vol. 5, no. 1, pp. 28–38, January 2010.

[42] X. Cheng, H. Shu, Q. Liang, and D. H. C. Du, "Silent positioning in underwater acoustic sensor networks," *IEEE Transactions on Vehicular Technology*, vol. 57, no. 3, pp. 1756–1766, May 2008.

[43] X. Shen, Z. Song, H. Fan, and Q. Fu, "RFS-based extended target multipath tracking algorithm," *IET Radar, Sonar Navigation*, vol. 11, no. 7, pp. 1031–1040, July 2017.

[44] M. B. Porter and Y.-C. Liu, "Finite-element ray tracing," *Theoretical and Computational Acoustics*, vol. 2, pp. 947–956, October 1994.

[45] W. H. Munk, "Sound channel in an exponentially stratified ocean, with application to SOFAR," *Journal of the Acoustical Society of America*, vol. 55, no. 2, pp. 220–226, February 1974.

[46] O. Carriere, J. P. Hermand, M. Meyer, and J. V. Candy, "Dynamic estimation of the sound-speed profile from broadband acoustic measurements," in *OCEANS 2007 - Europe*, Aberdeen, UK, June 2007, pp. 1–6.

[47] D. Helbing and P. Molnár, "Social force model for pedestrian dynamics," *Physical review E*, vol. 51, no. 5, pp. 4282–4286, May 1995.

[48] J. Møller, A. R. Syversveen, and R. P. Waagepetersen, "Log Gaussian Cox processes," *Scandinavian Journal of Statistics*, vol. 25, no. 3, pp. 451–482, December 1998.

[49] K. Granström, M. Baum, and S. Reuter, "Extended object tracking: Introduction, overview, and applications," *Journal of Advances in Information Fusion*, vol. 12, no. 2, pp. 139–174, December 2017.

[50] M. Feldmann, D. Franken, and W. Koch, "Tracking of extended objects and group targets using random matrices," *IEEE Transactions on Signal Processing*, vol. 59, no. 4, pp. 1409–1420, April 2011.

[51] K. Granstrom and U. Orguner, "A PHD filter for tracking multiple extended targets using random matrices," *IEEE Transactions on Signal Processing*, vol. 60, no. 11, pp. 5657–5671, November 2012.

[52] G. Vivone, K. Granström, P. Braca, and P. Willett, "Multiple sensor measurement updates for the extended target tracking random matrix model," *IEEE Transactions on Aerospace and Electronic Systems*, vol. 53, no. 5, pp. 2544–2558, October 2017.

[53] K. Granström and U. Orguner, "New prediction for extended targets with random matrices," *IEEE Transactions on Aerospace and Electronic Systems*, vol. 50, no. 2, pp. 1577–1589, April 2014.

[54] M. Feldmann and D. Franken, "Tracking of extended objects and group targets using random matrices – A new approach," in *11th International Conference on Information Fusion*, Cologne, Germany, June 2008, pp. 1–8.

[55] M. Schuster, J. Reuter, and G. Wanielik, "Probabilistic data association for tracking extended targets under clutter using random matrices," in *18th International Conference on Information Fusion*, Washington, DC, United States, July 2015, pp. 961–968.

[56] E. Sarıtaş and U. Orguner, "Posterior Cramér-Rao lower bounds for extended target tracking with random matrices," in *19th International Conference on Information Fusion*, Heidelberg, Germany, July 2016, pp. 1485–1492.

[57] K. Granstrom, C. Lundquist, and O. Orguner, "Extended target tracking using a Gaussian-mixture PHD filter," *IEEE Transactions on Aerospace and Electronic Systems*, vol. 48, no. 4, pp. 3268–3286, October 2012.

[58] K. Granström, C. Lundquist, and U. Orguner, "A Gaussian mixture PHD filter for extended target tracking," in *13th International Conference on Information Fusion*, Edinburgh, United Kingdom, July 2010, pp. 1–8.

[59] N. Wahlström and E. Özkan, "Extended target tracking using Gaussian processes," *IEEE Transactions on Signal Processing*, vol. 63, no. 16, pp. 4165–4178, August 2015.

[60] W. Wu, J. Jiang, W. Liu, X. Feng, L. Gao, and X. Qin, "Augmented state GM-PHD filter with registration errors for multi-target tracking by Doppler radars," *Signal Processing*, vol. 120, pp. 117–128, September 2016.

[61] Y. Huang, Y. Zhang, Z. Wu, N. Li, and J. Chambers, "A novel adaptive

Kalman filter with inaccurate process and measurement noise covariance matrices," *IEEE Transactions on Automatic Control*, vol. 63, no. 2, pp. 594–601, February 2018.

[62] E. A. Wan and R. Van Der Merwe, "The unscented Kalman filter for nonlinear estimation," in *Proceedings of the IEEE 2000 Adaptive Systems for Signal Processing, Communications, and Control Symposium*, Lake Louise, Alberta, Canada, August 2002, pp. 153–158.

[63] K. V. Mackenzie, "Nine-term equation for sound speed in the oceans," *Journal of the Acoustical Society of America*, vol. 70, no. 3, pp. 807–812, September 1981.

[64] T. Ringholm, "Target depth estimation using hull mounted active sonar," Master's Thesis, Norwegian University of Science and Technology, 2014.

[65] T. Kirubarajan, Y. Bar-Shalom, and D. Lerro, "Bearings-only tracking of maneuvering targets using a batch-recursive estimator," *IEEE Transactions on Aerospace and Electronic Systems*, vol. 37, no. 3, pp. 770–780, July 2001.

[66] C. R. Berger, S. Zhou, P. Willett, and L. Liu, "Stratification effect compensation for improved underwater acoustic ranging," *IEEE Transactions on Signal Processing*, vol. 56, no. 8, pp. 3779–3783, August 2008.

[67] C. Jauffret and Y. Bar-Shalom, "Track formation with bearing and frequency measurements in clutter," *IEEE Transactions on Aerospace and Electronic Systems*, vol. 26, no. 6, pp. 999–1010, November 1990.

[68] T. Kirubarajan, H. Chen, and Y. Bar-Shalom, "Parameter estimation and the CRLB with uncertain origin measurements," *Methodology and Computing in Applied Probability*, vol. 3, no. 4, pp. 387–410, December 2001.

[69] W. Blanding, P. Willett, and Y. Bar-Shalom, "ML-PDA: Advances and a new multitarget approach," *EURASIP Journal on Advances in Signal Processing*, vol. 2008, no. 1, pp. 1–13, November 2008.

[70] G. W. Pulford, "OTHR multipath tracking with uncertain coordinate registration," *IEEE Transactions on Aerospace and Electronic Systems*, vol. 40, no. 1, pp. 38–56, January 2004.

[71] S. Boyd and L. Vandenberghe, *Convex Optimization*. Cambridge University Press, 2004.

[72] D. E. Goldberg and J. H. Holland, "Genetic algorithms and machine learning," *Machine Learning*, vol. 3, no. 2, pp. 95–99, October 1988.

[73] M. Li and Y. Lu, "Maximum likelihood DOA estimation in unknown colored noise fields," *IEEE Transactions on Aerospace and Electronic Systems*, vol. 44, no. 3, pp. 1079–1090, July 2008.

[74] M. Li and Y. Lu, "Source bearing and steering-vector estimation using partially calibrated arrays," *IEEE Transactions on Aerospace and Electronic Systems*, vol. 45, no. 4, pp. 1361–1372, October 2009.

[75] S. Sedghizadeh and S. Beheshti, "Particle swarm optimization based fuzzy gain scheduled subspace predictive control," *Engineering Applications of Artificial Intelligence*, vol. 67, pp. 331–344, November 2018.

[76] V. Roberge, M. Tarbouchi, and G. Labonte, "Comparison of parallel genetic algorithm and particle swarm optimization for real-time UAV path planning," *IEEE Transactions on Industrial Informatics*, vol. 9, no. 1, pp. 132–141, February 2013.

[77] D. Willner, C. B. Chang, and K. P. Dunn, "Kalman filter algorithms for a multi-sensor system," in *IEEE Conference on Decision and Control including the 15th Symposium on Adaptive Processes*, Clearwater, FL, USA, December 1976, pp. 570–574.

[78] T. Fortmann, Y. Bar-Shalom, and M. Scheffe, "Sonar tracking of multiple targets using joint probabilistic data association," *IEEE Journal of Oceanic Engineering*, vol. 8, no. 3, pp. 173–184, July 1983.

[79] Y. Bar-Shalom and E. Tse, "Tracking in a cluttered environment with probabilistic data association," *Automatica*, vol. 11, no. 5, pp. 451–460, September 1975.

[80] W. R. Blanding, P. K. Willett, and Y. Bar-Shalom, "Offline and real-time methods for ML-PDA track validation," *IEEE Transactions on Signal Processing*, vol. 55, no. 5, pp. 1994–2006, May 2007.

[81] E. Castillo, *Extreme Value Theory in Engineering*. Elsevier, 2012.

[82] Y. Bar-Shalom, X. R. Li, and T. Kirubarajan, *Estimation with Applications to Tracking and Navigation*. NY: John Wiley and Sons, 2001.

[83] L. Dagum and R. Menon, "OpenMP: An industry standard API for shared-memory programming," *IEEE Computational Science and Engineering*, vol. 5, no. 1, pp. 46–55, January 1998.

[84] A. Asada, F. Maeda, K. Kuramoto, Y. Kawashima, M. Nanri, and K. Hantani, "Advanced surveillance technology for underwater security sonar systems," in *OCEANS 2007 - Europe*, Aberdeen, UK, June 2007, pp. 1–5.

[85] A. Lovik, A. R. Bakken, J. Dybedal, T. Knudsen, and J. Kjoll, "Underwater protection system," in *OCEANS 2007*, Vancouver, BC, Canada, September 2007, pp. 1–8.

[86] A. Ur-Rehman, S. M. Naqvi, L. Mihaylova, and J. A. Chambers, "Multi-target tracking and occlusion handling with learned variational Bayesian clusters and a social force model," *IEEE Transactions on Signal Processing*, vol. 64, no. 5, pp. 1320–1335, March 2016.

[87] P. Gipps and B. Marksjö, "A micro-simulation model for pedestrian flows," *Mathematics and Computers in Simulation*, vol. 27, no. 2, pp. 95–105, April 1985.

[88] S. Okazaki, "A study of pedestrian movement in architectural space, Part 1: Pedestrian movement by the application of magnetic models," *Transactions of the Architectural Institute of Japan*, vol. 283, pp. 111–119, 1979.

[89] P. Feng, W. Wang, S. Dlay, S. M. Naqvi, and J. Chambers, "Social force model-based MCMC-OCSVM particle PHD filter for multiple human tracking," *IEEE Transactions on Multimedia*, vol. 19, no. 4, pp. 725–739, April 2017.

[90] R. Ding, M. Yu, H. Oh, and W. Chen, "New multiple-target tracking strategy using domain knowledge and optimization," *IEEE Transactions on Systems, Man, and Cybernetics: Systems*, vol. 47, no. 4, pp. 605–616, April 2017.

[91] A. Rodningsby and Y. Bar-Shalom, "Tracking of divers using a probabilistic data association filter with a bubble model," *IEEE Transactions on Aerospace and Electronic Systems*, vol. 45, no. 3, pp. 1181–1193, July 2009.

[92] D. Musicki, S. Suvorova, M. R. Morelande, and B. Moran, "Clutter map and target tracking," in *7th International Conference on Information Fusion*, Philadelphia, PA, USA, July 2005, pp. 69–76.

[93] X. R. Li and N. Li, "Integrated real-time estimation of clutter density for tracking," *IEEE Transactions on Signal Processing*, vol. 48, no. 10, pp. 2797–2805, October 2000.

[94] X. Chen, R. Tharmarasa, M. Pelletier, and T. Kirubarajan, "Integrated clutter estimation and target tracking using Poisson point processes," *IEEE Transactions on Aerospace and Electronic Systems*, vol. 48, no. 2, pp. 1210–1235, April 2012.

[95] R. Mahler, "CPHD and PHD filters for unknown backgrounds II: Multitarget filtering in dynamic clutter," in *Proceedings of SPIE, Sensors and Systems for Space Applications III*, vol. 7330, Orlando, Florida, United States, May 2009.

[96] T. L. Song and D. Musicki, "Adaptive clutter measurement density estimation for improved target tracking," *IEEE Transactions on Aerospace and Electronic Systems*, vol. 47, no. 2, pp. 1457–1466, April 2011.

[97] X. Chen, R. Tharmarasa, T. Kirubarajan, and M. McDonald, "Online clutter estimation using a Gaussian kernel density estimator for multitarget tracking," *IET Radar, Sonar Navigation*, vol. 9, no. 1, pp. 1–9, February 2015.

[98] D. Musicki and R. Evans, "Clutter map information for data association and track initialization," *IEEE Transactions on Aerospace and Electronic Systems*, vol. 40, no. 2, pp. 387–398, April 2004.

[99] T. Hanselmann, D. Musicki, and M. Palaniswami, "Adaptive target tracking in slowly changing clutter," in *2006 9th International Conference on Information Fusion*, Florence, Italy, July 2006, pp. 1–8.

[100] R. Mahler, "CPHD and PHD filters for unknown backgrounds I: Dynamic data clustering," in *Proceedings of SPIE, Sensors and Systems for Space Applications III*, vol. 7330, Orlando, Florida, United States, May 2009.

[101] R. Mahler and A. El-Fallah, "CPHD and PHD filters for unknown backgrounds, part III: Tractable multitarget filtering in dynamic clutter," in *Proceedings of SPIE, Signal and Data Processing of Small Targets 2010*, vol. 7698, Orlando, Florida, United States, April 2010.

[102] R. P. S. Mahler, *Statistical Multisource-Multitarget Information Fusion*. Norwood, MA, USA: Artech House, Inc., 2007.

[103] X. R. Li and V. P. Jilkov, "Survey of maneuvering target tracking. Part I: Dynamic models," *IEEE Transactions on Aerospace and Electronic Systems*, vol. 39, no. 4, pp. 1333–1364, October 2003.

[104] M. Luber, J. A. Stork, G. D. Tipaldi, and K. O. Arras, "People tracking with human motion predictions from social forces," in *2010 IEEE International Conference on Robotics and Automation*, Anchorage, AK, USA, May 2010, pp. 464–469.

[105] E. J. Finnemore and J. B. Franzini, *Fluid Mechanics with Engineering Applications*. New York, USA: McGraw-Hill, 2002.

[106] T. Wei, R. Mark, and S. Hutchison, "The fluid dynamics of competitive swimming," *Annual Review of Fluid Mechanics*, vol. 46, pp. 547–565, January 2014.

[107] M. Nakashima, Y. Tanno, T. Fujimoto, and Y. Masutani, "Development of a simulation model for swimming with diving fins," *Multidisciplinary Digital Publishing Institute Proceedings*, vol. 2, no. 6:288, February 2018.

[108] M. Nakashima, "Modeling and simulation of human swimming," *Journal of Aero Aqua Bio-mechanisms*, vol. 1, no. 1, pp. 11–17, October 2010.

[109] A. Lyttle and M. Keys, "The use of computational fluids dynamics to optimise underwater kicking performance," in *22nd International Symposium on Biomechanics in Sports*, Ottawa, Canada, August 2004, pp. 438–441.

[110] G. K. Batchelor, *An Introduction to Fluid Dynamics*. Cambridge, UK: Cambridge University Press, 2000.

[111] R. P. Mahler, "Multitarget Bayes filtering via first-order multitarget moments," *IEEE Transactions on Aerospace and Electronic systems*, vol. 39, no. 4, pp. 1152–1178, October 2003.

[112] T. Li, M. Bolic, and P. M. Djuric, "Resampling methods for particle filtering: Classification, implementation, and strategies," *IEEE Signal Processing Magazine*, vol. 32, no. 3, pp. 70–86, May 2015.

[113] M. S. Arulampalam, S. Maskell, N. Gordon, and T. Clapp, "A tutorial on particle filters for online nonlinear/non-Gaussian Bayesian tracking," *IEEE Transactions on Signal Processing*, vol. 50, no. 2, pp. 174–188, August 2002.

[114] H. W. Sorenson and D. L. Alspach, "Recursive Bayesian estimation using Gaussian sums," *Automatica*, vol. 7, no. 4, pp. 465–479, July 1971.

[115] S. R. Rogers, "Tracking multiple targets with correlated measurements and maneuvers," *IEEE Transactions on Aerospace and Electronic Systems*, vol. 24, no. 3, pp. 313–315, May 1988.

[116] D. Song, R. Tharmarasa, T. Kirubarajan, and X. N. Fernando, "Multi-vehicle tracking with road maps and car-following models," *IEEE Transactions on Intelligent Transportation Systems*, vol. 19, no. 5, pp. 1375–1386, May 2018.

[117] S. J. Julier and J. K. Uhlmann, "New extension of the Kalman filter to nonlinear systems," in *Signal Processing, Sensor Fusion, and Target Recognition VI*, vol. 3068, Orlando, FL, United States, 1997, pp. 182–194.

[118] A. Brix and P. J. Diggle, "Spatiotemporal prediction for log-Gaussian Cox processes," *Journal of the Royal Statistical Society. Series B (Statistical Methodology)*, vol. 63, no. 4, pp. 823–841, 2001.

[119] C. Rasmussen and C. Williams, *Gaussian Processes for Machine Learning*. Cambridge, MA, USA: MIT Press, 2006.

[120] S. Sarkka, A. Solin, and J. Hartikainen, "Spatiotemporal learning via infinite-dimensional Bayesian filtering and smoothing: A look at Gaussian process regression through Kalman filtering," *IEEE Signal Processing Magazine*, vol. 30, no. 4, pp. 51–61, July 2013.

[121] R. P. Adams, I. Murray, and D. J. MacKay, "Tractable nonparametric Bayesian inference in Poisson processes with Gaussian process intensities," in *Proceedings of the 26th Annual International Conference on Machine Learning*, Montreal, Quebec, Canada, June 2009, pp. 9–16.

[122] L. Sun, J. Lan, and X. R. Li, "Extended target tracking using star-convex model with nonlinear inequality constraints," in *Proceedings of the 31st Chinese Control Conference*, Hefei, China, July 2012, pp. 3869–3874.

[123] J. W. Koch, "Bayesian approach to extended object and cluster tracking using random matrices," *IEEE Transactions on Aerospace and Electronic Systems*, vol. 44, no. 3, pp. 1042–1059, July 2008.

[124] K. Granström, C. Lundquist, and U. Orguner, "Tracking rectangular and elliptical extended targets using laser measurements," in *14th International Conference on Information Fusion*, Chicago, IL, United States, July 2011, pp. 1–8.

[125] J. Lan and X. R. Li, "Tracking of extended object or target group using random matrix – Part II: Irregular object," in *15th International Conference on Information Fusion*, Singapore, Singapore, July 2012, pp. 2185–2192.

[126] ——, "Tracking of maneuvering non-ellipsoidal extended object or target group

using random matrix," *IEEE Transactions on Signal Processing*, vol. 62, no. 9, pp. 2450–2463, May 2014.

[127] M. Baum and U. D. Hanebeck, "Random hypersurface models for extended object tracking," in *IEEE International Symposium on Signal Processing and Information Technology*, Ajman, United Arab Emirates, December 2009, pp. 178–183.

[128] Y. Guo, Y. Li, R. Tharmarasa, T. Kirubarajan, M. Efe, and B. Sarikaya, "GP-PDA filter for extended target tracking with measurement origin uncertainty," *IEEE Transactions on Aerospace and Electronic Systems*, October 2018. DOI: 10.1109/TAES.2018.2875555

[129] M. Kumru and E. Özkan, "3D extended object tracking using recursive Gaussian processes," in *21st International Conference on Information Fusion*, Cambridge, United Kingdom, July 2018, pp. 1–8.

[130] B. Habtemariam, R. Tharmarasa, T. Thayaparan, M. Mallick, and T. Kirubarajan, "A multiple-detection joint probabilistic data association filter," *IEEE Journal of Selected Topics in Signal Processing*, vol. 7, no. 3, pp. 461–471, June 2013.

[131] R. Mahler, "PHD filters for nonstandard targets, I: Extended targets," in *12th International Conference on Information Fusion*, Seattle, WA, United States, July 2009, pp. 915–921.

[132] A. Ur-Rehman, S. M. Naqvi, L. Mihaylova, and J. A. Chambers, "Multi-target tracking and occlusion handling with learned variational Bayesian clusters and

a social force model," *IEEE Transactions on Signal Processing*, vol. 64, no. 5, pp. 1320–1335, March 2016.

[133] T. De Laet, H. Bruyninckx, and J. De Schutter, "Shape-based online multi-target tracking and detection for targets causing multiple measurements: Variational Bayesian clustering and lossless data association," *IEEE Transactions on Pattern Analysis and Machine Intelligence*, vol. 33, no. 12, pp. 2477–2491, December 2011.

[134] O. Khatib, "Real-time obstacle avoidance for manipulators and mobile robots," in *1985 IEEE International Conference on Robotics and Automation*, St. Louis, MO, United States, March 1985, pp. 500–505.

[135] J. Guldner and V. I. Utkin, "Sliding mode control for gradient tracking and robot navigation using artificial potential fields," *IEEE Transactions on Robotics and Automation*, vol. 11, no. 2, pp. 247–254, April 1995.

[136] Y. K. Hwang and N. Ahuja, "A potential field approach to path planning," *IEEE Transactions on Robotics and Automation*, vol. 8, no. 1, pp. 23–32, February 1992.

[137] Y. Petillot, I. Tena Ruiz, and D. M. Lane, "Underwater vehicle obstacle avoidance and path planning using a multi-beam forward looking sonar," *IEEE Journal of Oceanic Engineering*, vol. 26, no. 2, pp. 240–251, April 2001.

[138] S. E. Houts and S. M. Rock, "Trajectory planning for motion-constrained AUVs in uncertain environments," in *Oceans - St. John's*, St. John's, NL, Canada, September 2014, pp. 1–5.

[139] T. M. Howard and A. Kelly, "Optimal rough terrain trajectory generation for wheeled mobile robots," *The International Journal of Robotics Research*, vol. 26, no. 2, pp. 141–166, February 2007.

[140] C. Veibäck, G. Hendeby, and F. Gustafsson, "Tracking of dolphins in a basin using a constrained motion model," in *18th International Conference on Information Fusion*, Washington, DC, United States, July 2015, pp. 1330–1337.

[141] K. Granström, A. Natale, P. Braca, G. Ludeno, and F. Serafino, "Gamma Gaussian inverse Wishart probability hypothesis density for extended target tracking using X-band marine radar data," *IEEE Transactions on Geoscience and Remote Sensing*, vol. 53, no. 12, pp. 6617–6631, December 2015.

[142] A. K. Gupta and D. K. Nagar, *Matrix Variate Distributions*. London, United Kingdom: Chapman and Hall/CRC, 1999.

[143] F. Lian, C.-Z. Han, W.-F. Liu, X.-X. Yan, and H.-Y. Zhou, "Sequential Monte Carlo implementation and state extraction of the group probability hypothesis density filter for partly unresolvable group targets-tracking problem," *IET Radar, Sonar Navigation*, vol. 4, no. 5, pp. 685–702, October 2010.

[144] T. Kirubarajan and Y. Bar-Shalom, "Probabilistic data association techniques for target tracking in clutter," *Proceedings of the IEEE*, vol. 92, no. 3, pp. 536–557, March 2004.

[145] T. Kirubarajan and Y. Bar-Shalom, "Low observable target motion analysis using amplitude information," *IEEE Transactions on Aerospace and Electronic Systems*, vol. 32, no. 4, pp. 1367–1384, October 1996.

[146] C. M. Bishop, *Pattern Recognition and Machine Learning (Information Science and Statistics)*. Berlin, Heidelberg: Springer-Verlag, 2006.

[147] P. Tichavsky, C. H. Muravchik, and A. Nehorai, "Posterior Cramér-Rao bounds for discrete-time nonlinear filtering," *IEEE Transactions on Signal Processing*, vol. 46, no. 5, pp. 1386–1396, May 1998.

[148] E. Saritaş, "Parametric and posterior Cramér-Rao low bounds for extended target tracking in a random matrix framework," Master's Thesis, Middle East Technical University, Turkey, 2015.

[149] H. Ramezani, H. Jamali-Rad, and G. Leus, "Target localization and tracking for an isogradient sound speed profile," *IEEE Transactions on Signal Processing*, vol. 61, no. 6, pp. 1434–1446, December.